LASING AND OPTICAL PROPERTIES OF
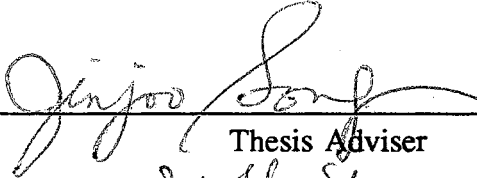
ZnSe BASED II-VI COMPOUNDS

By

XIAO HUA YANG

Bachelor of Science
Henan Normal University
Xinxiang, China
1984

Master of Science
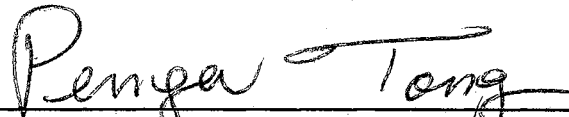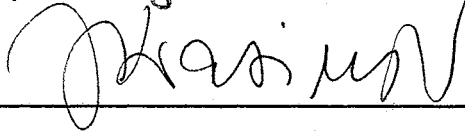Oklahoma State University
Stillwater, Oklahoma
1988

Submitted to the Faculty of the
Graduate College of the
Oklahoma State University
in partial fulfillment of
the requirements for
the Degree of
DOCTOR OF PHILOSOPHY
July, 1993

LASING AND OPTICAL PROPERTIES OF

ZnSe BASED II-VI COMPOUNDS

Thesis Approved:

_____
Thesis Adviser

_____

_____

_____

_____
Dean of the Graduate College

ACKNOWLEDGEMENTS

TABLE OF CONTENTS

LIST OF FIGURES

CHAPTER I

INTRODUCTION

ZnSe-based II-VI compound semiconductors are currently the best candidates for optoelectronic device applications in the blue-green region of the visible spectrum such as blue diode lasers and blue light-emitting diodes. There are still several serious obstacles which should be overcome before the successful diode lasers come to reality. These are the inability to achieve heavy p-type doping for the preparation of p-n junctions, as well as good Ohmic contacts. In addition, the optical properties of these materials and their lasing characteristics still remain to be thoroughly understood. It is the purpose of this work to present the results on the studies of certain aspects of optical properties and optically pumped lasing properties of ZnSe-based materials.

Chapter II presents a theoretical background. A historic perspective on the blue lasing of II-VI compounds is given. Special emphasis is given to optical pumping in various novel structures. The quantum size effect in a semiconductor quantum well is also briefly reviewed. Chapter III to Chapter VI presents detailed studies on the optically pumped lasing properties of ZnSe and ZnSSe samples. Chapter III studies the stimulated emission and lasing properties of ZnSe at room temperature. This includes the description of stimulated emission characteristics and the identification of lasing mechanisms at room temperature. Chapter IV describes the room temperature

1

operation of optically pumped lasing from ZnSe and ZnSSe laser bar samples. Record low lasing threshold values were observed from these laser bar samples without the optical coating on the laser cavity facets. In Chapter V, a two-photon pumped lasing study on ZnSe and ZnSSe samples is presented. The lasing properties were compared with one-photon pumping case and the lasing mechanism was identified. In Chapter VI optical gain measurements were performed. The obtained gain values are very useful in designing laser cavities. Chapter VII studies the quantum confinement effect of strained ZnS/ZnSe single quantum well systems. This study reveals the good sample quality in the strained layer samples with very sharp excitonic transitions observed. The strain in the quantum wells changes the band structures of the system, which has to be considered in energy band calculation. Chapter VIII presents a preliminary study on the nonlinear optical second harmonic generation with a transmission geometry. Finally, Chapter IX summarizes the results of this work.

CHAPTER II

BACKGROUND

Survey of Blue-green Lasing Work from

ZnSe Based II-VI Compounds

<u>Potential Applications</u>

Compact sources of blue light, such as blue light emitting diodes (LED's) and

blue lasers, will find wide applications in modern optoelectronic devices. Optical

information processing and optical data storage, compact disc players and large RGB

(red-green-blue) screen displays, as well as undersea communications, are a few

examples of the applications which illustrate the importance of the development of

small blue laser devices. An infrared emitting laser from III-V semiconductors is the

key component in the optical communication, laser printers and optical memories (

e.g. video and compact discs). Significant technological advantages are possible in the

enhancement of optical readout density and printing speed in the laser printers if the

wavelength of the semiconductor laser can be altered from infrared to blue. For

example, in the case of optical readout memories, such as compact discs, the storage

bit density, in diffraction limited optical systems, increases as the square of the spatial

cut off frequency $f_c = 2NA/\lambda$, where NA is the numerical aperture and λ is the laser

wavelength.[1] A change in wavelength from 800 to 400 nm produces a factor of 4 increase in the data storage rate. This increase in optical density will allow us to find more applications beyond the current capacity in video/compact disc optical information systems. A compact blue/green light source will also make large color screen display possible where blue and green are needed to make a full color display. The blue/green diode lasers will replace the bulky photo-tube now used in color TV sets to produce the primary colors: red-green-blue.

The application of blue lasers in under-water communications is due to the fact that the sea water absorbs colored lights at different rates; only the blue light can easily pass through the sea water with less absorption. This will provide faster and better communication between submarines. Laser beam communications would also be difficult to intercept and could transport a greater volume of information than present systems, such as sonar.

Electron Beam Pumping on II-VI Compounds

One of the commonly used excitation methods to obtain lasing in semiconductors is a beam of high energy electrons (e-beam) focused onto the semiconductor target to achieve high density carrier generation. In this case, high energy electrons of 20 keV or more are deposited on a semiconductor sample. These electrons penetrate several microns into the material and generate electron-hole pairs as they lose energy. Electron beam pumping was extensively used in the past for II-VI compound semiconductors where reliable diode laser structures are as yet difficult to

fabricate and where the optical pumping is limited by the available laser source. The first stimulated emission and lasing from semiconductors under e-beam pumping were reported more than twenty years ago on CdS.[2] Since then, electron beam pumped lasing has been demonstrated in most II-VI compounds. Some of the II-VI laser output efficiencies at low temperatures (4 K-77 K) are reported to be in excess of 0.26 for CdS.[3,4] At room temperature, efficiencies up to 0.18 were reported.[5] If proper cavity precautions are taken, high output powers can also be obtained from II-VI lasers. Up to 100 kW peak power has been obtained from both ZnO and CdS.[6,7] Unfortunately, these efficiencies and peak powers are not typical. In most experiments, one observes a few percent or less efficiency and a few watts or less peak power.

The disadvantage of the e-beam pumping is that in most cases, the density of the excitation required to achieve lasing threshold is too high. This will lead to various forms of sample degradation.[8,9] ZnSe is a typical example in which experiments have shown that very high excitation power densities are required to reach the lasing threshold. The threshold is usually so high that applications are impractical. Also, the thermal effects in the e-beam pumped lasers have to be dealt with since the excessive thermal loading of the material is present due to high conversion ratio of e-beam energy into heat.

Optical Pumping

Similar to the electron-beam pumping, optical pumping uses photons instead of electrons to excite semiconductors. A photon is absorbed by the semiconductor,

creating an electron-hole pair which then recombines and emits another photon with lower energy. This technique has been used to excite materials in which contact or junction technology is not adequately developed, or in high-resistivity materials where electroluminescence would be inefficient or impractical. The first optically pumped stimulated emission study on ZnSe was performed by R.J. Seymour in 1978.[10] The stimulated emission was observed from solution-grown bulk ZnSe samples by a nitrogen laser excitation. Based on energy position of the lasing line, the stimulated emission at 77 K was identified as due to the LO-phonon assistant free exciton recombination. Catalano et al performed the one- and two-photon pumped stimulated emission studies on the melt grown ZnSe.[11] Based on the experimental observations, they concluded that the ZnSe lasing mechanism under one photon excitation with pumping photon energy close to the sample energy gap is the exciton-exciton scattering, whereas under two-photon pumping the dominant laser action is related to LO-phonon assisted free exciton recombination. Baltrameyunas et al also studied the lasing mechanism of ZnSe at low temperatures (77K) and found that the main mechanism responsible for two-photon pumped lasing was a combination of exciton-phonon and exciton-exciton interactions.[12] Recently, Newbury et al re-investigated the stimulated emission mechanisms in MBE ZnSe epilayers.[13] Based on i) the peak energy position of stimulated emission line at threshold, ii) the kinetics of the emission intensity below threshold, and iii) a shift to lower energies of the lasing line with increased pump intensity, they concluded that the stimulated emission is due to inelastic exciton-exciton scattering.

The above studies are all made at low temperatures. Lasing at room temperature has not been achieved until very recently. Zmudzinski et al reported for the first time the room temperature photopumped lasing from bulk ZnSe by using a pump photon energy very close to the band gap of ZnSe and incorporating highly reflective coatings on the cavity ends.[14] The improved lasing properties were observed in our laboratory at room temperature in both bulk and epilayer ZnSe samples without the high reflective coatings.[15] Furthermore, we have identified the lasing mechanisms at room temperature for the first time.[16]

With advances in modern growth technology such as Molecular Beam Epitaxy (MBE) and Vapor Phase Epitaxy (VPE), sample qualities are much improved. GaAs is usually used as a substrate material in these epitaxial growth techniques for II-VI compounds. Stimulated emission and lasing have been observed in various types of quantum well structures based on ZnSe. The quantum well structures such as a double heterostructure (DH) can provide confinement to electronic carriers as well as to the photons. This will significantly reduce the threshold, resulting in the improved lasing characteristics compared to the bulk case. As a matter of fact, a $ZnSe/ZnS_{0.06}Se_{0.94}$ double heterostructure grown on the GaAs substrate has been lased at room temperature using a near resonant pumping.[17] The reason for selecting $ZnS_{0.06}Se_{0.94}$ as the cladding layer is that it is lattice matched to the GaAs substrate which will give rise to good sample quality. However, the small sulphur concentration used in the ZnSSe barrier provides limited optical and carrier confinements. The advantage of using the small sulphur concentration is that it reduces the strains in the ZnSe active

layer so that a thicker active layer can be grown without the generation of misfit dislocations.

The ZnSe/ZnSSe multilayer structures are favored material systems for blue lasing since the quantum confinement effects shift the lasing energy further into the blue. Lasing in a $ZnSe/ZnS_{0.12}Se_{0.88}$ multilayer structure has been observed up to 180K.[18] The same group has also improved the sample structure design with higher heterobarriers ($ZnSe/ZnS_{0.18}Se_{0.82}$) and with an average lattice constant of the multilayers matched to that of the GaAs substrate.[19] In this way, they observed lasing up to near room temperature (280K). Later on, they observed the low threshold lasing by a near resonant pumping, which directly excites the active ZnSe layer.[20] Lasing up to 400 K was observed.[20] Another group reported lasing in $ZnSe/ZnS_{0.19}Se_{0.81}$ superlattice structures in the temperature range of 100-300K.[21] Very recently, high output powers of 24 W (10 ns, 8 Hz) was observed from a photopumped $ZnSe/ZnS_{0.18}Se_{0.82}$ blue laser operating at room temperature with high quantum efficiency.[22] The improved lasing property is attributed to the improved waveguiding structure as well as the crystalline property of the active layer.[22] The lasing mechanism was studied by measuring the temperature and the excitation level dependence of the emission spectra. The stimulated emission mechanism was concluded to be the result of electron-hole plasma.[23]

Another material system which has been studied intensively is the ZnSe/ZnCdSe multilayer structures. Due to the fact that high quality ZnCdSe crystals can be easily grown and that the crystal can provide the unique tunability in the range

of yellow-to-red, the lasing properties of ZnCdSe alloy have been studied.[24] The

wavelength of lasing achieved varies from 620 nm (red) at room temperature to 585

nm (yellow) at 100K. The main reason in considering ZnSe/ZnCdSe as the prime

candidate for realizing the p-n diode laser emission results from a consideration of

conduction and valence band offsets in II-VI heterostructures. While a number of

structures were found to possess either rather small valence band offset

(ZnSe/ZnMnSe[25,26] and CdTe/ZnTe[27,28]) or too small conduction band offsets (

ZnSe/ZnSSe system),[29,30] $ZnSe/ZnCd_xSe_{1-x}$ system was found to have reasonable

confinement on both electrons and holes (for example, with x=0.2, the band offset

ratio is $\Delta E_c/\Delta E_v=70/30$).[31,32] Optically pumped lasing has been realized in

ZnSe/ZnCdSe single quantum well structures[33] as well as multiple quantum well

structures.[34,35] This leads to the historic development of the first II-VI diode lasers

emitting in the blue-green spectral region in 1991.[36,37] After this initial success in

making the diode laser, efforts continued to improve the lasing properties, such as

lowering the lasing threshold, increasing the operation life time, and increasing the

lasing temperatures in order for it to be practically used.[38] Also, some novel structure

designs such as $Zn_{0.80}Cd_{0.20}Se/ZnS_{0.08}Se_{0.92}$ have been studied to improve the lasing

properties.[39] Meanwhile, efforts are also made toward the identification of the

mechanisms responsible for the lasing.[40-42]

Other material systems have also been studied by using optical pumping

techniques. Since it is still difficult to obtain p-doped ZnSe and ZnTe is grown

naturally p-type, it is believed that the ZnSe/ZnTe quantum well structure should

provide a good choice for the p-n junction carrier injection lasers. However, the difficulty in this system is the large lattice constant mismatch (7.4%) and possibly a type-II band offset.[43] These problems may be solved by using a ZnSeTe alloy system.[44] As an alternative, a $Zn_{0.75}Cd_{0.25}Te/ZnTe$ structure has been designed to reduce the strain and has been studied for optically pumped lasing at room temperature.[45] Quasi-continuous lasing was also observed in ZnCdTe/ZnTe quantum wells up to room temperature.[46, 47] Another well studied lasing system is the ZnSe/ZnMgSe multiple quantum wells.[48] Very recently, blue laser diodes were successfully fabricated from ZnMnSSe/ZnSe structures which operate at 77 K.[49]

Quantum Size Effect

When a single layer of material A with a smaller energy band gap is embedded between two layers of material B with a larger band gap, the band discontinuities are such that both electrons and holes are confined in the A materials. In the case that the thickness of the material A is much less than the other two dimensions, $L_z \ll L_x, L_y$, and is comparable to the DeBroglie wavelength of the carrier, quantization of the particle motion in the z-direction occurs. The electrons and holes in such a heterostructure may be viewed as a two-dimensional electron gas. This is the so-called Quantum Size Effect which was discovered over 20 years ago.

In the approximation of the envelope wave function[50], the situation can be viewed as the one-dimensional motion of a particle of mass m confined by a finite barrier. The problem is well-known, and the solution can be found in any quantum

mechanics textbook. The Schrodinger equation can be written as

$$[-\frac{h^2}{2m^*(z)}\frac{d^2}{dz^2}+V_c(z)]\psi_n=E_n\psi_n$$

$$V_c=0 \quad for \quad |z|<\frac{L_z}{2}$$

$$V_0 \quad for |z|>\frac{L_z}{2}$$

(II.1)

where $m^*(z)$ is the effective mass of the carrier in A or B material, and L_z is the thickness of material A. Since the problem has an inversion symmetry around the center of the well, which is taken as the center of coordinates, the solution wave functions of Eq. (II.1) can only be even or odd. They can be written as

$$\Psi_n=A\cos kz, \quad for \quad |z|<\frac{L_z}{2}$$

$$=B\exp[-\kappa(z-L_z/2)], \quad for \quad z>\frac{L_z}{2}$$

$$=B\exp[\kappa(z+L_z/2)], \quad for \quad z<-\frac{L_z}{2}$$

(II.2)

or

$$\Psi_n=A\sin kz, \quad for \quad |z|<\frac{L_z}{2}$$

$$=B\exp[-\kappa(z-L_z/2)], \quad for \quad z>\frac{L_z}{2}$$

$$=B\exp[\kappa(z+L_z/2)], \quad for \quad z<-\frac{L_z}{2}$$

(II.3)

where

$$E_n = \frac{h^2 k^2}{2m_A^*} - V_0; \qquad E_n = -\frac{h^2 \kappa^2}{2m_B^*}; \qquad -V_0 < E < 0 \qquad \text{(II.4)}$$

The eigenvalues E_n can be obtained by matching Ψ and $[1/m^*(z)][d\Psi/dz]$ at the interfaces which gives the transcendental equation

$$\tan\sqrt{\frac{2m_A^* L_z^2 E_n}{h^2}} = \frac{2\sqrt{m_A^* m_B^*}\sqrt{\frac{E_n}{V_0}(1-\frac{E_n}{V_0})}}{(m_A^* + m_B^*)\frac{E_n}{V_0} - m_B^*} \qquad \text{(II.5)}$$

The above equation holds for both electrons and holes. The potential V_0 is called the band offset. The ratio of the conduction band offset over the valence band offset is an important parameter in calculating the quantized energy levels. Obviously, the quantized energy levels will depend on the potential barrier V_0, as well as the well width L_z. By changing L_z, one can change the optical transition wavelength. The photoluminescence technique usually can detect the transition between the first quantized electron and hole energy levels.

CHAPTER III

OPTICALLY PUMPED STIMULATED EMISSION STUDIES

IN ZnSe AT ROOM TEMPERATURE

Introduction

Direct wide band gap II-VI compound semiconductors have been studied for more than twenty years for their potential applications in optoelectronics such as blue laser diodes and light emitting devices.[51] ZnSe is one of the most extensively studied II-VI materials. In recent years, great progress has been made in lasing ZnSe based materials.[10,36,37,52] This includes the first successful operation of the diode lasers in the blue-green portion of the spectrum.[36,37] The photopumped lasing work has been mainly confined to low temperatures. The mechanisms responsible for stimulated emission (SE) at low (~10 K) temperatures have been studied extensively. The proposed mechanisms for SE at low temperatures were free exciton-exciton inelastic scattering or a combination of exciton-exciton and exciton-phonon process.[13,53] Much less work has been done for lasing ZnSe at room temperature. This is probably due to the poor sample qualities which make it difficult to lase at room temperature. Although photopumped lasing has been observed in ZnSe at room temperature (RT) in recent years with improved sample qualities,[14,15,52] the origin responsible for lasing at RT has

not yet been studied in detail, partially due to the lack of experimental data and the difficulty of generating tunable blue laser beams for excitation. In order to improve the lasing characteristics and eventually fabricate RT injection diode lasers, it is important to identify the mechanism responsible for room temperature lasing.

In this chapter, we present a detailed study of the photopumped stimulated emission process in ZnSe at RT. Samples used in this study include the ZnSe bulk as well as MBE epilayers. The properties of SE were studied under near resonant pumping with the excitation photon energy very close to the fundamental band gap of ZnSe. Tuning of the lasing temperature, as well as the pumping wavelength, is applied in this study. We show that the SE is due to inelastic exciton-free carrier scattering, the exciton-hole interaction being the dominant process.

Experimental Procedure

Two types of ZnSe samples were used in this experiment. The bulk samples were grown by the seeded physical vapor-phase transport (SPVT) technique. The SPVT technique can grow large single crystal ZnSe with a diameter as large as 5 cm uniformly without twinning. A large piece of SPVT ZnSe wafer was mechanically polished and then chemically etched using $NaOH/H_2O$ at a concentration of 14 molar at 90° C for 5 minutes to reduce the surface related effects. The final thickness of the wafer was 0.8 mm. Samples of size 5x5 mm^2 were manually cleaved from the wafer by using a razor blade. Other samples studied were MBE grown ZnSe on (100) GaAs substrates. The growth temperature of the MBE samples was 350^0 C. Two undoped

samples with layer thicknesses of 2.42 μm and 7.64 μm were used.

The samples were mounted on the cold finger of a closed cycle liquid helium refrigerator using vacuum grease. The sample temperatures were adjusted in the range of 10-400 K with this dewar. In this study, we used a doubled Nd-YAG laser (Quanta-Ray GCR-3)-pumped dye laser (Lambda Physik, FL3002) as the primary excitation source with a pulse width of 10 ns and repetition rate of 10 Hz. Several dyes were used to generate a broad range of pump wavelengths needed to study the effect of the pump photon energy on the stimulated emission. A frequency tracking doubler (Inrad, Autotracker II) was then used to double the near-infrared photon energy of the dye laser. The laser beam was focused on the sample surface using a quartz cylindrical lens to form a stripe. The laser light intensity were attenuated continuously using a variable neutral density filter, and the excitation power densities were measured by a pyroelectric power meter (Molectron, J4-05). The stimulated emission signal was collected from one cleaved facet of the sample and detected by a Spex 0.6 m triple-grating spectrometer in conjunction with a thermoelectrically cooled charge coupled device (CCD) (Princeton Instruments, ICCD 576LDG/RB). A photomultiplier tube (RCA) was also used to detect the emission signal and then fed to a boxcar averager (EG&G, 4402) triggered by the excitation laser pulses for time resolved emission profile measurements. This data acquisition system was interfaced to a personal computer. The experimental layout is shown in Fig. 1.

Pulse Dye Laser

Nd-YAG Laser
With Second Harmonic Generator (SHG)

SHG

SHG

Optical
Multichannel
Analyzer (OMA)

LHe (10K) Cryostat
with Sample Enclosed

Triple
Spectrometer

Cylindrical Lens

Collection Lens

Computer
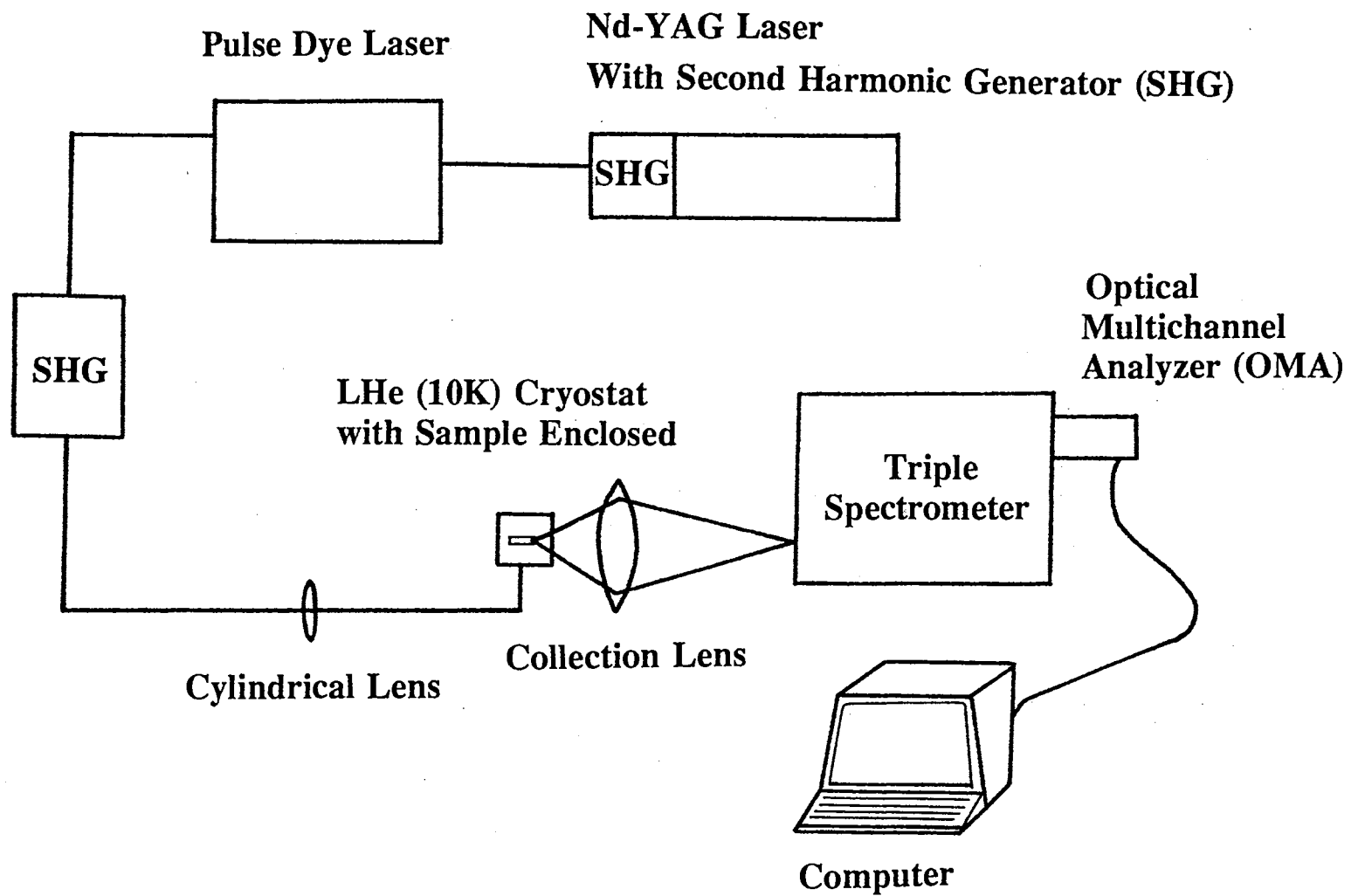
Figure 1. Side-pumping configuration.

Theoretical Background

The optical properties of highly excited direct gap II-VI semiconductors such as CdS, ZnO have been extensively studied.[54] The high external optical excitation induces electronic excitations such as excitons and excitonic molecules in these semiconductors. These electronic excitations, in turn, interact strongly with each other and/or with the excitation photon field. Transversal singlet excitons are strongly coupled to the light field. In order to simplify the Hamiltonian of the interacting field, Hopfield[55] first diagonalized the Hamiltonian of the interacting exciton-photon system by a linear transformation. By this transformation, one finds new quasiparticles, which are mixed exciton-photon states, called (excitonic) polaritons. This polariton concept is of great importance in the study of various recombination processes in dense excitonic systems. These scattering processes were first introduced in 1968 by Benoit a la Guillaume et al.[56] In these processes, one polariton is scattered from the exciton-like part of its dispersion curve into the lower energy photon-like part. A photon can then be emitted from the photon-like polariton in crystal. By conservation of energy and momentum, another particle is scattered into a higher energy state. This particle can be another exciton or a free carrier such as an electron or a hole. These processes, together with the recombination process of an exciton under simultaneous emission of M LO-phonons (M=1,2,...), have been fully treated quantum mechanically by deriving the rate equations describing the processes.[57,58] The gain spectra and the spectra of the spontaneous recombination for these processes can be obtained from the theory.[57,58]

The inelastic exciton-exciton scattering occurs preferentially at lower temperatures where the excitons are not thermally dissociated. At higher temperatures, exciton-free carrier interaction dominates where excitons and free carriers coexist. For the exciton-free carrier interaction, the maximum emission band shifts to lower energies with increasing lattice temperature faster than the band gap. These theoretical results have been compared with experimental results in II-VI compound materials such as CdS, ZnO, and ZnTe, where the theory was found to match the experimental data well.[58,59]

In the exciton-free carrier scattering process, the dominant free carriers are usually electrons. This is due to the smaller effective electron mass compared to holes. At a given temperature, the high energy states with smaller wavevectors are occupied due to thermal excitations for electrons. This will make the exciton-electron scattering process more probable in that the electrons near the bottom of a conduction band can be scattered into higher energy states. Exciton-electron scattering has been observed in most II-VI materials. In a p-type semiconductor, however, the exciton-hole scattering process can dominate due to the excess concentration of holes. This exciton-hole process has been observed in p-doped ZnTe.[58]

For ZnSe, the origins of SE has been investigated mainly at low temperatures (up to 100 K).[13,53] At low temperatures, the SE due to exciton-exciton scattering process dominates.[13,53] Along with this process, exciton-M LO phonon processes have been reported.[53] At room temperature, the spontaneous emission due to free exciton-free carrier interactions were reported by Era et al[60] and by Fan et al.[61] Similar results were reported for the RT blue electroluminescence in forward-biased ZnSe diodes.[62]

In the exciton-free carrier scattering process, the polariton with momentum **K** is scattered from the exciton-like part of the dispersion curve to the photon-like part and transmits the whole momentum to the free carrier, which is scattered from **k** to **k'**. Energy and momentum conservation give

$$E_0 + \frac{h^2 K^2}{2M} + E_G + \frac{h^2 k^2}{2m} = h\nu + E_G + \frac{h^2 k'^2}{2m} \tag{III.1}$$

$$K + k = k' \tag{III.2}$$

where E_0 is the energy of exciton at K=0, E_G is the energy of the band gap, M is the exciton mass, m is the free carrier mass, and $h\nu$ is the photon energy. Fig. 2 shows the schematic representation of an exciton-electron scattering process. In the calculation it is necessary to know the distribution of the excitons and carriers in their momentum space. Boltzmann distribution is assumed for both systems. Integration over all possible exciton-carrier configurations results in[70]

$$S(h\nu) = \int \exp\left(-\frac{h^2 K^2}{2M k_B T}\right) I(h\nu, K, T) d^3 K \tag{III.3}$$

with

$$I(h\nu, K, T) = \int \exp\left(-\frac{h^2 K^2}{2m k_B T}\right) \delta [E_0 - h\nu + \frac{h^2 K^2}{2}(\frac{1}{M} - \frac{1}{m}) - \frac{h^2 K \cdot k}{m}] d^3 k \tag{III.4}$$

These integrals can be solved after variable substitution by a Laplace transformation. This gives
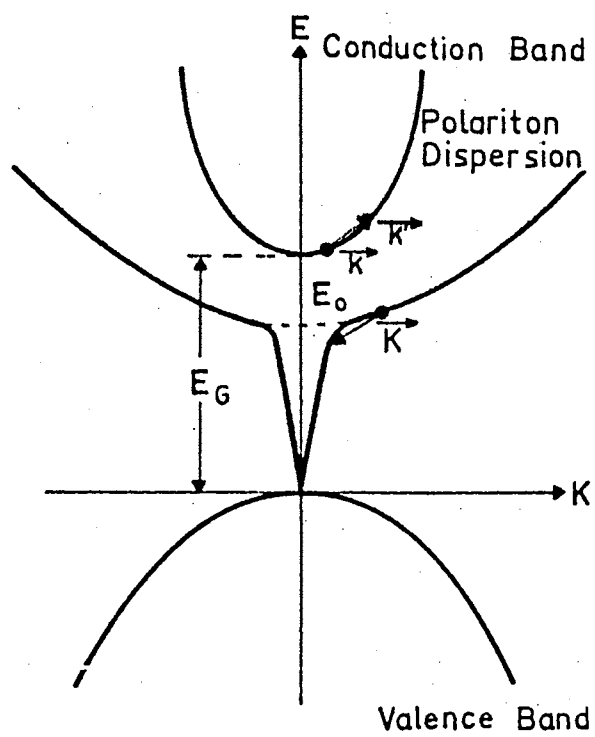
Figure 2. Exciton-electron scattering process.

$$S(hv) = \frac{1}{2}\pi(\frac{m^2}{\beta})\exp(A\beta x)BxK_1(C\beta x)$$

(III.5)

where $A=(M-m)/2M$, $B=2/h^2(M+m)$, $C=(M+m)/2M$, $\beta=1/k_bT$, $x=E_0-hv$, K_1 being the modified Bessel function. The maxima of the emission can be determined by differentiation of $S(hv)$ which gives the transcendental equation

$$\frac{1}{x}+A\beta+\frac{1}{K_1}\frac{dK_1(\beta Cx)}{d(\beta Cx)}\beta C=0$$

(III.6)

With recursion formulae for the modified Bessel functions we can simplify this equation to

$$\frac{A}{C}=\frac{K_0(\beta Cx)}{K_1(\beta Cx)}$$

(III.7)

From the above equation we can solve numerically for x, which in turn gives the peak energy as a function of temperature. Experimental results will be compared to the above equation to determine the type of free carriers involved in the scattering process.

Results

Shown in Fig. 3 are room temperature stimulated emission spectra of SPVT ZnSe taken with the pumping wavelength of 460 nm (2.695 eV) at several different excitation power densities. Under low excitation, the spectrum is characterized by a broad emission band located around 2.61 eV, which is presumably related to the emission from impurities introduced into the sample during the crystal growth process.
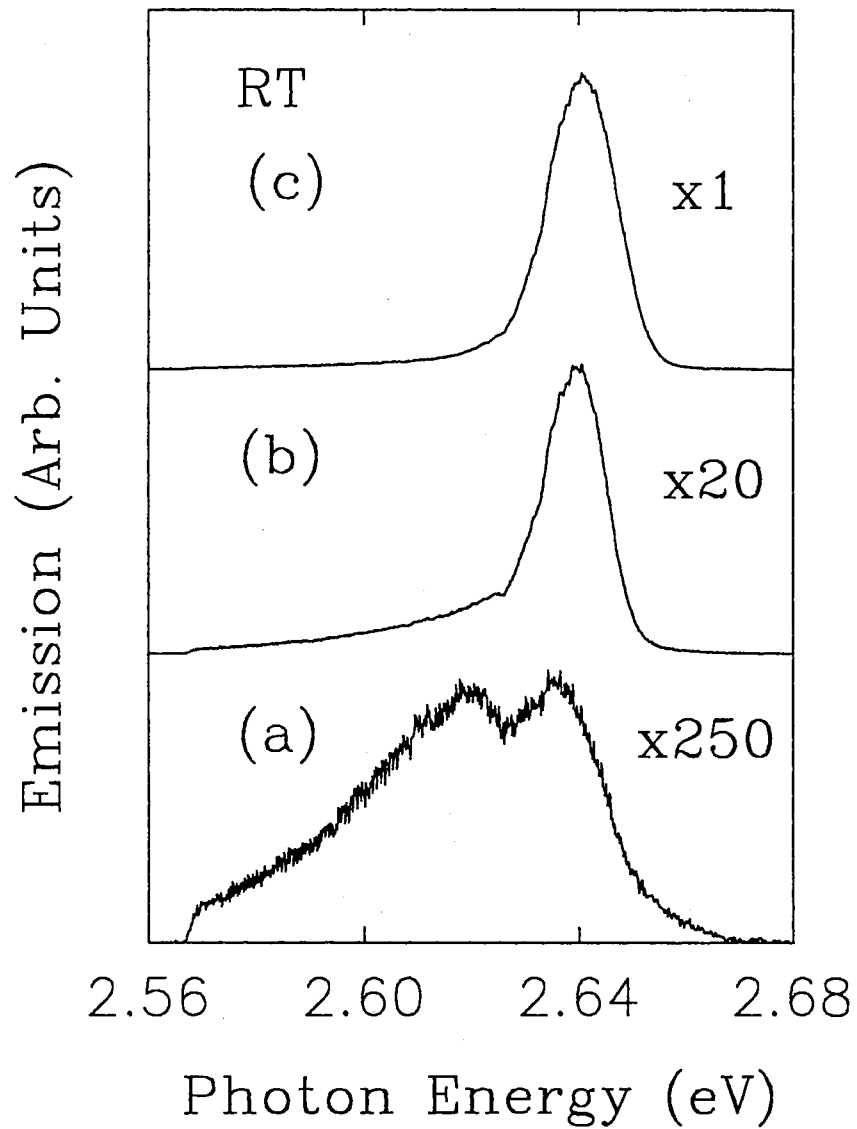
Figure 3. Typical emission spectra from a SPVT ZnSe sample pumped at 460 nm with pump power densities of (a) $0.9I_{th}$, (b) $1.2I_{th}$, and (c) $1.8I_{th}$. The threshold pump power density I_{th} was determined to be 60 kW/cm^2.

With increasing excitation power densities, a second emission band peaked at 2.64 eV appears, as shown in Fig. 3(a). The intensity of this emission band increases superlinearly and becomes predominant and much sharpened, as seen in Figs. 3(b) and (c). The full width at half maximum (FWHM) of this spectral feature is about 12 meV. Fig. 4 shows a plot of the intensity of this high energy emission band as a function of the pumping power density. The sharp rising of the curve defines the stimulated emission threshold and gives a value of ~60 kW/cm^2. The low energy emission band is suppressed at high pumping powers. This spectral narrowing as well as the sharp rising of the emission intensity versus pumping power density curve implies that the high energy emission band is caused by stimulated recombination.

Similar results were observed in MBE samples. The stimulated emission spectra for a 2.42 µm thick sample are shown in Fig. 5(a) at the onset of stimulated emission and in Fig. 5(b) above the stimulated emission threshold. Note that when the pumping power density increases by a factor of less than 1.5, the emission intensity increases by a factor of more than 20. Fig. 6 shows the emission intensity versus pumping power density curve, which gives a stimulated emission threshold of ~45 kW/cm^2, comparable to that of SPVT samples.

Under close scrutiny, one finds that the stimulated emission peak positions of SPVT and MBE samples are not coincident under the same pumping power densities. The SPVT samples have a higher emission peak energy. Fig. 7 shows a comparison of emission spectra for two different samples under the same pump power density of ~125 kW/cm^2. It can be seen that the emission peak energy of the SPVT sample is
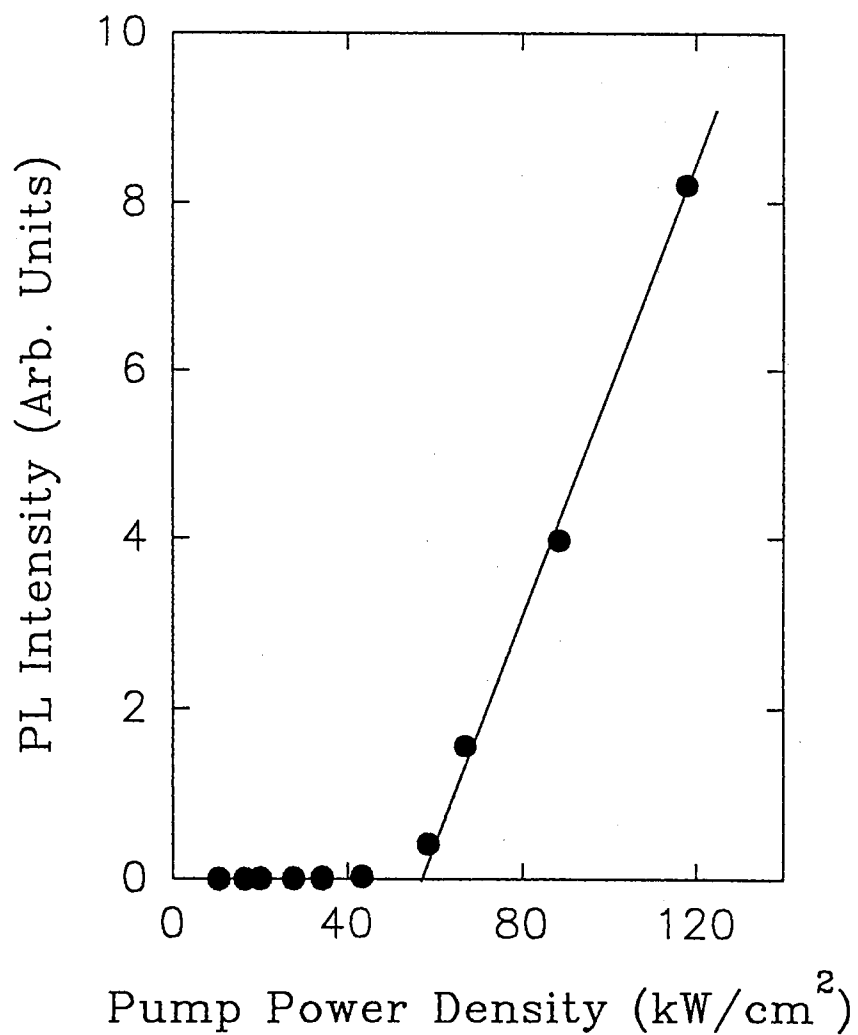
Figure 4. Emission output versus optical pumping power densities for the sample in Fig. 3. The vertical axis is linear in intensity. The dots are data points and the line is a guide to the eye.
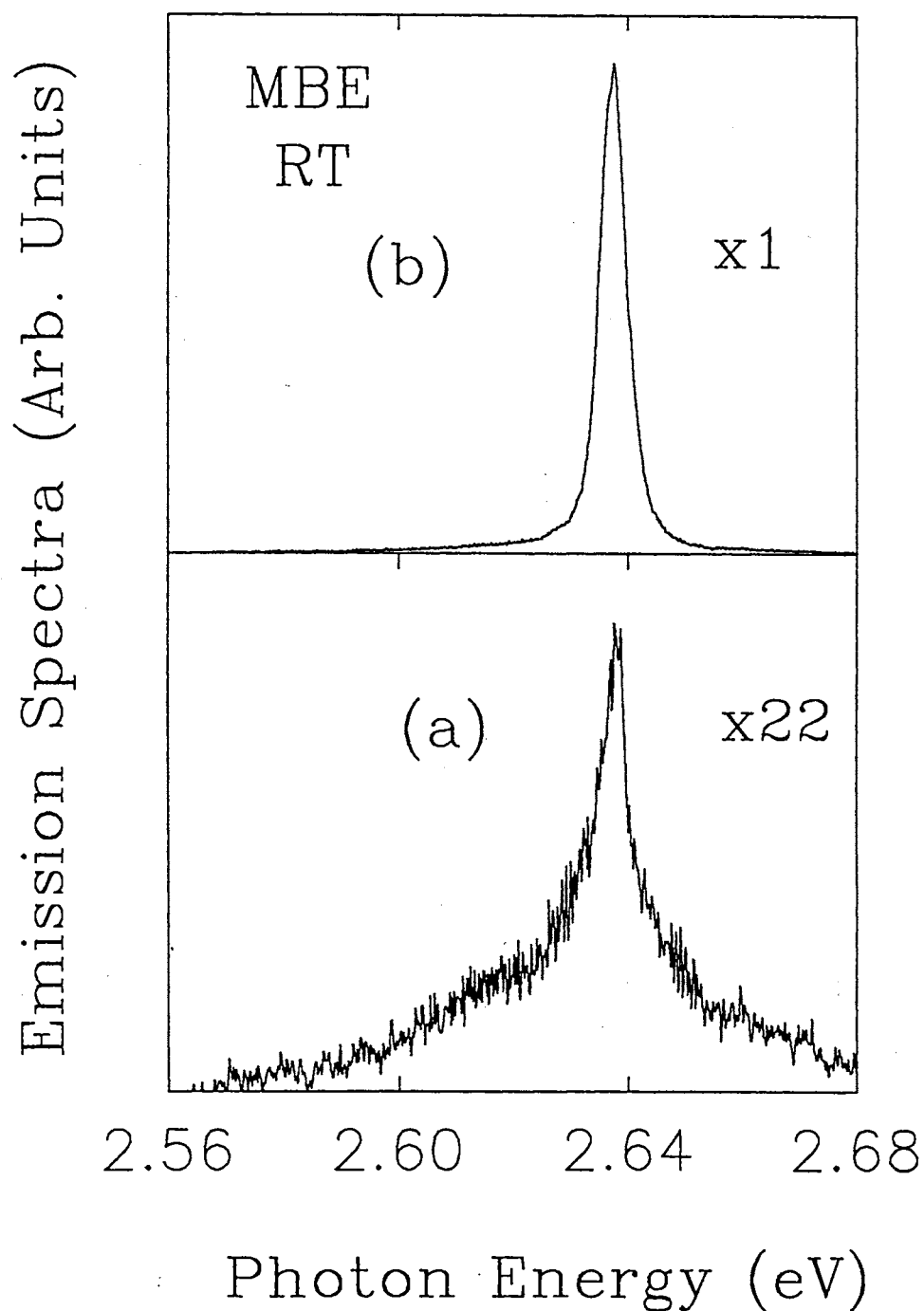
Figure 5. Stimulated emission spectra from a 2.42 μm thick MBE sample pumped at 460 nm with power densities of (a) 36 kW/cm², and (b) 50 kW/cm².
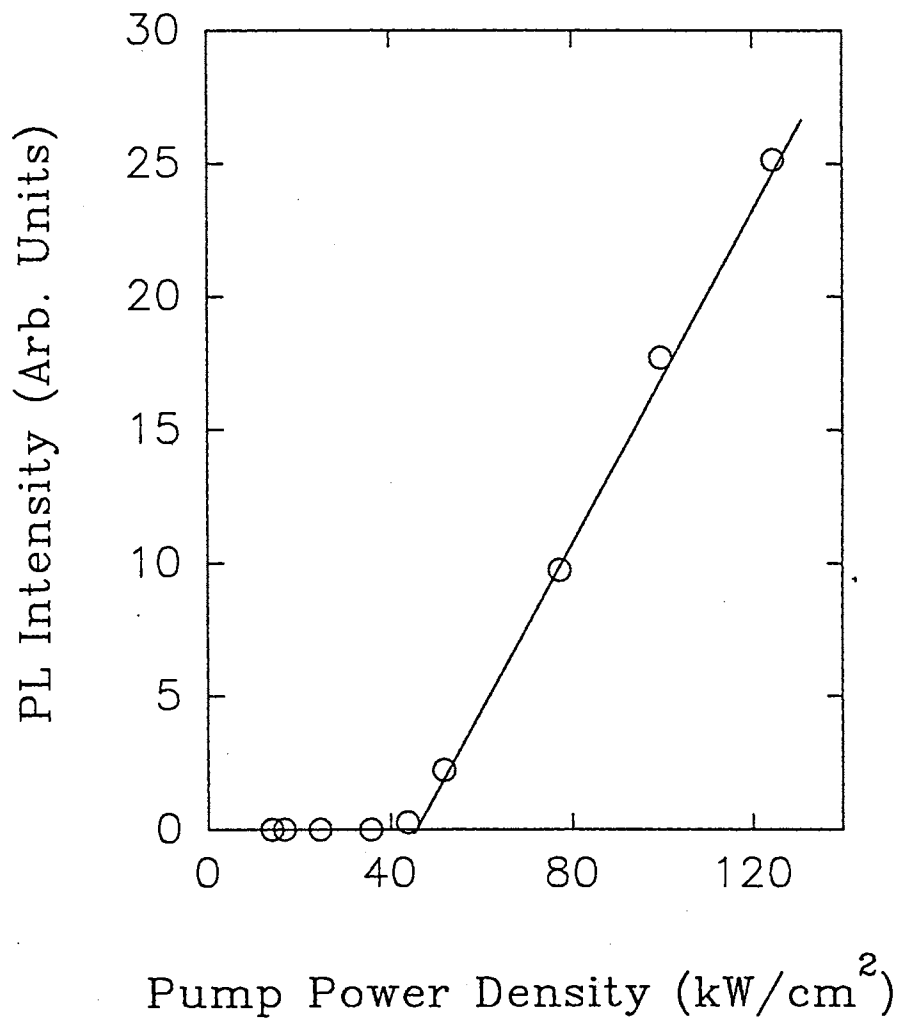
Figure 6. Emission output versus pumping power densities for the MBE sample in Fig. 5. The vertical axis is linear in intensity. The dots are data points and the line is a guide to the eye.
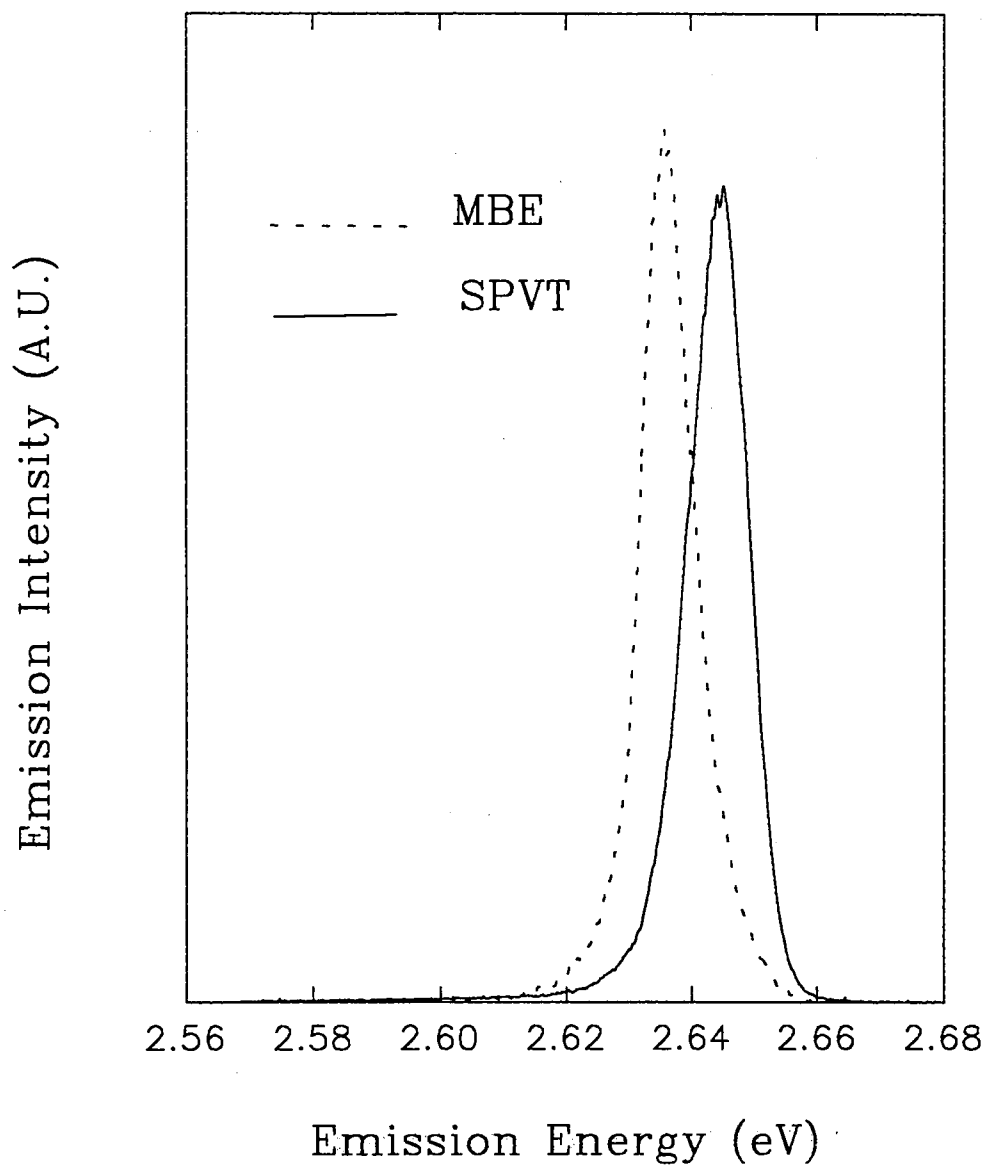
Figure 7. Comparison of emission spectra for MBE and SPVT samples pumped at 460 nm under similar pump power densities. The thickness of the MBE sample is 2.42 µm.

about 6 meV above the peak of the MBE emission band. This energy difference may be ultimately related to the effects due to the growth technique difference. The two growth techniques can introduce different impurity species with different densities into the samples. The impurities will modify the conduction band and valence band structures and will affect the recombination wavelength as well. Another possible contribution to the energy difference is the strain effect on MBE sample. The strain effect on thick ZnSe/GaAs films has been studied extensively.[63-65] ZnSe has a larger lattice constant than GaAs. The coherently grown layers of ZnSe on GaAs will suffer a biaxial compressive strain by adopting the GaAs lattice constant in the plane perpendicular to the growth direction. As the thicker layers were grown, misfit dislocations are induced, which will gradually relax the ZnSe to its bulk lattice structure. However, due to the difference in the thermal expansion coefficient between ZnSe (6.8×10^{-6} K^{-1})and GaAs (5.6×10^{-6} K^{-1}), the relaxed thick layers (> 1μm) at growth temperature will be under biaxial tensile strain once the sample is cooled down to room temperature. As a result, the thick ZnSe/GaAs epilayers will suffer a biaxial tensile strain, and the resulting strain will affect the band structure of ZnSe, i.e. lifting the degeneracy of valence band by splitting the heavy- and light-hole band at Γ point and shrinking the band gap. It is noted that the energy shift of the heavy hole branch of the valence bands caused by strain is smaller than that of the light hole branch. In the case of biaxial tensile strain, the separation between the light-hole band and the lowest conduction band gives the minimum band gap energy. Ohkawa et al[64] treated this subject and found an emission peak energy shift to lower energy by as much as 5

meV from bulk to strained epilayers at low temperature (12 K). This energy shift is expected to be smaller at room temperature. In our case, an energy shift of 6 meV is observed in SE. Such a large value could be due to an enhancement of the energy shift in the stimulated emission process, as will be discussed in the discussion section.

We have also performed time-resolved photoluminescence measurements to trace the temporal profiles of the excitation pulse, the photoluminescence under low excitation power density (low energy emission band), and the emission under high excitation power density (SE band). The results are shown in Fig. 8 for a SPVT sample. It is evident that the higher energy emission band observed under high excitation power has a temporally narrowed profile. Notice that this narrowed pulse may have a much shorter width, possibly in the sub-nanosecond region, which can not be resolved with our apparatus. The pulse width under low excitation is longer than the excitation pulse width. This temporal narrowing is typical of the behavior of time-resolved SE.

Stimulated emission was observed up to 400 K. The light output versus pumping power density characteristics at different temperatures are shown in Fig. 9. The SE wavelength increased from 470.01 nm at 293 K to 478.42 nm at 400 K. At all temperatures there was clear evidence of SE above the threshold pumping power density, at which the slope of the output intensity rises sharply. It is noted that differential quantum efficiency does not change appreciably although the threshold changes substantially from ~50 kW/cm^2 at 293 K to 150 kW/cm^2 at 400 K. Above room temperature, SE has been previously observed in ZnSSe/ZnSe heterostructures,[37]
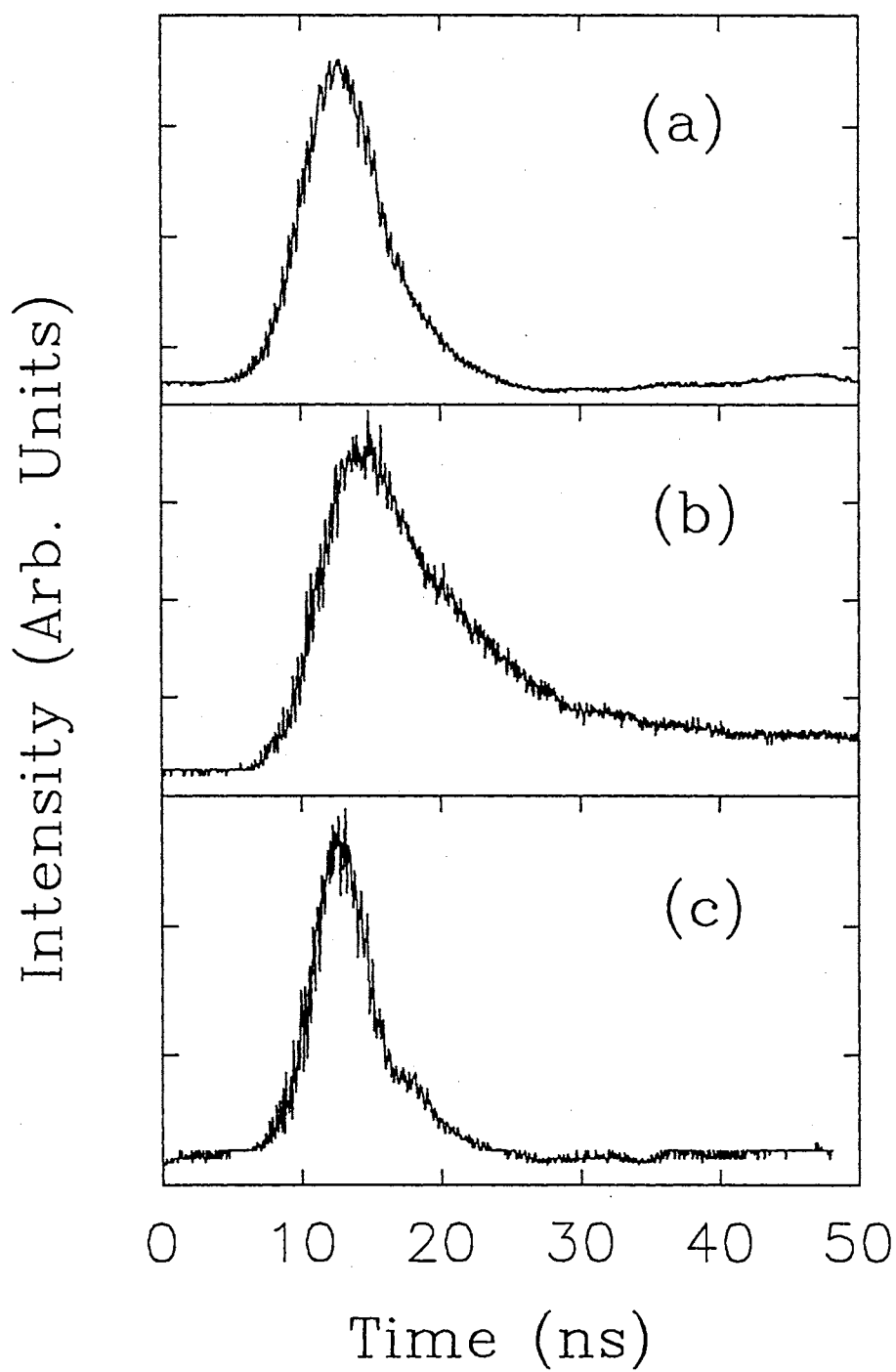
Figure 8. The comparison of temporal profiles of the excitation pulse (top), spontaneous emission (middle), and stimulated emission (bottom) from a SPVT sample at room temperature. The zero point of time is arbitrary.
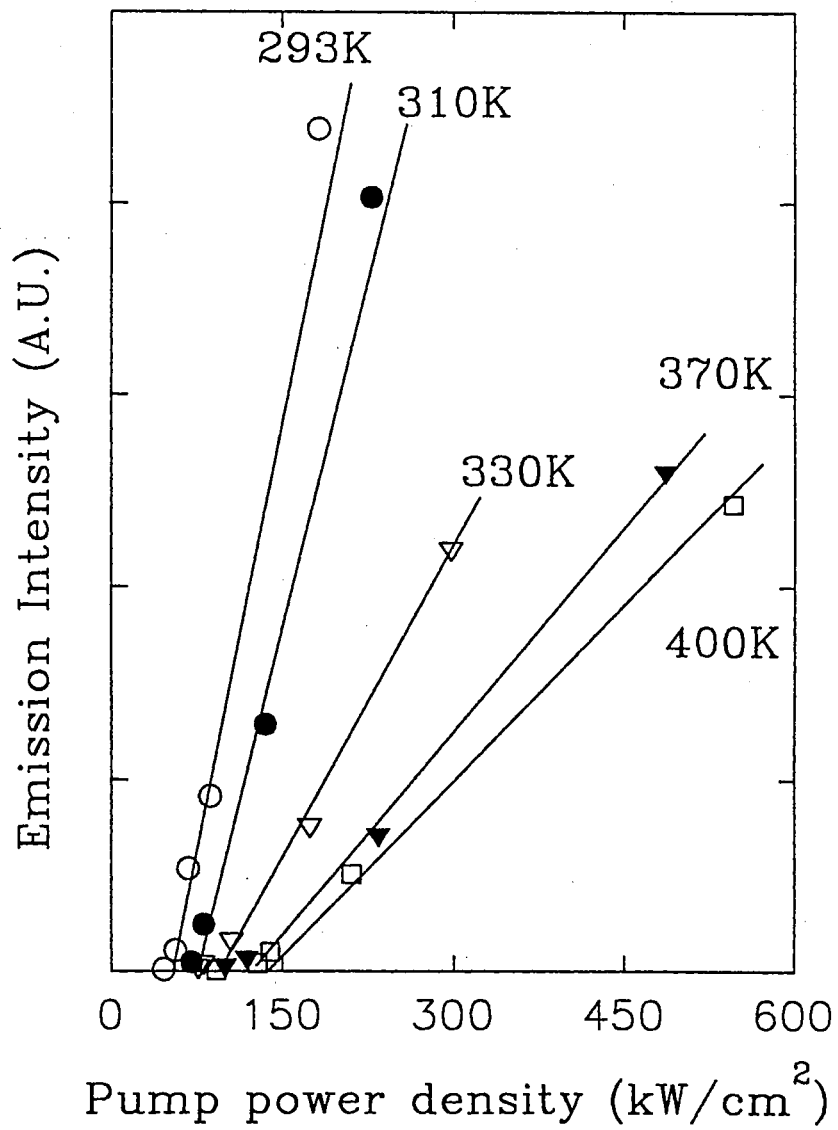
Figure 9. Emission output versus pumping power density at different temperatures for a SPVT sample. The lines are guides to the eye.

as well as in ZnCdSe/ZnSSe MQW structures.[39]

Another interesting result in this study is the dependence of the stimulated emission peak energy on the excitation photon wavelength. The energy position of the SE peak shifts monotonically to lower energy by about 8 meV as the pumping wavelength is tuned from 455 nm to 460 nm while keeping the excitation power density constant. This behavior is shown in Fig. 10 for a SPVT sample. This effect was also observed in ZnS_xSe_{1-x} alloys.[66] This implies that the lasing is not likely to occur via some extrinsic recombination channels such as native impurity bound excitons, shallow donor or acceptor levels since their energy levels should be independent of the excitation photon energy. The lasing is most likely of intrinsic origin.

We have also performed the so-called off-band-edge pumping, i.e., using an excitation photon with energy much higher than the ZnSe band gap, by using a tripled YAG laser output at 355 nm (~3.49 eV) and a doubled dye laser at 408 nm (~3.04 eV). Only spontaneous recombination spectral features could be observed at RT under pumping power densities equal to or higher than the power densities used with near resonant pumping. This may be due to the competition of the non-radiative recombination near the sample surface with the stimulated recombination; with the excitation photon energy tuned far above the band gap, the penetration depth of the light is very short due to the large absorption coefficient of the sample and the scattering losses due to many body effects.[53] As a result, the photo-excited carriers are concentrated near the surface where the surface related recombination centers may
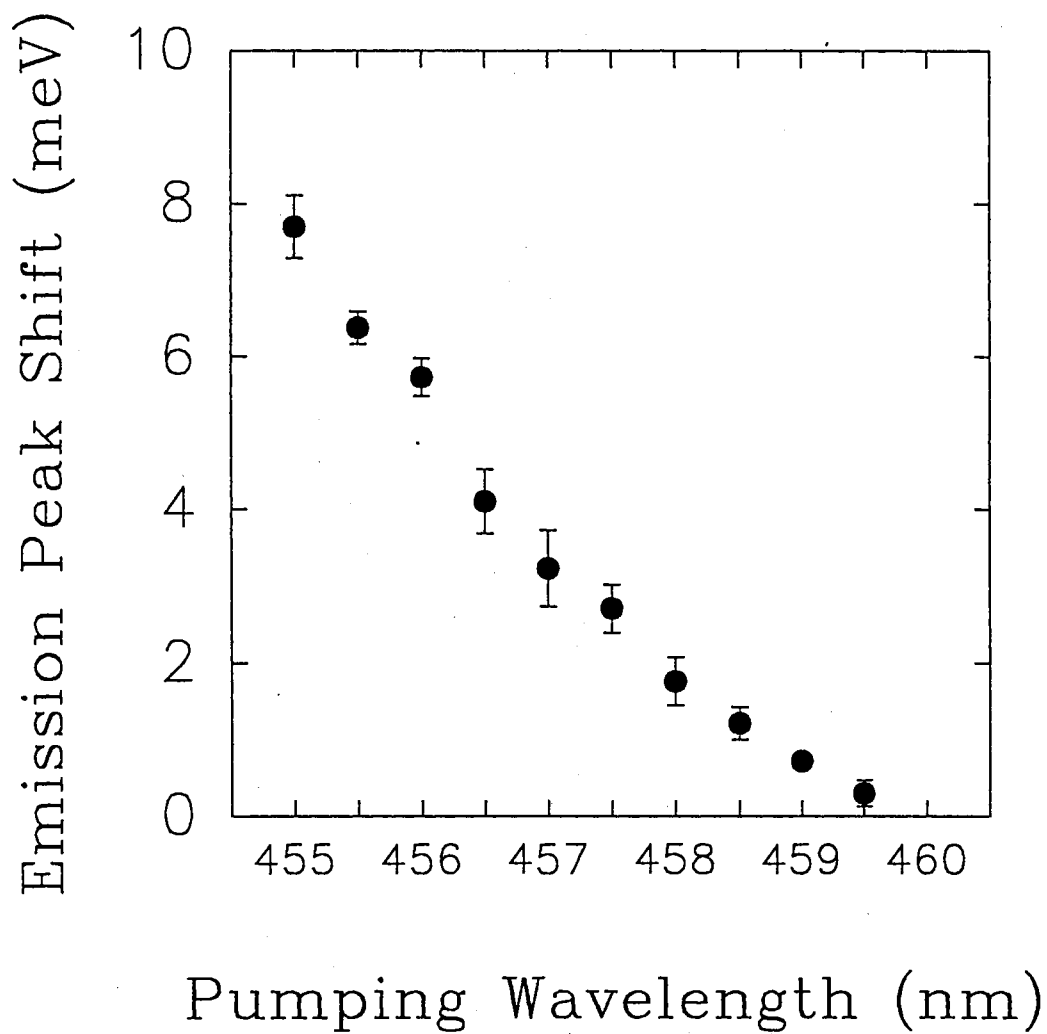
Figure 10. The dependence of the stimulated emission peak energy on the pumping wavelength. The stimulated emission blue shifts about 8 meV with the pumping wavelength change from 460 nm to 455 nm.

compete strongly with the stimulated emission process. This results in a high SE

threshold which makes it difficult to observe SE at RT. Another contribution to the

high SE threshold is the thermal effect caused by the pump photons with energy much

higher than the band gap. On the other hand, if excitation photon energy is tuned very

close to the band gap, the light penetration depth increases and thermal effect

decreases, resulting in a much reduced SE threshold.

Discussion

In the present study, we propose that the SE of ZnSe at RT is due to exciton-

free carrier scattering processes by examining different possible processes and by

calculating the emission energy position.

From the experimental results above we have excluded the possibility of

extrinsic origin of SE at RT. The SE should be due to intrinsic effects. The electron-

hole plasma (EHP) effect can be excluded since the thresholds for our samples, when

converted to an exciton density, are estimated to be lower than the Mott critical

density for ZnSe (5×10^{17} cm^{-3}).[67] In addition, the narrowness of the SE lines (FWHM

of ~7 meV for MBE samples) indicates that EHP is not involved in this process which

would otherwise show much broader emission lines (up to 50 meV).[68] Furthermore, we

have tuned the pumping photon energy below the band gap of ZnSe at RT and have

found the SE characteristics virtually unchanged. Such near band gap pumping is less

likely to produce an EHP.[13]

There are three possible excitonic scattering processes which will give a

positive gain: exciton-exciton, exciton-free carrier, and exciton-M LO phonon processes. The exciton-M LO phonon process will usually have a positive gain at low temperatures where there are not many thermal phonons which would otherwise enhance the absorption process. This process has a large probability when large volumes are excited, e.g. by two-photon pumping. In the present case, we can exclude this mechanism as contributing significantly.

Comparing exciton-free carrier and exciton-exciton processes, the scattering cross-section of exciton-free carrier interaction is considerably larger than that of exciton-exciton process, since the former is of charge-dipole type while the latter is of dipole-dipole type process. This was verified by the observation of exciton-free carrier interaction at very low temperatures where the number of free carriers is much smaller than that of excitons.[69] Exciton-exciton scattering processes usually occur at low temperatures where there is a higher density of free excitons than free carriers.

At room temperature, we can exclude the exciton-exciton interaction by the following argument about the emission peak energy. The energy gap of ZnSe at RT is 2.673 eV, as verified by photoreflectance measurements.[16] Assuming that the exciton binding energy is the same at RT and at low temperature (21 meV), this will give a free exciton energy of 2.652 eV. The SE peak observed has an energy of 2.64 eV when pumped at 460 nm. The energy difference between the free exciton and SE peak is about 12 meV. Notice that part of this energy shift is caused by pumping wavelength variation, i.e. with higher pump photon energy, the emission peak will shift to higher energy, as demonstrated in Fig. 10. This energy difference is much

smaller than the exciton binding energy. Saito et al[69] has shown that in the exciton-exciton scattering process, one exciton is scattered to the bound excitonic state n=2 at low temperature (for ZnSe, T=40 K). At higher temperatures, the scattering to the continuum state would become dominant. At RT, even if we only consider the case of excitons being scattered into n=2 states, an energy difference of 15 meV should be derived. If the exciton's kinetic energy is taken into consideration, a value greater than 15 meV should result. This energy discrepancy between experimental results and theoretical estimation clearly excludes the exciton-exciton scattering process as being responsible for SE of ZnSe at RT.

The only mechanism left is exciton-free carrier interaction. In order to verify that this is indeed the process which occurs at RT and also to determine the type of carriers (electron or hole) dominating in the process, we calculated the SE peak position using the method developed by Fischer et al.[70] In this calculation, energy and momentum conservations are satisfied. Also, the Boltzmann distribution for both excitons and free carriers in their momentum space is assumed. The equation determining the peak energy is derived from Eq. (III.7)

$$\frac{(M-m)}{(M+m)} = \frac{K_0(\beta Cx)}{K_1(\beta Cx)} \tag{III.8}$$

For ZnSe, $M=(m_e+m_h)=0.17+0.6=0.77$, in units of the free electron mass. We then obtain $h\nu=E_0-1.18k_bT$ for exciton-electron interaction, and $h\nu=E_0-0.04k_bT$ for exciton-hole interaction. At RT, $k_bT=25.9$ meV, so $E_0-h\nu=30.6$ meV for electrons, and 1.04

meV, for holes, respectively. When pumped at 460 nm, the energy difference between the SE peak and free exciton is about 12 meV. When the pumping wavelength is tuned into 455 nm, this energy difference becomes ~4 meV. The exciton-hole interaction gives a value closer to the experimental value. Based on this estimation, we propose that the SE of ZnSe at RT is due to exciton-free carrier interactions, the exciton-hole process being the dominant process. The exciton-hole scattering mechanism is sketched in Fig. 11. This is consistent with a report by Maier et al,[71] in which the RT spontaneous emission of high-resistivity ZnSe samples at high excitations is ascribed to exciton-free carrier scattering, with the exciton-hole interaction being dominant. The reason that exciton-hole scattering rather than exciton-electron scattering is dominant in ZnSe is not clear at this point.

In order to verify the dominance of the exciton-hole scattering process, we plotted the temperature dependence of the SE peak energy position near RT for a SPVT sample in Fig. 12. The pump power densities were kept constant. Also shown in Fig. 12(a) is the energy gap of ZnSe obtained using the formula given by Shirakawa et al.[72] We can see that the SE peak almost follows the gap. This is consistent with the predictions of the exciton-hole process that the energy difference between free exciton and SE peak should be insensitive to temperature. Under closer scrutiny, we found that the SE peak actually shifts to lower energy with increasing temperature slower than that of the band gap. Fig. 12(b) plots the temperature dependence of energy difference between the gap and the SE peak. The energy difference at 400 K was arbitrarily chosen to be zero. We can see that the energy difference decreases as
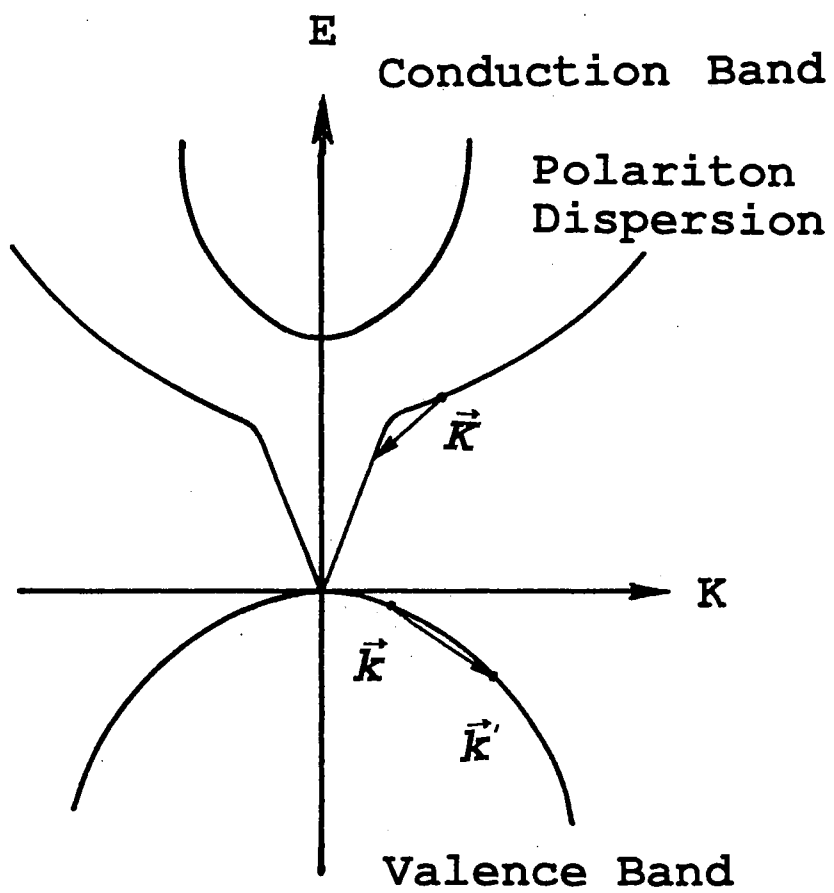
Figure 11. Schematic representation of the exciton-hole scattering process.
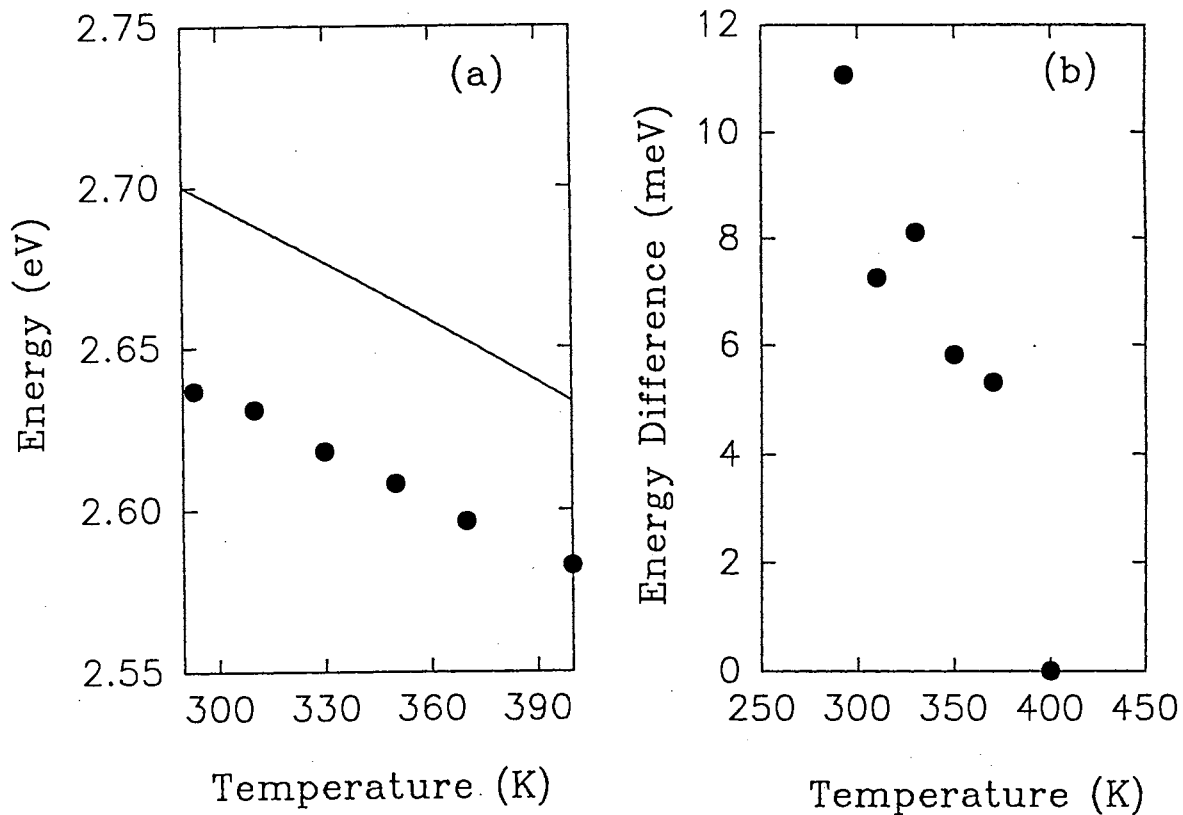
Figure 12. (a) Stimulated emission peak energy versus temperature near room
temperature for a SPVT sample. The line is the energy gap given
by the formula from Ref. 31. (b) Temperature dependence of the
difference between the band gap energy and stimulated emission
peak.

temperature increases. This can be explained as being due to the influence of the pump wavelength. As the temperature increases, the energy difference between the excitation and the band gap increases. This increase will increase the emission energy due to the wavelength dependence effect which we described above. This once again supports our proposal that exciton-hole interaction is the dominant process.

The emission peak difference between the ZnSe/GaAs epilayer and the bulk samples can also be accounted for by the exciton-hole interaction. The in-plane tensile strain in the epilayer samples will shift the light hole band above the heavy hole band.[64] Thus the holes will be populated in the light hole band instead of heavy hole band upon near resonant excitation. Light holes will be scattered rather than heavy holes. Due to the small effective mass of the light hole, the dispersion is relatively large. When a polariton is scattered from the exciton-like polariton branch to the photon-like branch with a certain momentum change, more energy will be transferred to light holes compared to that for a heavy hole scattering case, resulting in a larger energy decrease of emission photons. In this way, the strain effect manifests itself by the energy gap reduction, as well as larger dispersion of the free carriers.

The effect of pumping wavelength on the SE peak energy is not totally understood at this point. The change of pumping photon's energy should not affect the distribution of excitons and free carriers at thermal equilibrium. The pumping wavelength dependent effect may ultimately be related to the interaction (relaxation) mechanisms of the exciton-polariton dispersion near the bottleneck region. The emission peak shift of the transverse exciton throughout the bottleneck region in

response to the variation of pumping energy was reported in CdS.[73]

Summary

In summary, we have described stimulated emission from ZnSe bulk as well as MBE epilayers at temperatures up to 400 K. The SE peak energy of MBE samples are lower than that from a bulk sample. One possible cause of this energy difference is the in-plane tensile strain in the thick MBE epilayers due to the difference in the thermal expansion coefficients between ZnSe and GaAs. This tensile strain then reduces the band gap of the MBE sample. The importance of pumping wavelength selection was demonstrated by using the near resonant or off resonant pumping. The SE can only be observed with near resonant pumping. This is explained as being primarily due to the elimination of competition from surface-related recombination and thermal effect of pump photons. A peak shift of SE is observed by the pumping wavelength tuning. Different possible physical origins were examined, and the origin of SE at RT was proposed to be the exciton-free carrier scattering, the exciton-hole interaction being the dominant process.

CHAPTER IV

PHOTOPUMPED LASING OF ZnSe AND ZnSSe SAMPLES

AT ROOM TEMPERATURE

Introduction

In recent years the wide-band-gap II-VI compounds have attracted much

attention for their technological importance appropriate for optoelectronic

applications.[74,75] ZnSe is one of those most extensively studied materials duo to its

zinc-blende structure with a band gap ~2.7 eV at room temperature corresponding to a

spontaneous emission band peaked at the wavelength around 465 nm. Optical pumping

(band-to-band excitation) techniques, in particular by using pulsed lasers, are widely

used to investigate the lasing properties of ZnSe bulk and epilayers and the physical

dynamics involved in the lasing process. So far most of such work has been done

below 200K rather than at room temperature.[10,11,13,33,48] We have previously observed

stimulated emission from ZnSe and Zmudzinski and co-workers have reported the

observation of laser emission of a resonator with reflective coatings on the sample

surface[14] at room temperature. Such observation of room temperature laser emission is

important for development of a practical blue-light laser system. In both studies the

excitation photon energies were chosen to be very close to the ZnSe band gap to result

in an enhancement of the carrier generation rate.

Although room temperature photopumped lasing has been observed in both ZnSe bulk[14] and epilayers,[52] as well as ZnSe-ZnS$_{0.06}$Se$_{0.94}$ double heterostructures (DH)[17] using an excitation photon energy very close to the band gap energy, one of the problems associated with the epilayers grown on a GaAs substrate is the lattice mismatch between the ZnSe epilayer and the GaAs substrate. This can cause the presence of misfit dislocations when the epilayer is thicker than the critical thickness of ~1500Å which would adversely affect both device performance and operation lifetime.[18] As a result, the epilayer samples should be restricted to a layer thickness of less than 1500Å. But for photopumped lasing studies, the penetration depth of the light is usually larger than 1500Å, especially in the case of the near band gap pumping. Thus the active gain volume for ZnSe grown on GaAs is limited by the critical length, resulting in a high lasing threshold.[52] In order to improve the electronic and optical confinement, a DH structure was used in Ref. 17. However, since the total band-gap energy difference between ZnSe and ZnS$_{0.06}$Se$_{0.94}$ is only ~36 meV and most of this difference is taken up in the valence band offset, the electron confinement is very poor (This is true in general for any ZnSe-ZnS$_x$Se$_{1-x}$ system, 0<x<1).[17] Also, the optical confinement is very poor due to the small index of refraction difference in this system (less than 1%). New sample structures with different combinations of binary and ternary systems are needed to optimize the lasing properties.

While various superlattice structures have been lased with some successes, there have not been many photopumped lasing studies on the ZnS$_x$Se$_{1-x}$ alloys. Along with ZnSe, other properties of ZnS$_x$Se$_{1-x}$ alloys have been extensively studied.[76-79] Due

to the lattice match between ZnS_xSe_{1-x} (with $x\sim 5\text{-}6\%$) and GaAs, the photoluminescence (PL) efficiency from lattice matched ZnS_xSe_{1-x} samples is at least one order of magnitude larger than that from ZnSe films,[77,80] indicating the high quality of the sample with less non-radiative recombination due to the misfit dislocations. Thus, ZnS_xSe_{1-x} can be an alternative in blue optoelectronic applications.

In this chapter, we report new experimental results on the optically pumped lasing of bulk and epilayer ZnSe at room temperature after our previous observation of room temperature stimulated emission of ZnSe samples. We also report the first observation of room-temperature photopumped lasing in bulk $ZnS_{0.05}Se_{0.95}$ alloy samples. We have succeeded in making ZnSe and ZnSSe laser with significantly low threshold intensity of pumping power density (7 kW/cm^2 for ZnSe) without high reflective coating on the sample edge facets. A few longitudinal cavity modes could be well resolved from the room temperature laser emission spectra. To our knowledge, this is the best experimental evidence of room temperature optically pumped lasing of bulk ZnSe ever observed.

Sample Preparation

The ZnSe and ZnSSe bulk materials used in this work were strain free single crystals grown by the SPVT technique. Large pieces of (111) oriented SPVT ZnSe and $ZnS_{0.05}Se$ wafer were mechanically polished and chemically etched with 0.5% bromine/methanol for 5 min to reduce the thickness and surface roughness, then were manually cleaved to small pieces of bar-like sample edge facets. The cleaved sample

bars were attached to a copper mount with Ni/Au plating by master bond thermal epoxy with an aluminum nitride filler so as to let the cleaved faces of the bar be positioned horizontally and the pump face be illuminated from the top. Eleven laser bar samples were made from ZnSe and 10 samples were made from ZnSSe. The cavity lengths were ranging between 200 μm to 400 μm. The thickness of the sample was about 100 μm and the length, about 1.27 mm. For MBE grown ZnSe/GaAs epilayer samples, the GaAs substrate was first polished to make it easier to cleave. Eight laser bar samples with cavity lengths ranging from 200 μm to 500 μm were made from a sample with an epilayer thickness of 2.4 μm. The samples were mounted on a sapphire plate by the 5 minutes epoxy to reduce the thermal heating effect. The experimental setup used is the same as that described in Chapter III.

Lasing from Bulk and MBE ZnSe

Under the condition of high-excitation power densities with the pumping beam wavelength tuned close to the room temperature band gap of ZnSe, the output of the laser emission from ZnSe bar-like sample was extremely strong and the laser light was found to have a polarization along the direction of the bar. Blue laser emission from the ZnSe samples is visible to the naked eye. In Fig. 13 we show typical laser emission spectra taken from two SPVT ZnSe samples with resonator lengths 0.376 mm (sample lot number C-3) and 0.302 mm (B-3), respectively, pumped at 460 nm wavelength with about 10-11 kW/cm^2 pumping power density. The spectra are characterized by sharp, narrow line shapes consisting of a few spectrally spaced
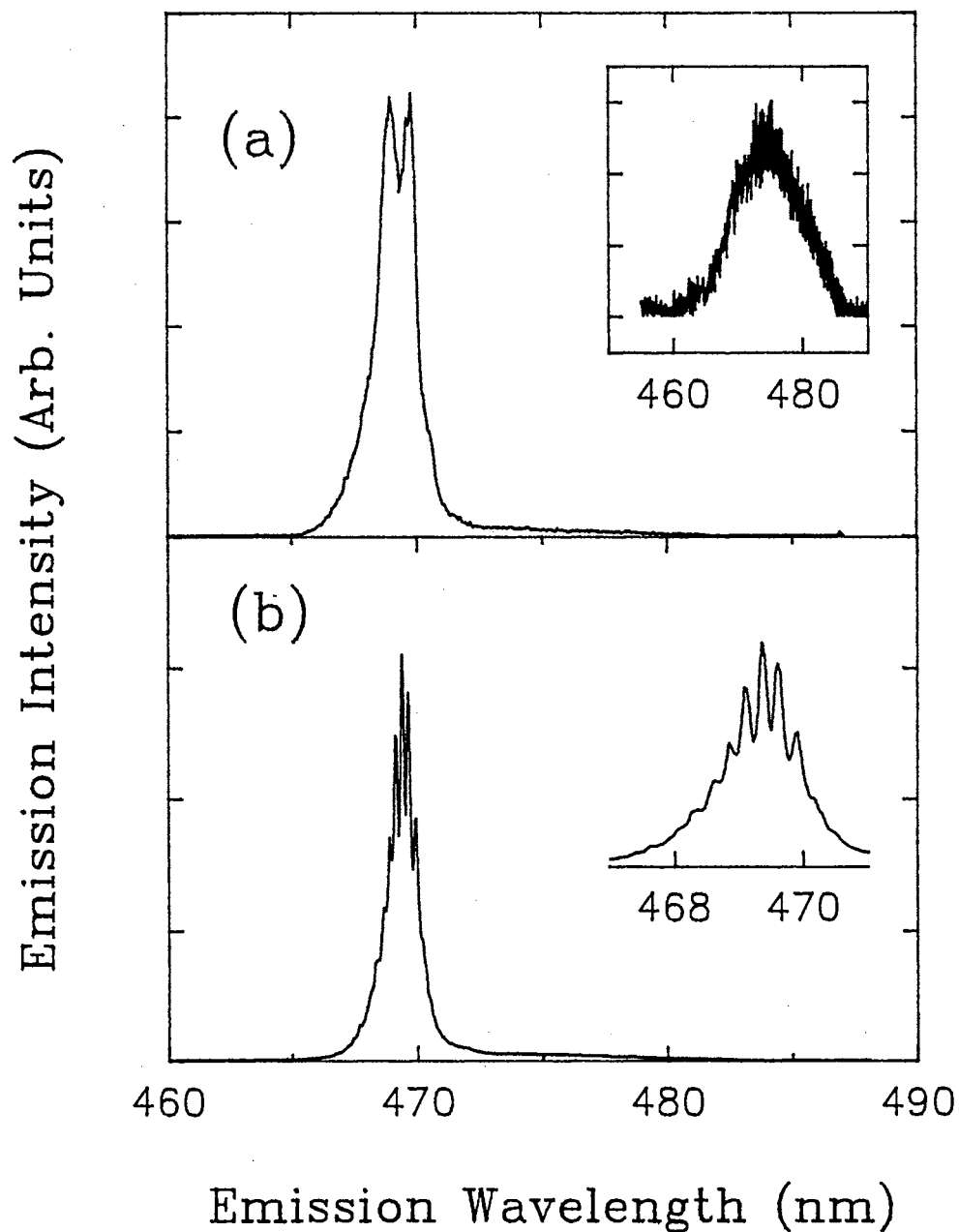
Figure 13. Typical lasing spectra taken from two ZnSe samples (C-3 and B-3)
pumped at 460 nm wavelength. Fabry-Perot interference fringes are
well observable. (a) Sample C-3, cavity length is 0.376 mm,
pumping power density 10.5 kW/cm². The inset shows the line shape
of the spontaneous emission band observed at low-excitation power
density. (b) Sample B-3, cavity length is 0.302 mm, pumping power
density 11.0 kW/cm². The inset shows the detailed laser mode
structures.

fringes. For example, the overall full width at half maximum of the total laser emission band of the sample C-3 is 10 meV under the excitation power density of 10.5 kW/cm^2. Those spectrally resolvable fringes correspond to the longitudinal cavity modes resulting from the reflection from the cleaved facets of the sample and the dispersion in the index of refraction for ZnSe. There is considerable dispersion in the index of refraction near the band edge[81] which influences the distribution of allowed modes oscillating in the Fabry-Perot resonant cavity formed by mirror like cleaved sample faces. A broad emission band located at lower energy (~5 nm below the lasing emission band) was observed below the threshold excitation intensity for laser emission. This spectral feature presumably corresponds to some radiative recombination processes associated with the presence of impurities such as Si, Ba, and Ni.[82] The Si contamination could be introduced into ZnSe bulk during the crystal growth most likely due to the quartz ampoules used for growing samples at about 1200 ^{0}C. The source of Ba and Ni contamination is not clear at present. Similar results were observed from the MBE samples. Fig. 14 shows the laser emission spectra from a sample with a cavity length of 436 μm just at the threshold of lasing (Fig. (14a)) and above threshold (Fig. (14b)).

The onset of the steep rising slope of the emission intensity plotted against pumping power densities in Fig. 15 is defined as the threshold for lasing. The lasing threshold pump power at room temperature was determined to be 7 kW/cm^2 for the SPVT sample which is a surprisingly low value. This value is approximately two orders of magnitude less than that reported in Ref. 14, using a high reflection coated
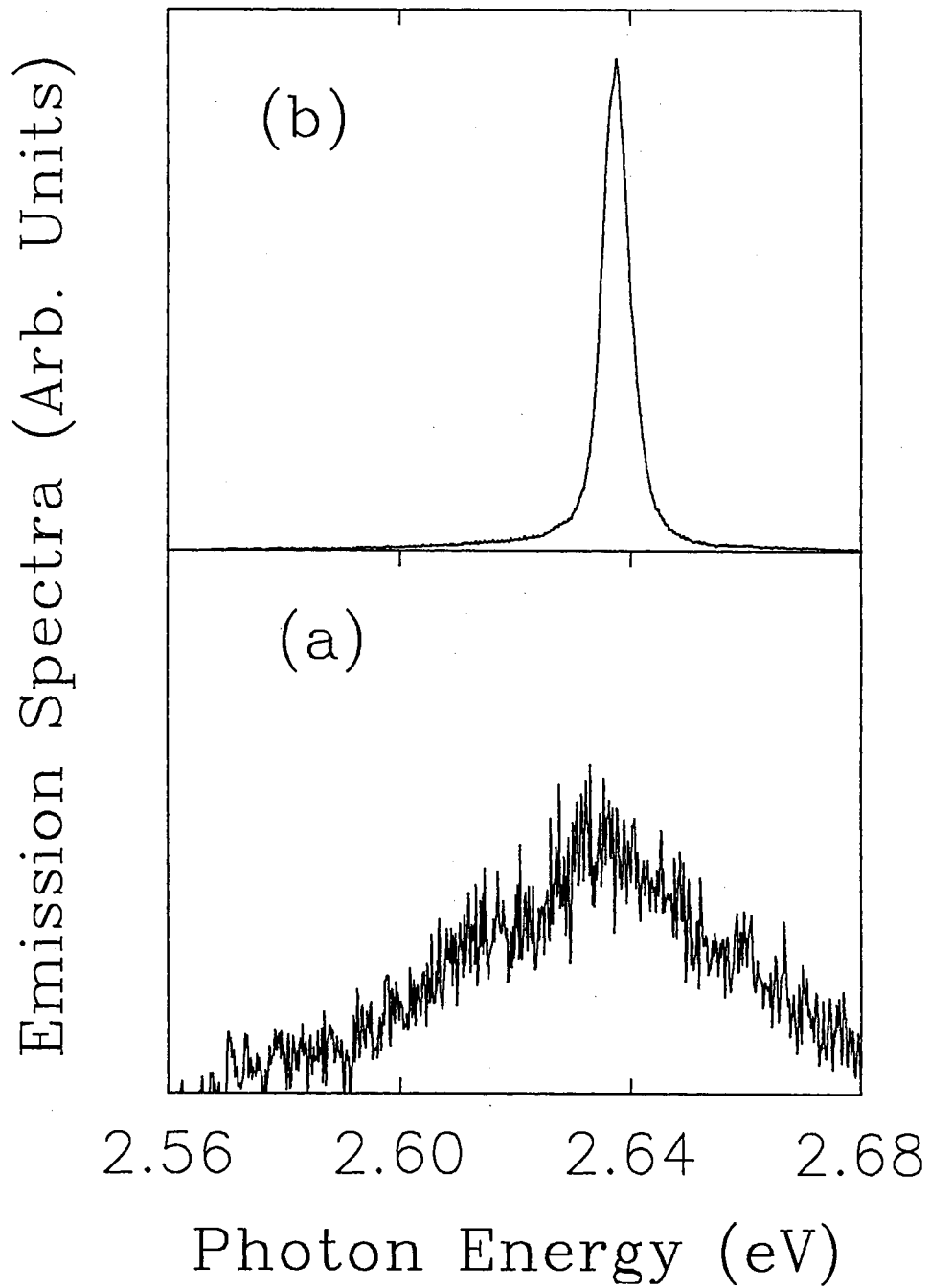
Figure 14. Lasing spectra of a 2.42 μm thick MBE sample with a cavity length of 436 μm under pumping power densities below (a) and above (b) the lasing threshold.
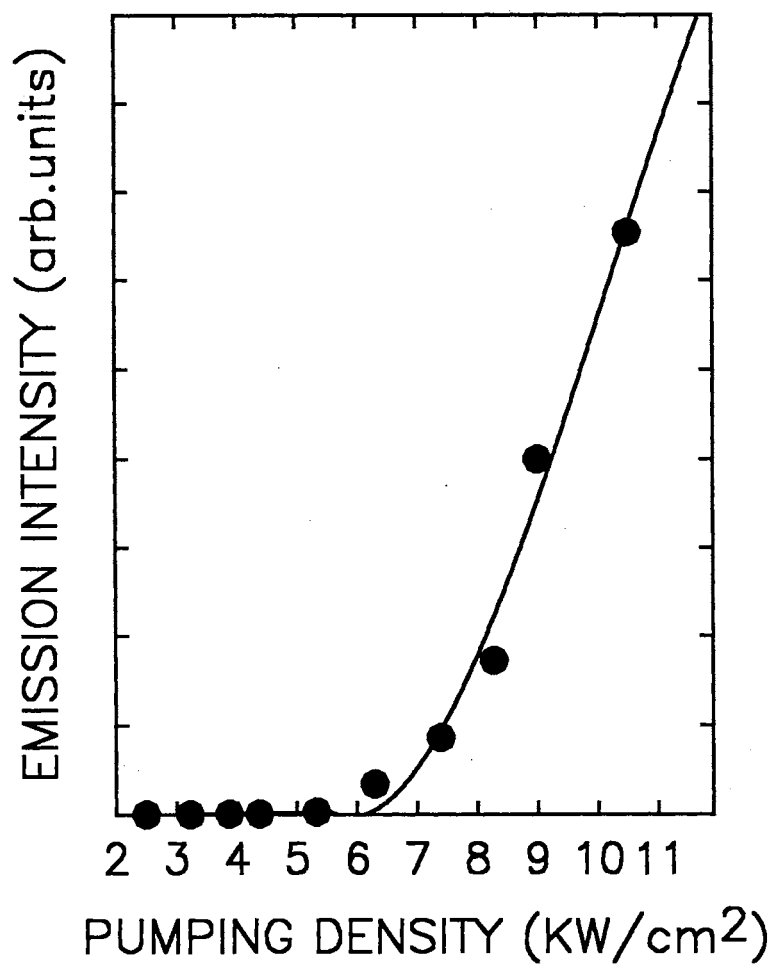
Figure 15. Emission output vs optical pumping power densities for the ZnSe
sample with a resonator cavity length of 0.376 mm, showing a linear
rise at low-excitation densities and a superlinear rise beyond 7
kW/cm^2 at pumping wavelength of 460 nm.

ZnSe laser resonator. The lasing threshold can be severely affected by pump-beam-dependent parameters and sample-dependent parameters. The main influence of pumping-beam-dependent parameters on the threshold in this work is from the excitation photon energy as far as the experimental setup is concerned. When the pumping wavelength is tuned to be very close to the ZnSe band gap, the sample can be efficiently pumped due to the enhancement of the carrier generation rate as observed in this work. More important influence on the lasing threshold is from the sample itself. This can be further classified into two groups: one is associated with its bulk material properties such as impurities, crystallinity, and defects; another is related to laser cavity length, the quality of cleaved edge facets of the sample (which formed the oscillation cavity in our case here), and the sample surface quality. It is known that the surface condition of II-VI compound semiconductors samples can greatly affect the efficiency of radiative recombination and poor surface quality causes surface recombination losses.[83,84] It is evident from our experimental results that the ZnSe samples have a high degree of uniformity and the cleaved edges of the samples have a fairly high efficiency of reflection so that the surface recombination losses, which compete with the radiative-recombination emission, were sufficiently reduced. Though the lasing threshold achieved in this work is relatively low, we still expect that even lower threshold with much stronger room-temperature laser emission can be obtained if reflective coatings are used on the sample. Furthermore, there have been some new developments on the techniques of making heavily n- and p-doped ZnSe materials.[85-89] This means that the practical, convenient and useful p-n junction structure of ZnSe

may fabricated and low-threshold, high-power, current-injection ZnSe laser can be developed to operate in the blue range in the near future.

In conclusion, optically pumped room temperature laser emission of bulk and MBE epilayer ZnSe samples by tuning excitation photon energy close to the ZnSe band gap has been observed and the cavity modes corresponding to the laser oscillation within a resonator formed by cleaved sample facets were clearly resolvable. Our observation of laser emission of ZnSe demonstrates that ZnSe single crystals have the quality sufficient for low-threshold, high-power output blue laser operation.

Lasing of ZnSSe Alloys

The sulphur concentration of the ZnS_xSe_{1-x} alloy was determined by x-ray rocking curves and room temperature optical absorption measurements. For optical absorption measurements, a linear interpolation was used to determine the x value from the change in the band gap (2.83 eV for ZnSe and 3.84 eV for ZnS at 4 K). The x-ray measurements yield an x value of 5.17% and the optical absorption yields a value of 5-6%. An example of the low temperature (10K) photoluminescence emission spectra taken using a continuous wave (cw) HeCd laser at 325 nm as the excitation source is shown in Fig. 16. The sharp, high energy peaks at 436.63 nm and 437.50 nm are identified as neutral donor and neutral acceptor bound excitons respectively.

In the lasing experiments, the output from one of the cleaved facets was directed to a distant spectrometer with and/or without a collection lens. The basic lasing characteristics of these two experimental arrangements, such as the differential
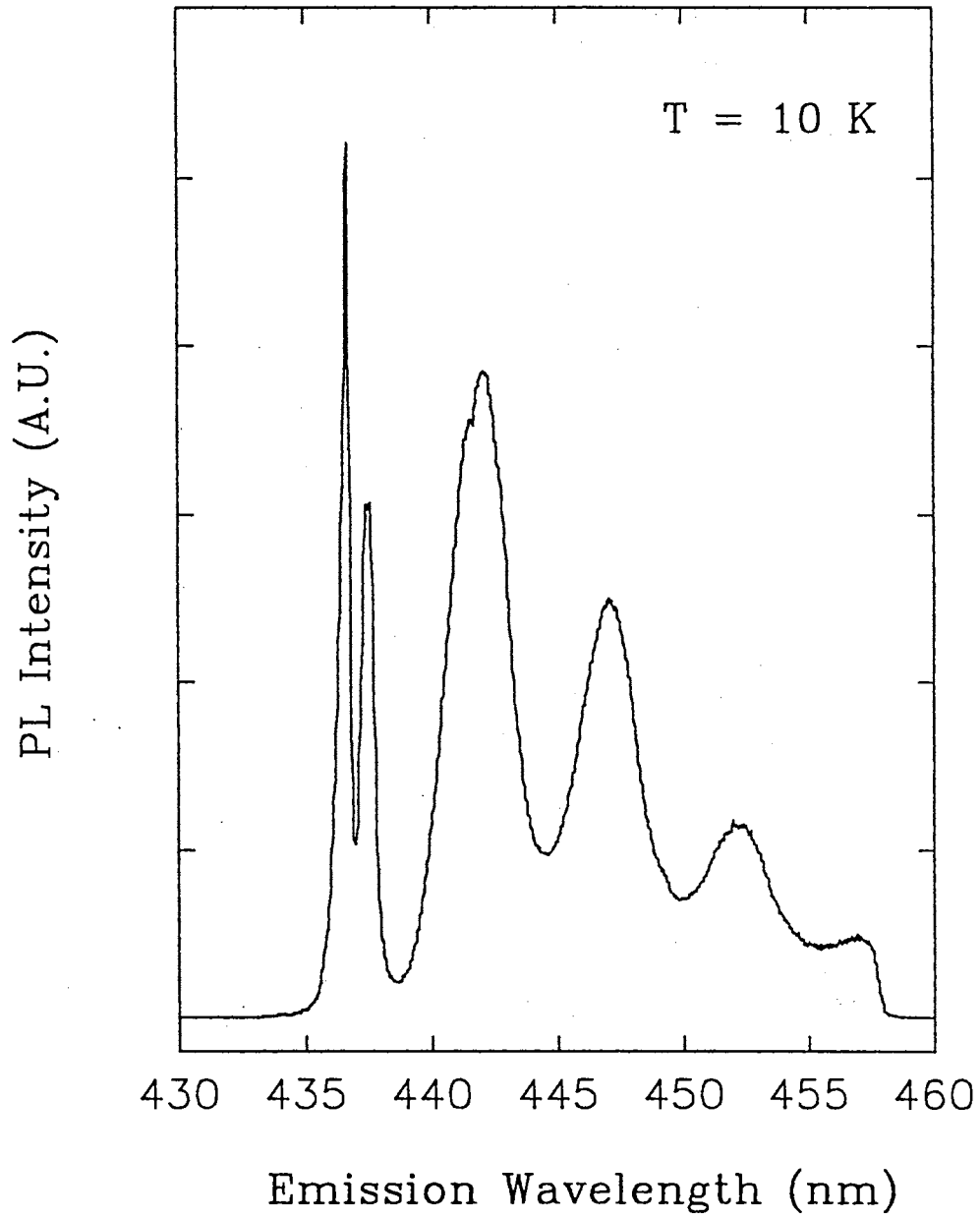
Figure 16. Continuous wave photoluminescence spectrum of ZnSe$_{1-x}$S$_x$, with x=0.05. The excitation source is a HeCd laser operating at 325 nm. The sharp high energy peaks at 436.63 and 437.50 nm are identified as neutral donor and neutral acceptor bound excitons.

quantum efficiency, lasing threshold power density, are the same except that the signal levels are higher with the collection lens. This implies that in this experimental configuration the influence from the scattered spontaneous emission is negligible with a collection lens. As a result, the data presented in the following are taken with a collection lens because of the higher sensitivity. The emission spectra taken with a 10 nanosecond pulsed laser, below and above the estimated threshold pumping power density, are plotted in Fig. 17 for a sample with the cavity length 399 µm with the excitation wavelength at 459 nm. The spontaneous emission has a broad spectral feature located around 467 nm, as shown in Fig. 17(b). A sharp peak appears at 464 nm as shown in Fig. 17(a) with an increase of the pumping power density. This peak has a full width at half maximum of 5 meV. This spectra narrowing is a clear indication of lasing. Under close examination, the longitudinal mode structures due to the reflection from the cleaved facets of the sample and the dispersion of the index of refraction of ZnS_xSe_{1-x} are resolvable, as shown in the inset of Fig. 17.

Fig. 18 demonstrates the well-defined lasing threshold observed at two different excitation wavelengths for the sample with a cavity length of 399 µm. The onset of lasing action was evidenced by the spectral narrowing, as well as the steep rise of the emission intensity-vs-pumping intensity curve. The threshold powers are found to be 350 kW/cm^2 for a pump wavelength of 459 nm and 96 kW/cm^2 for a wavelength of 455 nm. These values are one order of magnitude higher than the photopumped lasing threshold for bulk ZnSe in our previous report.[15] However they are still comparable to those reported for an antiguiding ZnSe epilayer structure[52] and DH structures.[17] The
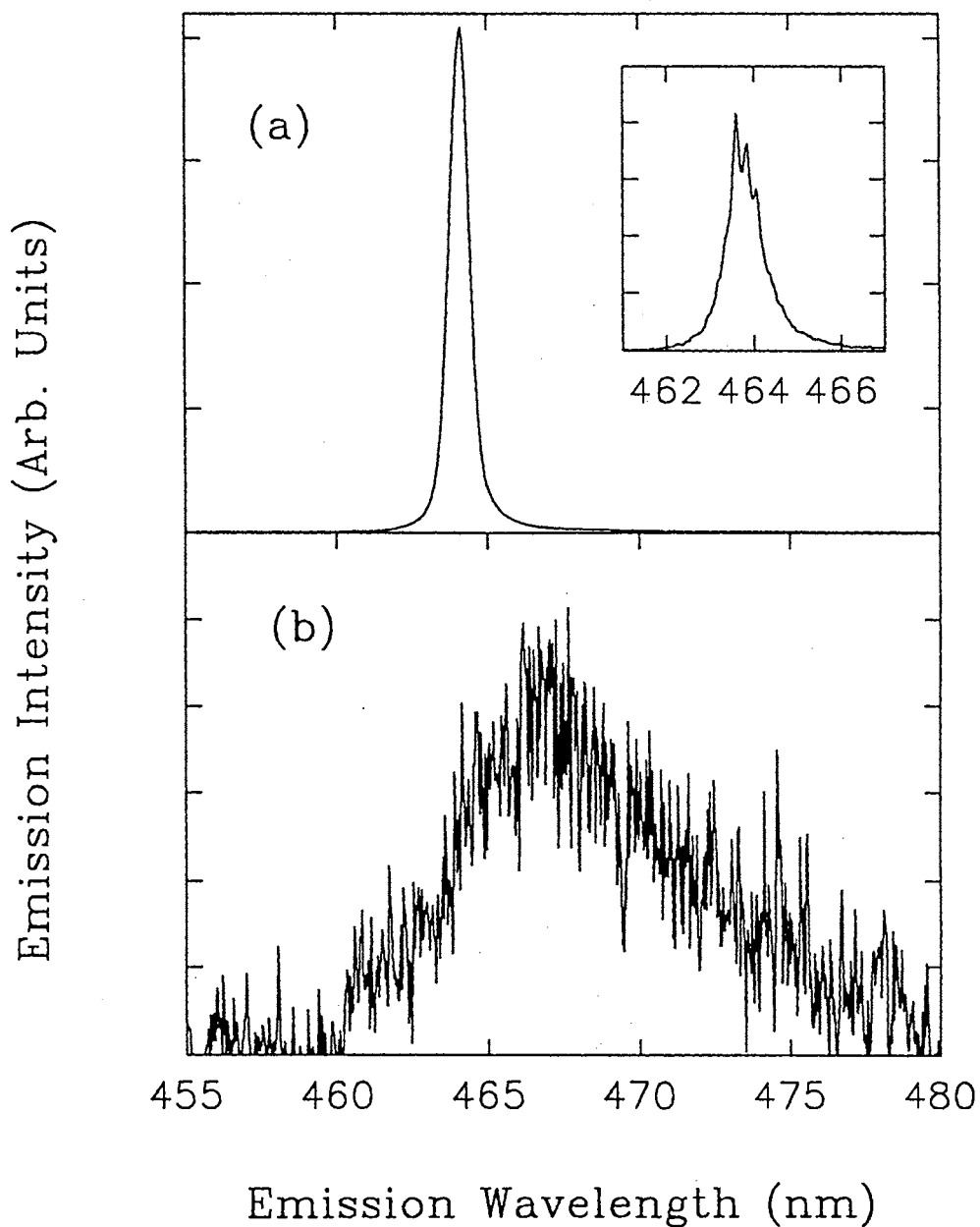
Figure 17. Typical emission spectra from a $ZnS_{0.05}Se_{0.95}$ sample with a cavity length of 399 μm pumped at 459 nm with pump power densities of (a) $1.4I_{th}$ and (b) $0.76I_{th}$. The threshold pump power density I_{th} was determined to be 350 kW/cm^2. The inset shows the longitudinal modes.
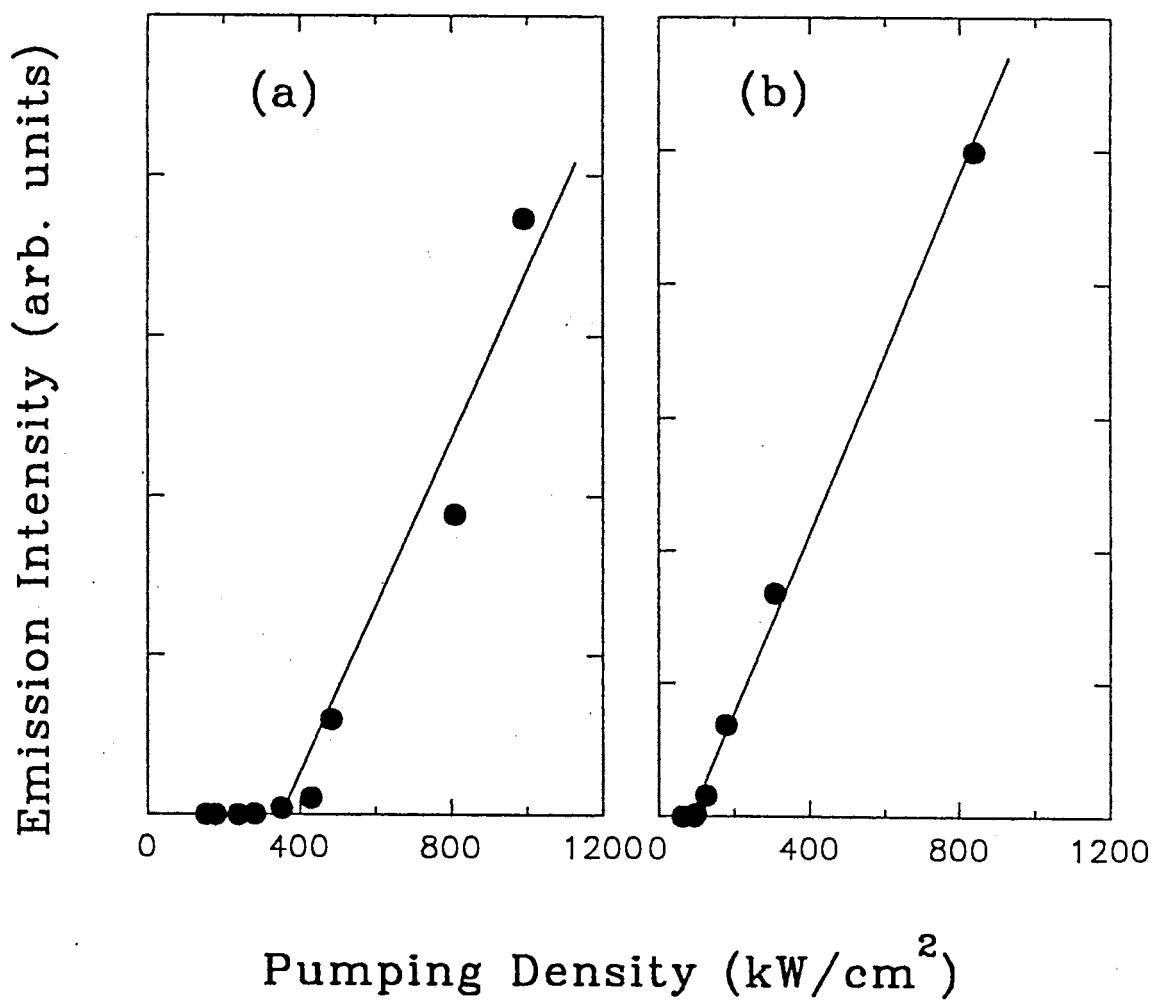
Figure 18. Emission output versus optical pumping power densities for the sample used in Fig. 17 pumped at 459 nm (a), 455 nm (b). The vertical axis is linear in intensity.

threshold could be reduced when the ZnS_xSe_{1-x} alloy sample quality is further improved or a ZnS_xSe_{1-x} epilayer grown on the lattice-matched GaAs substrate is used.

The effect of excitation photon wavelength λ_p on the lasing characteristics was also observed. There are several noteworthy results. The first is the dependence of the lasing threshold pump power density on λ_p, as illustrated in Fig. 18. We attempted lasing the sample with λ_p=433 nm and shorter, i.e. with an excitation energy much higher than the ZnS_xSe_{1-x} band gap. Only the spontaneous emission similar to Fig. 17(b) can be observed under pumping power densities equal to or higher than the threshold power densities needed to lase when pumping at 459 nm. This may be due to the competition of the non-radiative recombination near the surface with the stimulated recombination; with the excitation photon energy tuned far above the band gap, the penetration depth of the light was very short due to the large absorption coefficient of the alloy sample and the scattering losses due to many body effects.[53] As a result, the photo-excited carriers are concentrated near the surface where the surface related recombination centers may compete strongly with the stimulated emission process. This results in a high lasing threshold which makes it difficult to observe lasing. On the other hand, if λ_p is tuned very close to the band gap, the light penetration depth increases and this extends the excitation volume into the bulk of the sample where there are much less surface-related defects, resulting in a much reduced lasing threshold. This is supported by the observation of lasing when λ_p is tuned into the range between 460 nm and 455 nm. When λ_p is tuned from 460 nm to 455 nm, the lasing threshold decreases monotonically from 450 kW/cm² to 96 kW/cm². This may

be due to some resonant pumping effect although the exact origin is not known at this point.

The shift of the emission peak with λ_p is also observed. The peak shifts from 464.5 nm to 462.6 nm when λ_p is tuned from 460 nm to 455 nm while keeping the excitation power density fixed. This shift was also observed in ZnSe bulk[16] and epilayers.[52] This implies that the lasing is not likely to occur via some extrinsic recombination channels such as native impurity bound excitons, shallow donor or acceptor levels since their energy levels should be independent of the excitation photon energy. The lasing is most likely of intrinsic origin. The full understanding of this shift requires further study of the lasing mechanisms.

In summary, we have observed photopumped blue lasing at room temperature for $ZnS_{0.05}Se_{0.95}$ alloy samples using a near band gap pumping photon energy. Our results demonstrate the feasibility of using lattice-matched ZnS_xSe_x as an active light emitting region in place of ZnSe in most applications where the device is grown on GaAs substrate. For example, a DHs can be grown on a GaAs substrate using the $ZnS_{0.05}Se_{0.95}$ as an active region. The barrier layers can use ZnS_ySe_{1-y} with y greater than 5%. In this situation, the active layer can be grown coherently for a large layer thickness as long as the barrier layer is grown below its critical thickness. This DHs can therefore have a large gain volume as well as reduced strain induced defects. Also, a buffer layer of a superlattice structure $ZnS_xSe_{1-x}/ZnSe$ with low x values, for example, x=0.1, of equal well and barrier thickness can be inserted on top of GaAs substrate to smooth the subsequent growth since the average lattice constant of this

buffer layer is lattice-matched to the GaAs substrate.[20,22] The laser emission peaked at

464 nm, which is about 35 meV higher in energy compared to the result of ZnSe. The

emitting light wavelength can be tuned further into the blue by varying the ZnS_xSe_{1-x}

alloy concentration.

CHAPTER V

TWO-PHOTON PUMPED BLUE LASING IN BULK ZnSe AND ZnSSe

Introduction

The lasing characteristics of ZnSe and ZnSSe have been studied both by optical and electron beam pumping.[14,15,35,34,36,66,90] In general, the optical excitation was achieved in the one-photon absorption regime by using excitation photon energies above the band gap of ZnSe. The blue lasing from ZnSe and ZnSSe bulk samples have been previously obtained by using one photon pumping (OPP) method.[14,15,35,36,66] In this chapter, we report new experimental results on the study of laser action of ZnSe and $ZnS_{0.05}Se_{0.95}$ bulk samples in the near resonant two-photon absorption regime by using the two photon pumping (TPP) method. One difference between the TPP technique and the OPP method is that in TPP case a much larger volume inside the sample can be effectively pumped, so that the influence of the sample surface related defects is greatly reduced. In addition, different transition selection rules are involved in two-photon pumping, compared with one- photon pumping. TPP can induce optical transitions between levels having the same parity, which are forbidden under OPP condition. As a result, TPP is complimentary to OPP in studying the laser action and its physical origins. By using a tunable near infrared nanosecond laser (830-890 nm),

the two-photon pumped blue lasing could be observed up to room temperature and the lasing threshold was measured to be ~7 MW/cm^2. This observation of infrared-pumped visible laser action in ZnSe and ZnSSe single crystals indicates the applicability of using GaAs based III-V semiconductor compound diode lasers as a pumping source to excite the ZnSe-based materials for the frequency up-conversed lasing.

Experimental Results

Samples used in this study were ZnSe and $ZnS_{0.05}Se_{0.95}$ laser bars as described in Chapter IV. The difference of current experimental setup and the single photon pumping setup described in Chapter IV is in the use of a near infrared dye laser as optical pumping source, rather than in use of a frequency tracking doubler to double the near-infrared laser beam for excitation.

The laser emission generated by TPP in both ZnSe and $ZnS_{0.05}Se_{0.95}$ samples is very strong. The blue light emitted from samples is visible to the naked eye at ambient room illumination. The emission spectra from a ZnSe sample with a cavity length of 430 μm measured at 10 K are shown in Fig. 19(a). The excitation wavelength is 850 nm. From the figure one can see that the spontaneous emission from the sample has a few relatively broad peaks. Under high excitation conditions the dominant emission spectral feature is a narrow peak at ~446.4 nm whereas the other features present in the spontaneous emission spectrum are suppressed. The longitudinal cavity mode structures are also resolvable in the laser emission spectrum. The threshold of the excitation power for lasing was measured to be 7 MW/cm^2. The emission spectra
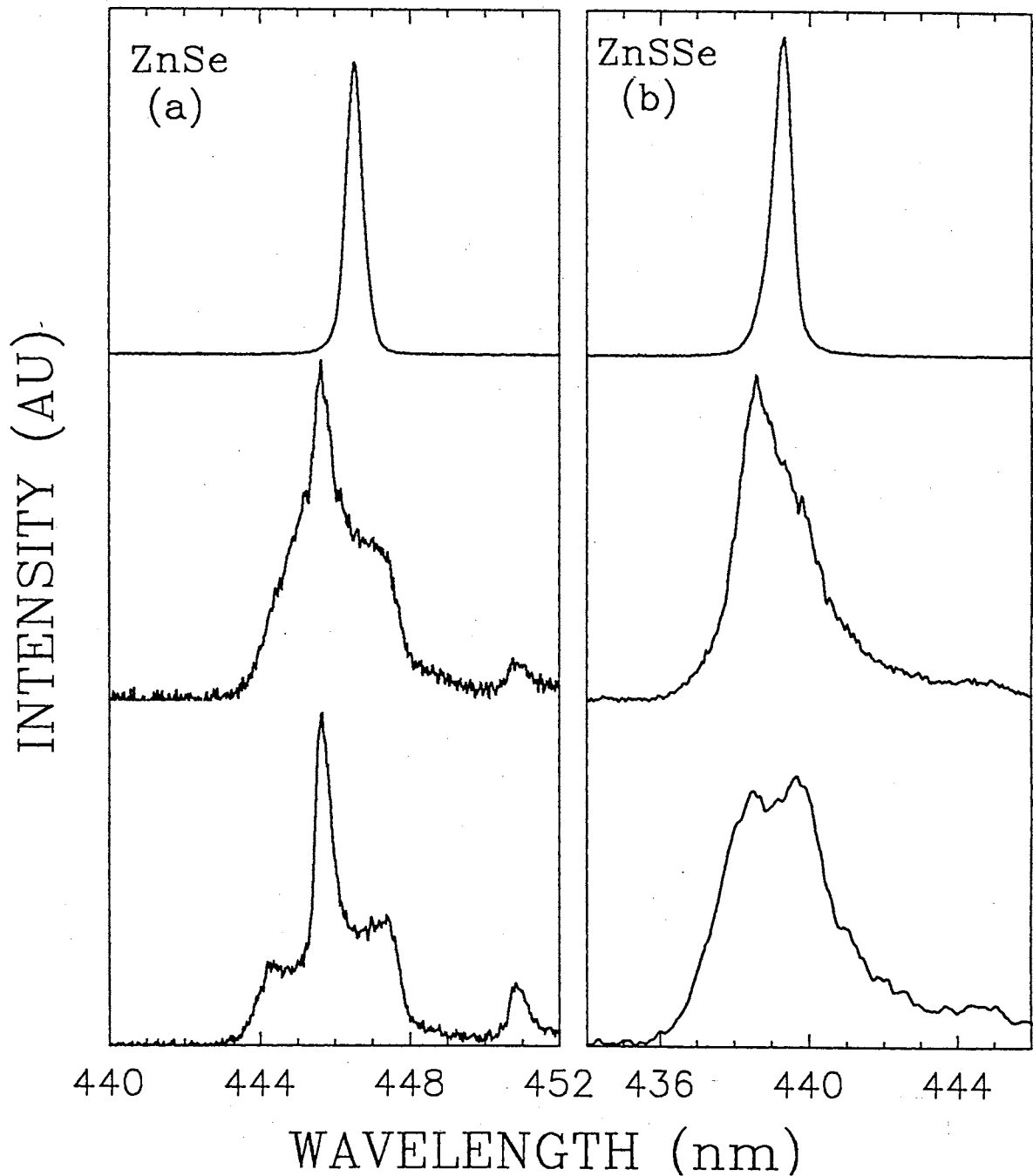
Figure 19. Typical emission spectra from ZnSe (a) and $ZnS_{0.05}Se_{0.95}$
(b) at 10 K with the excitation wavelength at 850 nm
under different pump intensities. Lower spectra: (a)
2.3 MW/cm^2, (b) 8 MW/cm^2, middle: (a) 5 MW/cm^2, (b) 13
MW/cm^2; upper: (a) 16 MW/cm^2, (b) 21 MW/cm^2.

taken from $ZnS_{0.05}Se_{0.95}$ samples are similar to those from ZnSe samples and are shown in Fig. 19(b). Due to the alloying effect the laser emission peak shifts to ~438 nm in $ZnS_{0.05}Se_{0.95}$ samples. Fig. 20 shows the emission intensity versus pumping power density for the ZnSe sample. A functional form of x^n with n=5.2 can be derived from the curve above the lasing threshold for the ZnSe sample. This power characteristic, together with the spectral narrowing, are manifestations of laser action resulting from TPP.[91] Similar results were observed for ZnSSe samples. A functional form of x^6 could be obtained before the onset of saturation of the laser emission in this sample.

The laser action could be observed up to room temperature for ZnSe and 200 K for ZnSSe samples. In Fig. 21 we show the experimentally measured energy position of lasing peaks as a function of temperature. The solid line in the figure is the temperature dependence of energy position of free exciton in ZnSe.[92] Typical spectra of the lasing output are shown in the inset of the figure. The lasing threshold power density increases by a factor of about three when the temperature changes from 10 to 200 K. The linewidth is broadened by a factor less than two (from ~4.9 to 7.3 meV in full width at half maximum) and the longitudinal modes could be also observed even at 200 K. While tuning the pumping wavelength from 830 nm to 867 nm, the laser action could be observed at 10 K from all the samples used in this study. When the pumping wavelength is longer than 867 nm, the laser action quenches regardless of the pumping power density used. Compared to the OPP situation, where the laser action could be observed with pumping wavelengths as long as 442 nm, it appears that the two-photon pumped lasing process requires a higher
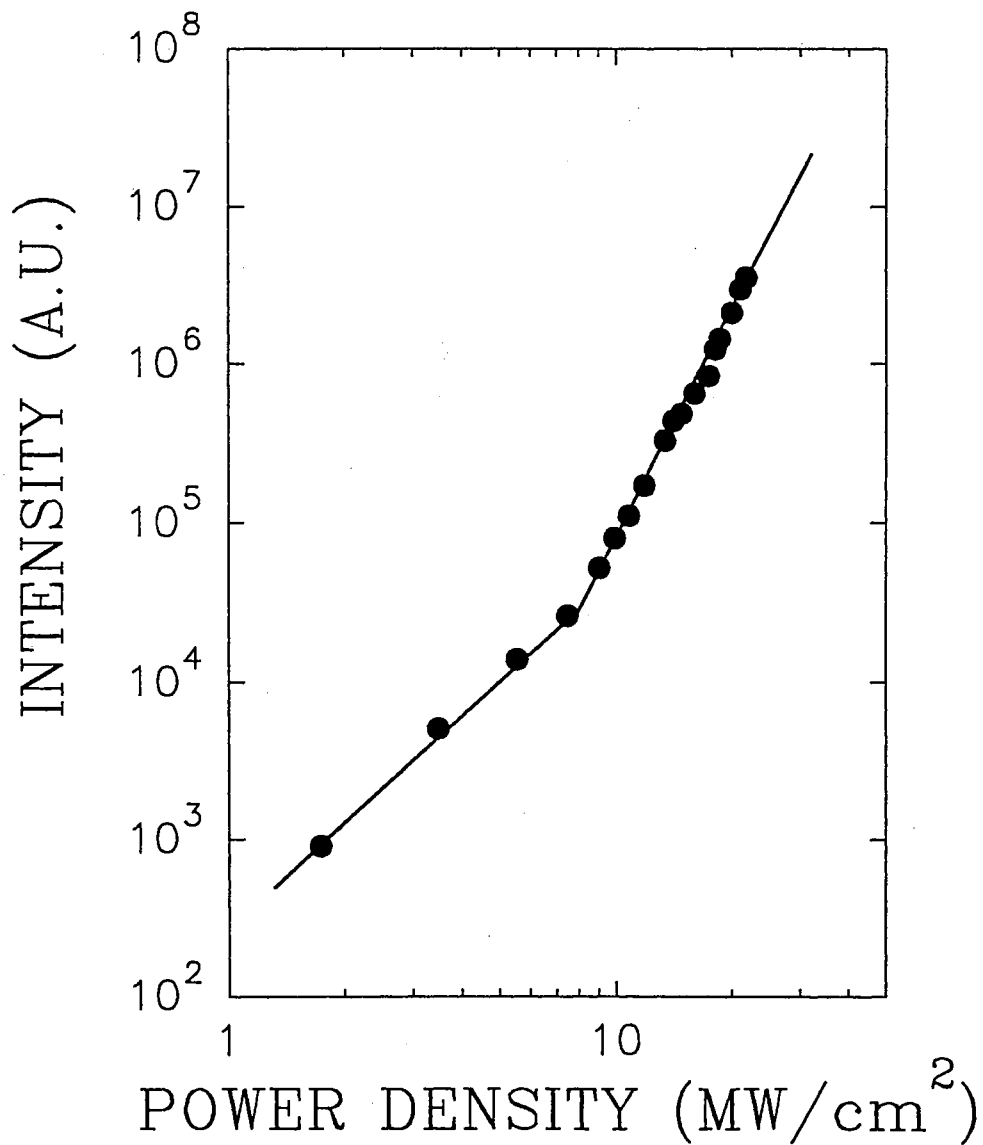
Figure 20.   The lasing emission intensity dependence of the ZnSe
              sample with 420 μm cavity length on the pumping power
              density at 10 K. The solid line through the data
              points is a guide for the eye.
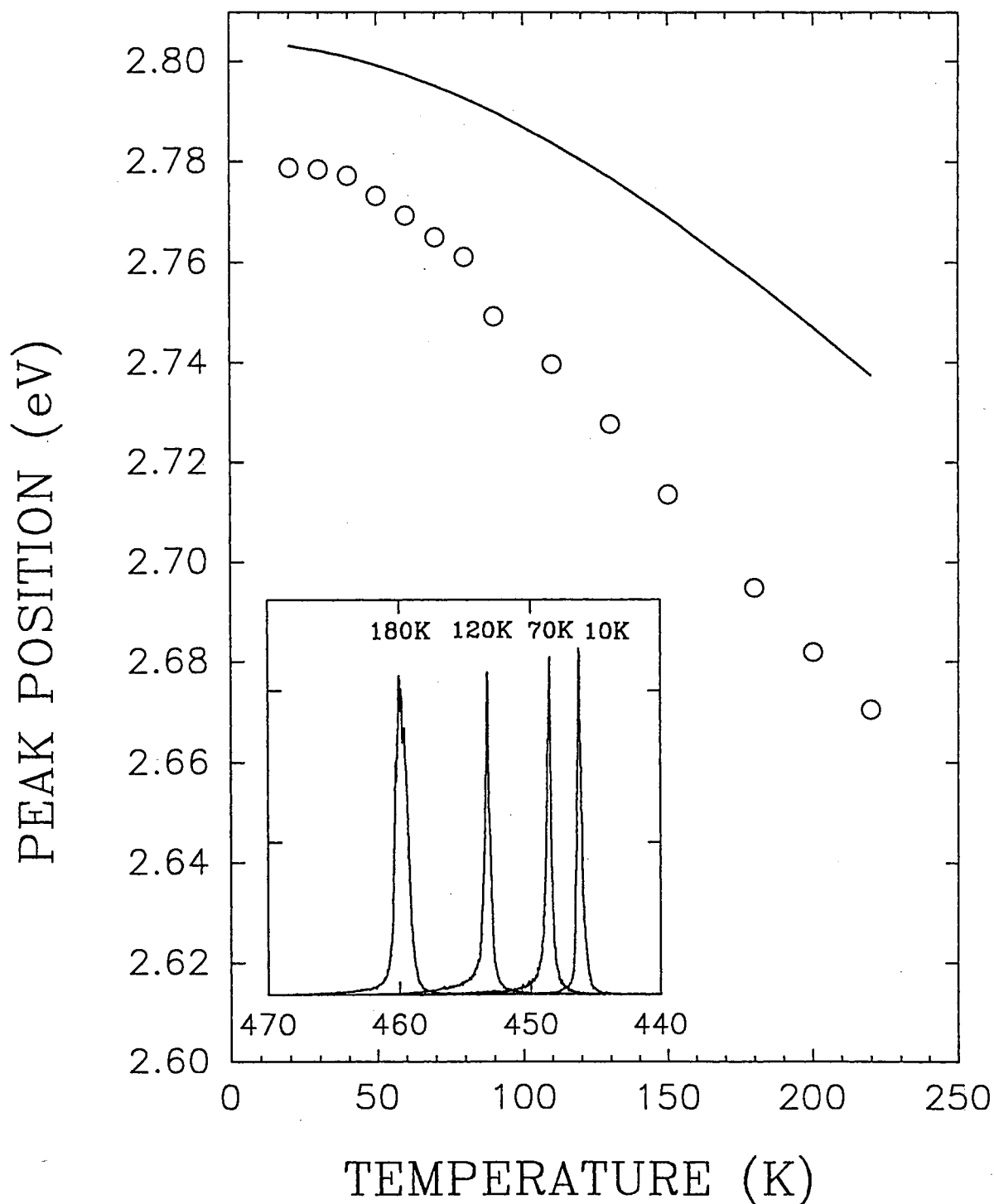
Figure 21. Variation of the measured lasing energy position with temperature. The solid line in the figure is the temperature dependence of energy position of free exciton in ZnSe. The inset shows lasing spectra of a ZnSe sample at different temperatures.

effective excitation energy (twice of the pumping photon energy). One of the reasons

responsible for this difference has been suggested to be due to the fact that the two-

photon absorption coefficient changes much more drastically with incident laser

wavelength than the one-photon absorption coefficient for semiconductor materials.[91,93]

We have also found that the TPP lasing peak position at threshold pump powers for

ZnSe samples is approximately the same as those of our previous OPP experimental

results.[94] Nearly the same lasing peak positions of TPP and OPP suggests that the TPP

lasing process might be of the same physical origin as OPP lasing processes.

Discussion and Conclusion

In wide band-gap II-VI compound semiconductor materials excitons are known

to play important roles in lasing processes.[35] The LO-phonon assisted free exciton (FE)

recombination, i.e. a FE-phonon scattering process, was proposed to be the dominant

lasing mechanism under two photon pumping.[11] However as shown in Fig.21, the laser

transition shifts to lower energy with increasing temperature more rapidly than the FE

energy. This shift cannot be explained with recourse to the FE-phonon scattering

process. The sample heating effect can be also excluded. The low average excitation

intensity of the near-infrared dye laser with a pulse of 10 ns and a repetition rate of 10

Hz and small two-photon absorption coefficients of ZnSe and ZnSSe at the near-band-

gap region are not likely to cause significant heating on the samples. By monitoring

the peak position of the LO-phonon assisted deep acceptor bound exciton line in ZnSe

as a function of excitation intensity, we found that it is independent of the excitation

intensity. Another alternative is a free-exciton free-exciton (FE-FE) scattering process. In such a scattering process, one exciton is scattered into a lower energy photon-like part of polariton dispersion curve then annihilated to emit a photon while the recoiling exciton is scattered into a higher energy state, which could be the continuum of free electron and hole states. In the case of high excitation, a high density of free carriers could be created resulting in the occurrence of band filling effect. When the FE-FE interaction process takes place, the free carriers created must obtain sufficient kinetic energy from the exciton in order to reach the higher lying unfilled states in the bands. Consequently, the exciton scattered into the photon-like branch of polariton will lose more energy. A red shift of the lasing transition is therefore expected to occur with increasing carrier densities originating from the pumping power density increase. Such a red shift with the pump intensity was indeed observed in this work as shown in Fig. 22. The solid line in the figure is a fit of the lasing peak energy shift ΔE as a function of TPP density using the equation

$$\Delta E = a(I_p - I_{p0})^2 + b$$

(V.1)

Here a and b are fitting parameters and I_{p0} is TPP lasing threshold. Recently, Newbury et al have studied one-photon pumped stimulated emission in ZnSe epilayers[13] and suggested that, by energy conservation, the red-shift of the lasing peak (ΔE) should equal the kinetic energies of the recoiling electron and hole obtained due to FE-FE scattering with the assumption that all carriers relax down to the bottom of their respective bands. Therefore the total energy required to reach the lowest unfilled states
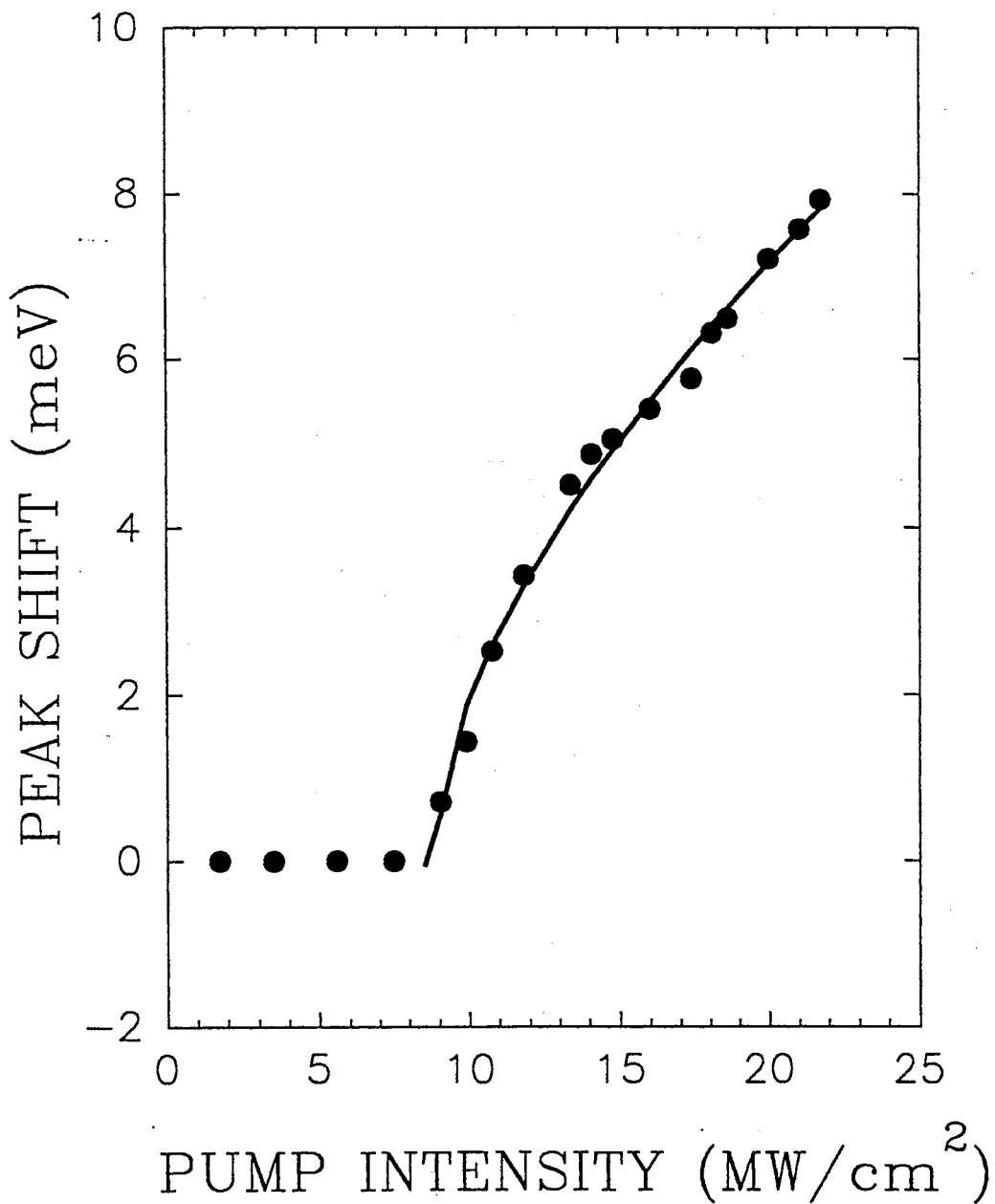
Figure 22.   The lasing peak energy shift of a ZnSe sample vs
            pumping intensities. The solid line is a theoretical
            fit to the experimental data.

of free-carrier continuum is proportional to two thirds power of the generated free carrier concentration.[13] One the other hand, the free electron (hole) concentration is proportional to the square root of the free-carrier generation rate for the FE-FE scattering process and in the two-photon absorption regime the generation rate is proportional to the square of the pumping intensity.[54] This means that the free-carrier (either electron and/or hole) concentration is a linear function of the two photon pumping density. Therefore, theoretical estimation gives N=2/3 in Eq.(1). By using fitting parameters a=2.02 and b=0.58, along with the measured I_{p0}=7 MW/cm^2, the best fitting gives N=0.64. This value is close to the value of 2/3 derived from the theoretical estimation based on the FE-FE scattering process. Hence our results suggest that the FE-FE scattering dominates the low-temperature lasing process in ZnSe and ZnSSe alloy crystals.

In summary, we have studied the laser actions of SPVT ZnSe and $ZnS_{0.05}Se_{0.95}$ alloy crystals in the two photon absorption regime. The infrared pumped visible lasing has been observed in both ZnSe and ZnSSe alloy samples up to room temperature by tuning the pumping light wavelength in the range of 830-890 nm. These experimental results indicate the possibility of using near infrared GaAs based III-V compound diode lasers as excitation sources to pump ZnSe based II-VI materials for blue lasing. Based on the peak energy position and the red shift of the lasing line above threshold, the dominant physical mechanism of lasing is attributed to the free-exciton free-exciton scattering and resultant band filling processes.

CHAPTER VI

GAIN MEASUREMENTS OF BULK ZnSe

Introduction

In previous chapters, we have demonstrated that ZnSe samples have qualities

sufficient for low-threshold, high-power output blue laser operation. One important

parameter in evaluating the possible utility of laser systems is the optical gain. In this

chapter, we study the stimulated emission effects and investigate the gain in SPVT

ZnSe single crystals using the single beam method by varying the length of

excitation.[95] Since this technique does not require the fabrication of the crystal into an

optical cavity, and utilizes only one pumping beam, it has been used extensively to

study stimulated emission effects in various materials.[96-98] If the spontaneous emission

occurs uniformly in the excited volume, the light emission intensity I for an excited

region of length l is given by[99]

$$I(l) = I_0 \exp(gl) \tag{VI.1}$$

where g is the gain which is given by[99]

$$g(v)=\sigma(v)[N_2-\frac{u_2}{u_1}N_1]$$ (VI.2)

where v is the emitted photon energy, and N_1, N_2 denote the number of carriers in the

lower and upper energy states, respectively. The factor u_1 and u_2 are the degeneracies

of the lower and upper states, and $\sigma(v)$ is the stimulated emission cross section at v. It

is clear that, for low excitation powers, the population should vary linearly with the

excitation power density, and thus, the emission intensity has an exponential

dependence upon the excitation power density. By varying the excitation length l, we

can monitor the emission intensity at fixed pump powers. An exponential increase in

the emission intensity as a function of excitation length indicates stimulated emission,

and the gain can be derived from the intensity versus excitation length curves.

Experimental Setup

In this study, we have used a 10 ns pulsed dye laser as the excitation source.

The dye laser (Lamda Physik 3002, LDS 765 dye from Exciton) operating at 750 nm

was frequency doubled to 375 nm (3.31 eV) by a wavelength-mixer. This photon

energy of the pump source is well above the band gap energy of ZnSe at 10K. The

gain measurements were made by employing a side-pumping geometry. The excitation

length of a focused beam on the sample surface was varied by translating a sharp

razor blade mounted on a micrometer head. The detection system is the same as

described in previous chapters.

The ZnSe samples used in this work were (100) oriented SPVT ZnSe single

crystals. The samples were nominally undoped, and the sample surfaces were mechanically polished initially. In order to study surface related effects, some of the samples were chemically etched using 0.5% bromine dissolved in methanol. The etching time varied from 0.5 to 2 minutes. The samples are large enough so that the cavity effects were eliminated. All experiments were carried out at 10K.

Results and Discussion

Fig. 23 shows the emission spectra from a 2 minutes etched sample taken at different pump power levels. For this etched sample, the spectra show a peak at 2.779 eV which grows rapidly with increasing pump power. This peak (A) is very close in energy to the so-called FE-(1s-2s) peak.[100] The FE-(1s-2s) peak is due to an inelastic scattering of free exciton at neutral donors so that its energy lies below the free exciton energy by the amount of the donor 1s-2s separation energy.[100] These donors can be Cl, Al, Ga, or In.[100] Another possibility is that peak (A) is due to an exciton-exciton inelastic scattering since the peak is located about one binding energy (~20 meV) below the free exciton peak. The former case is of extrinsic origin, and the latter is of intrinsic origin. Free exciton-exciton scattering is the more probable mechanism since it can also explain the square dependence of the emission intensity on the input power before the onset of stimulated emission, as shown in Fig. 25.[11] The other three peaks at the lower energy side are attributed to the phonon replica of peak A. The energy separation between these peaks is ~31 meV, corresponding to LO phonon energy of ZnSe.[101] At lower pump power densities, there is another peak (B) at 2.795

Figure 23. Stimulated emission spectra of the 2 minutes etched ZnSe taken at 10 K for several pump powers. The power used for spectra (a), (b), and (c) are 3, 4, and 10 kW/cm^2, respectively. The inset shows the stimulated emission peak taken at a pump power of 64 kW/cm^2.

eV. This peak coincides with the I_x peak in energy. The I_x peak is due to a radiative

recombination of bound excitons at neutral donors. At higher pump power levels,

peak B is suppressed by peak A, as shown in the inset of Figure 23. With an increase

of the pump power, peak A rises rapidly and becomes dominant. It is this peak which

we investigated carefully, as will be discussed below.

Fig. 24 shows the emission spectra of the unetched sample taken at different

pump powers. Comparing with Fig. 23, one clear difference is the absence of peak B.

Other spectra features are similar to those in Fig. 23. However, the signal level of the

2 minutes etched sample was found to be about 10 times greater than that of the

unetched sample. The enhanced emission after etching is probably related to the

increased sample surface quality, which results in a decrease of nonradiative

recombination channels as well as an increase of the beam penetration depth.

In Fig. 25, we show the pump power dependence of peak A emission intensity

plotted on a log-log scale for both of the samples shown in Figs. 23 and 24. The

squares are the experimental points, and the dashed lines are shown as a visual guide.

Curves 25a and 25b correspond to 2 minutes etched and unetched samples,

respectively. For the etched sample, the output signal increases by about four orders of

magnitudes with the input power change of less than 70 times. The rapid rise of the

output signal is a clear indication of stimulated emission. It can be seen that the curves

rise slower at lower powers than at higher powers. At low pump powers, the slope is 2

which means that the emission intensity varies with the square of the pump power.

This kind of kinetic behavior is typical in exciton-exciton scattering processes.[13] At
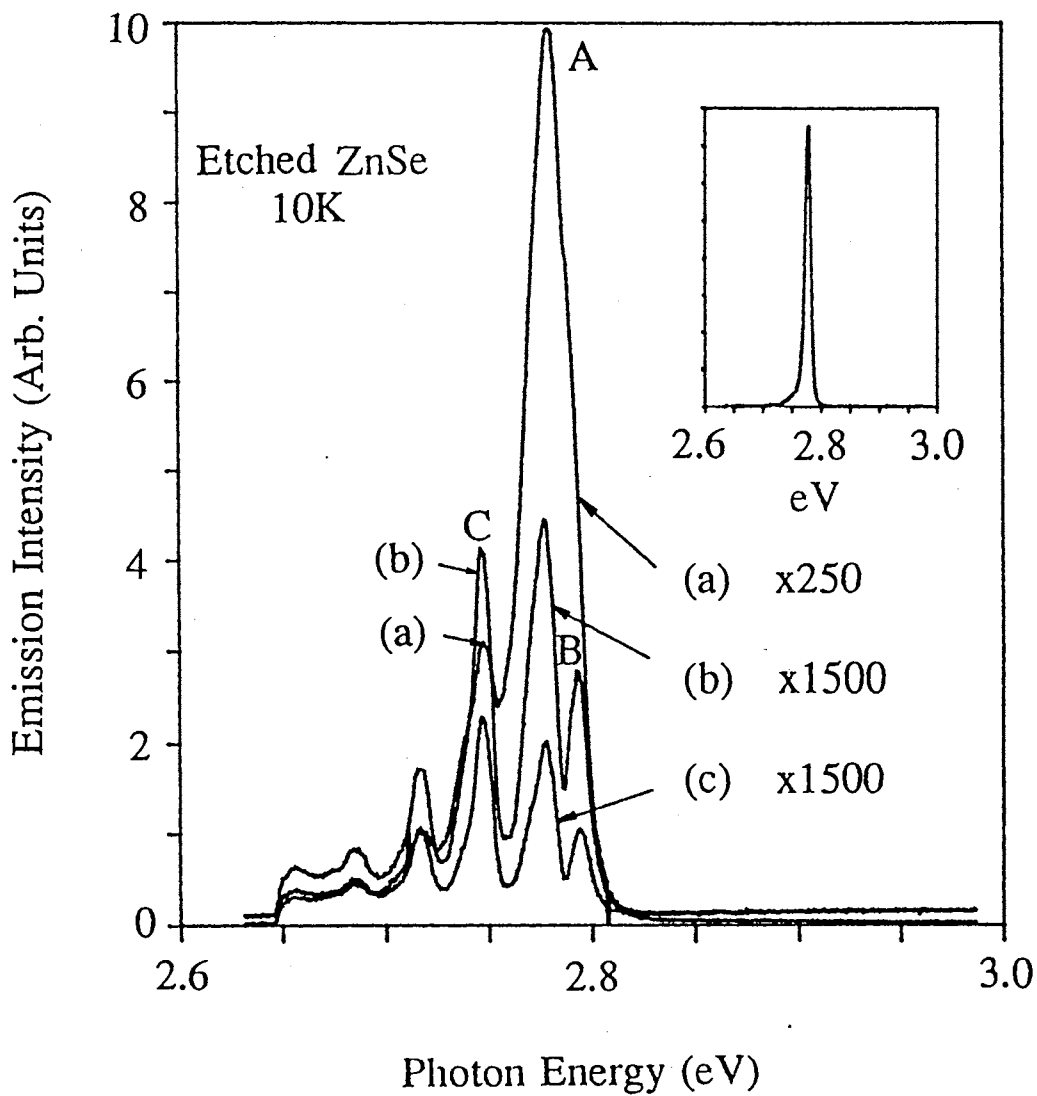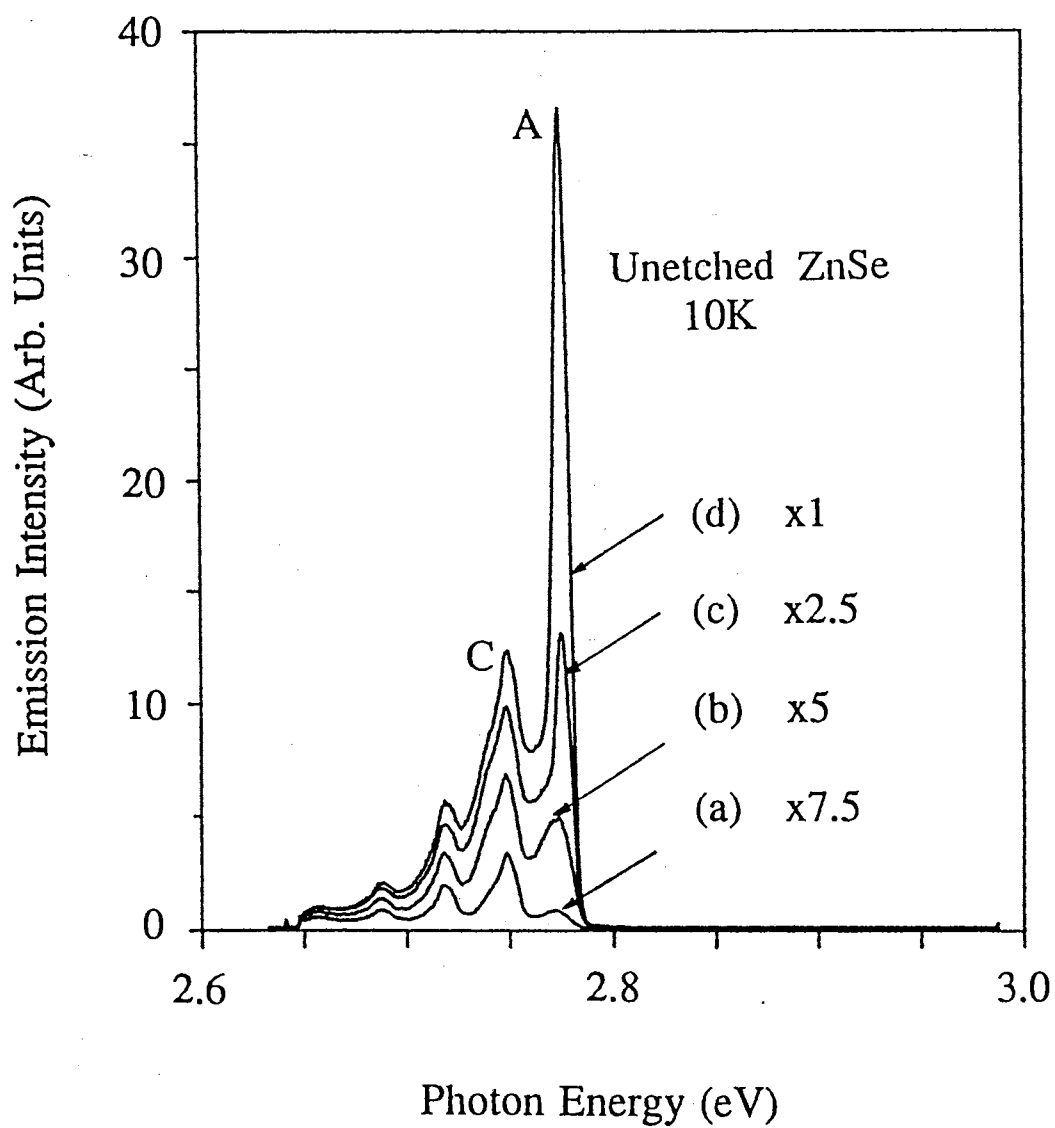
Figure 24. Stimulated emission spectra of the unetched ZnSe taken at 10 K for several pump powers. The powers used for spectra (a), (b), (c), and (d) are 6, 16, 25, and 39 kW/cm_2, respectively.
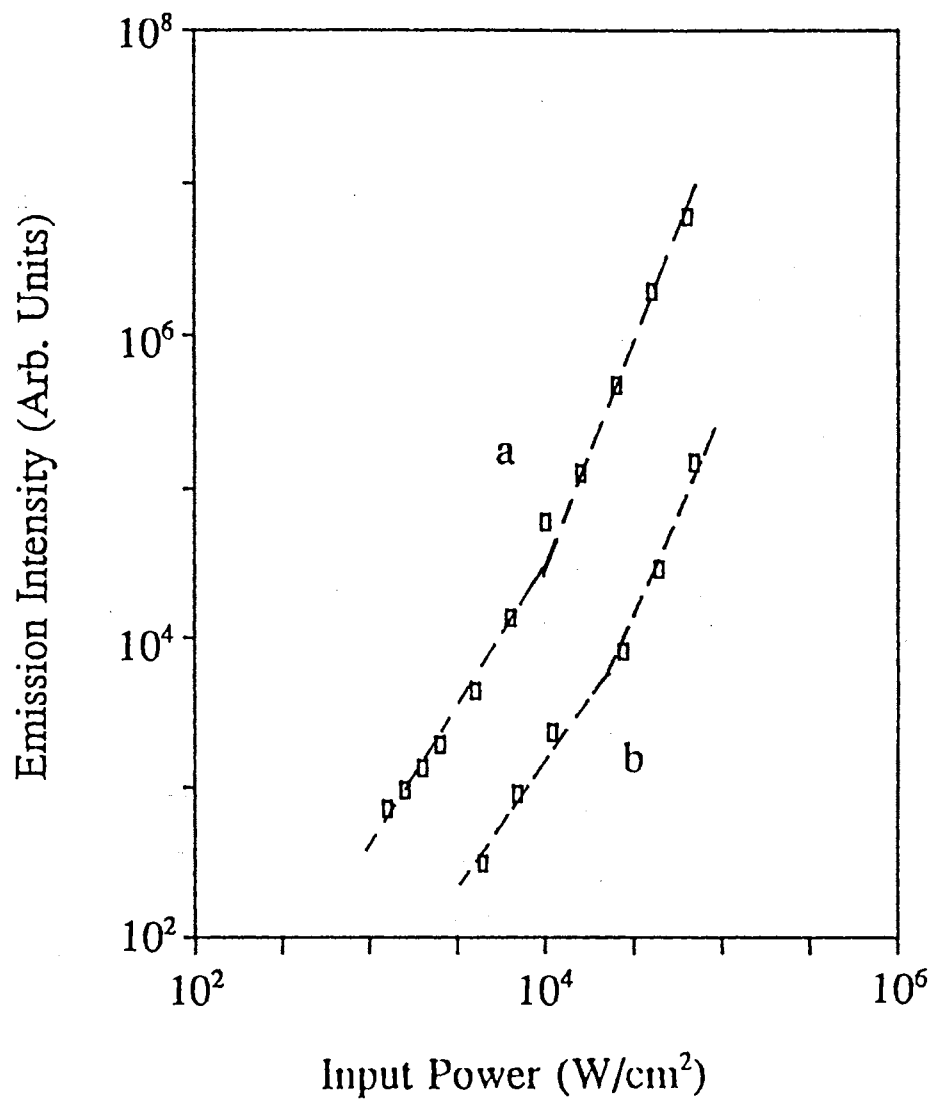
Figure 25. Pump power dependence of emission intensity for: (a) 2 minutes etched; (b) unetched ZnSe samples.

higher pump powers, the curves can be fitted to straight lines with slopes greater than 2, a clear indication of gain. This slope change of the power dependence curve is commonly seen in stimulated emission.[18,102,95] This represents the transition from spontaneous emission to stimulated emission. The transition point provides an estimation for the stimulated emission threshold.[18] The thresholds for both samples are about 10 kW/cm^2, as seen from Fig. 25. The saturation levels are not reached at the present power levels in both samples.

Peak B as well as peak C are located close to peak A, and this causes the partial overlapping of these peaks. In order to check the effect caused by the neighboring peaks on the stimulated emission of peak A, we also investigated the power dependence of peak B emission for the etched sample and peak C for both samples. We have found that initial increases of these peaks at low powers are comparable to peak A. However, these peaks increase at slower rates than peak A at higher pump power levels. Also, at high pump power levels the relative intensities of these neighboring peaks are much smaller than peak A. This suggests that the effect of the other peaks on the stimulated emission of peak A is insignificant. Therefore, we took the peak height of peak A as a measure of the stimulated emission intensity.

In order to obtain the gain value of the stimulating peak A, we measured the emission spectra at fixed power densities by varying the length of the excitation beam hitting the sample. Fig. 26 shows the emission intensity of peak A plotted as a function of the excitation length l at a fixed pump power for both samples. The curves can be fitted to a straight line before they reach the saturation point around l=0.7 mm.
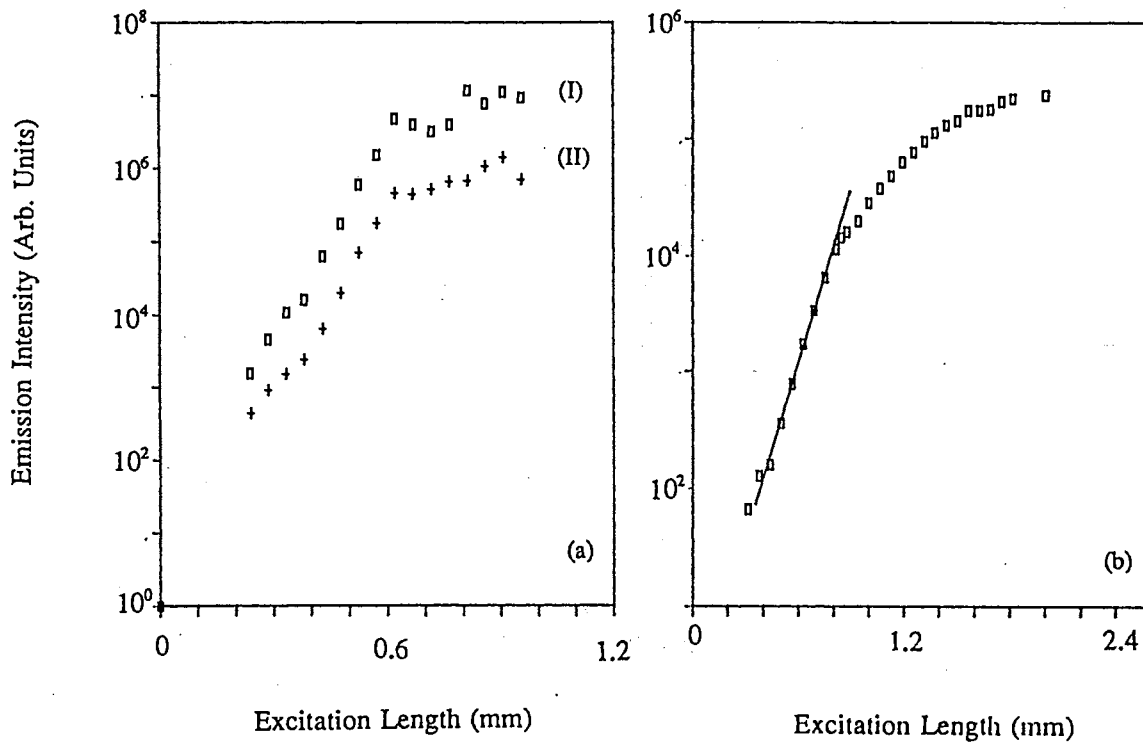
Figure 26. Plot of the stimulated emission intensity as a function of the excitation length for ZnSe samples. The two curves in (a) are for the etched sample at two different pump powers; (b) is for the unetched sample.

The gain values can be derived from the slope of the straight lines. The two curves in Fig. 26a are for the 2 minutes etched samples measured at two different pump power levels. The power used for the curve I is 63 kW/cm^2, which is 2.5 times that used for curve II. The gain value is 160 cm^{-1} for curve I and slightly smaller for curve II. These results indicate that the gain is rather insensitive to the pump power in this power range. At both pump powers, the gain saturation effects occur at l~0.7 mm.

As shown in Fig. 26b, the gain value for the unetched sample at 27 kW/cm^2 is about 120 cm^{-1}, which is smaller than the value for the 2 minutes etched sample. We have also measured the gain for a 1 minute etched sample and found a gain value between the gain of the unetched and 2 minutes etched samples. These gain values of ZnSe are comparable to those for CdS and GaP.[103] The increase in gain value after the etching of the sample may be due to the reduced surface effect. This can either be due to the improvement of the surface quality after etching or the decrease of the competing non-radiative recombination channels. Clearly, the etching improves the stimulated emission in ZnSe, both in terms of the emission signal level and the gain values.

Conclusion

We have observed optically pumped stimulated emission and measured the gain in SPVT ZnSe at 10 K for the first time. Compared with reported values[10,14], much lower threshold pump powers were observed for stimulated emission in bulk ZnSe. The gain values were measured by means of the variable excitation length method.

The saturation length determined from these gain measurements can be a valuable information when designing a laser cavity. The effect of etching on the gain was also examined, and the gain was found to be 160 cm^{-1} for the 2 minutes etched sample and 120 cm^{-1} for the unetched one. The etching of the ZnSe surface was found to increase the emission signal levels substantially, but only with a slight increase of the gain coefficients. These properties make ZnSe samples attractive blue laser materials.

CHAPTER VII

QUANTUM CONFINEMENT AND STRAIN EFFECTS

IN ZnSe/ZnS SINGLE QUANTUM WELLS

Introduction

With the advent of modern epitaxial growth techniques such as molecular-beam

epitaxy, it has become possible to grow semiconductor superlattices and quantum well

structures and tailor the band structures to achieve the desired properties and device

applications. Strained-layer quantum well structures give an additional degree of

freedom by allowing heteroepitaxial growth of lattice-mismatched systems without

creating misfit dislocations.[104] The strain energy in these structures is taken up by the

elastic deformation of the lattice. Wide band gap II-VI compound multilayer structures

are eminently suitable for various optoelectronic devices covering from the visible to

the ultraviolet spectral range. In particular, $ZnSe/ZnS_xSe_{1-x}$ MQWs are potentially

useful for electron-beam-pumped blue lasers[21] for printing applications and various

other optoelectronic devices including blue-light-emitting diodes and blue injection

lasers. For such applications, the growth of high quality, thin epitaxial layers is very

important. Unlike the case of $GaAs/GaAl_xAs_{1-x}$, where the hetero-layers are very well

lattice matched, ZnSe/ZnSSe epilayers are under considerable strain due to the lattice

mismatch present between them (~5%). However, it has been shown that if sufficient thin epilayers are used, then the lattice mismatch may be accommodated by elastic deformation only, and thereby, high quality multiple quantum well (MQW) structures may be grown.[105]

Recently, growth of ZnSe/ZnSSe superlattice by low-pressure organo-metallic vapor phase epitaxy (PL OMVPE) was reported in which very large blue shift was observed for the very thin layers.[106] Also ZnSe/ZnS superlattices have been grown on (100) GaAs substrates by hot wall epitaxy[107] and MBE.[108] In this chapter, we present the photoluminescence (PL) study on ZnSe/ZnS single quantum wells (SQW's) grown by a combination of MBE and atomic layer epitaxy (ALE). This combination of growth techniques can provide very good sample qualities as reflected by the narrowness of the PL peak. Single sharp PL peaks were observed in the energy range of (2.9-3.2) eV. The energy positions correlate with the quantum well size through the quantum size effect. Calculation based on a simple square well potential model fits the experimental data very well. Incorporation of strain effects can be seen to improve the fitting with the experimental results. The broadening of PL peaks from thin well samples (1-2 monolayer) was explained in terms of the interface roughness which induces the lateral quantum confinement effect in quantum slabs formed on islands and valleys at the interface.

Experimental Procedure

The samples were grown in the Electrotechnical Laboratory (JAPAN) by Dr. T.

Yao. Fig. 27 shows a schematic picture of a ZnS/ZnSe SQW structure. A 0.15 μm

thick GaAs buffer layer was grown on a (100) GaAs substrate by MBE in a separate

growth chamber. The sample was transferred to the II-VI growth chamber via

magnetic feed through and a ZnS barrier layer whose thickness ranged from 0.1 to 0.5

μm was subsequently by MBE. The typical growth rate was 0.1 μm/hr. Although the

lattice mismatch between GaAs and ZnS is 4.5%, the ZnS layer was thick enough to

be fully relaxed. The ZnSe well layer was grown by ALE. In the ALE growth,

constituent elements are alternately deposited onto the substrate so that the film growth

occurs stepwise.[109] Therefore, precise control of film thickness in the atomic layer

scale is easily attainable. The ALE growth conditions were examined by RHEED

investigations.[110] The thickness of the ZnSe well ranged from 1 to 20 monolayers

(ML's). Finally, a ZnS barrier layer whose thickness ranged from 0.03 to 0.1 μm was

grown by MBE. The substrate temperature during growth of II-VI compounds was

varied between 130 to 210⁰ C. PL spectra were measured at 10 K using the 325 nm

line from a He-Cd laser as an excitation source. The signal was dispersed with a spex

1403 double monochromator and detected with a photomultiplier tube.

Experimental Results and Discussion

Photoluminescence (PL) spectra from some of the ZnSe/ZnS SQWs are shown

in Fig. 28 as a representative. The PL spectra show dominant excitonic emission band

due to radiative annihilation of free exciton. The full width at half maximum of the

peaks at 10 K is about 20 meV for the three samples shown in Fig. 28. The linewidth

ZnS	← ~ 1000 Å MBE
ZnSe	← 1~20 ML ALE
ZnS	← ~ 5000 Å MBE
GaAs buffer	← ~ 1500 Å MBE
GaAs (001) substrate (Cr-0 doped)	T_{sub}~ 200 °C G_{ZnS} ~1000 Å/hr
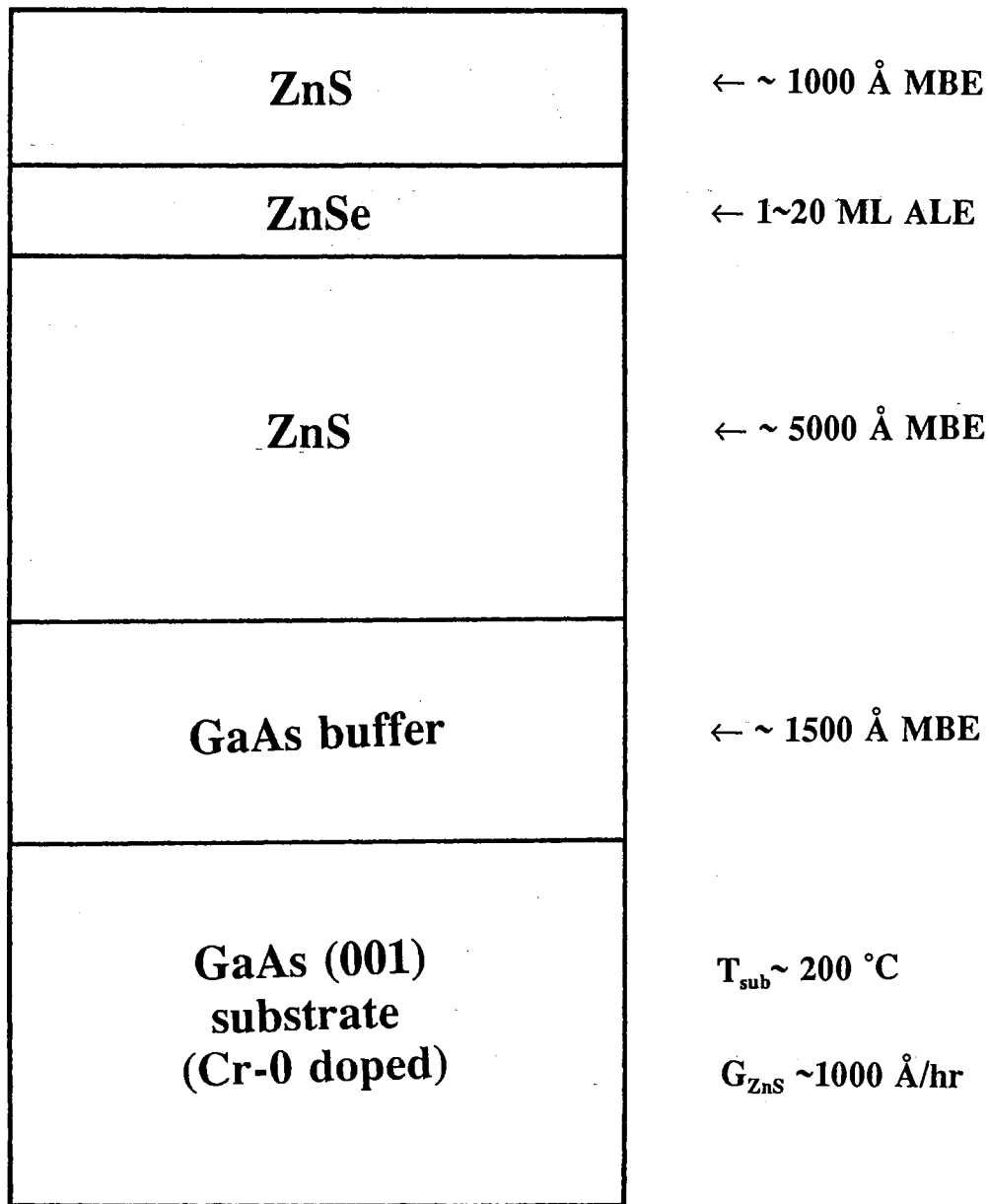
Figure 27. Schematic structure of fabricated single quantum well structures.
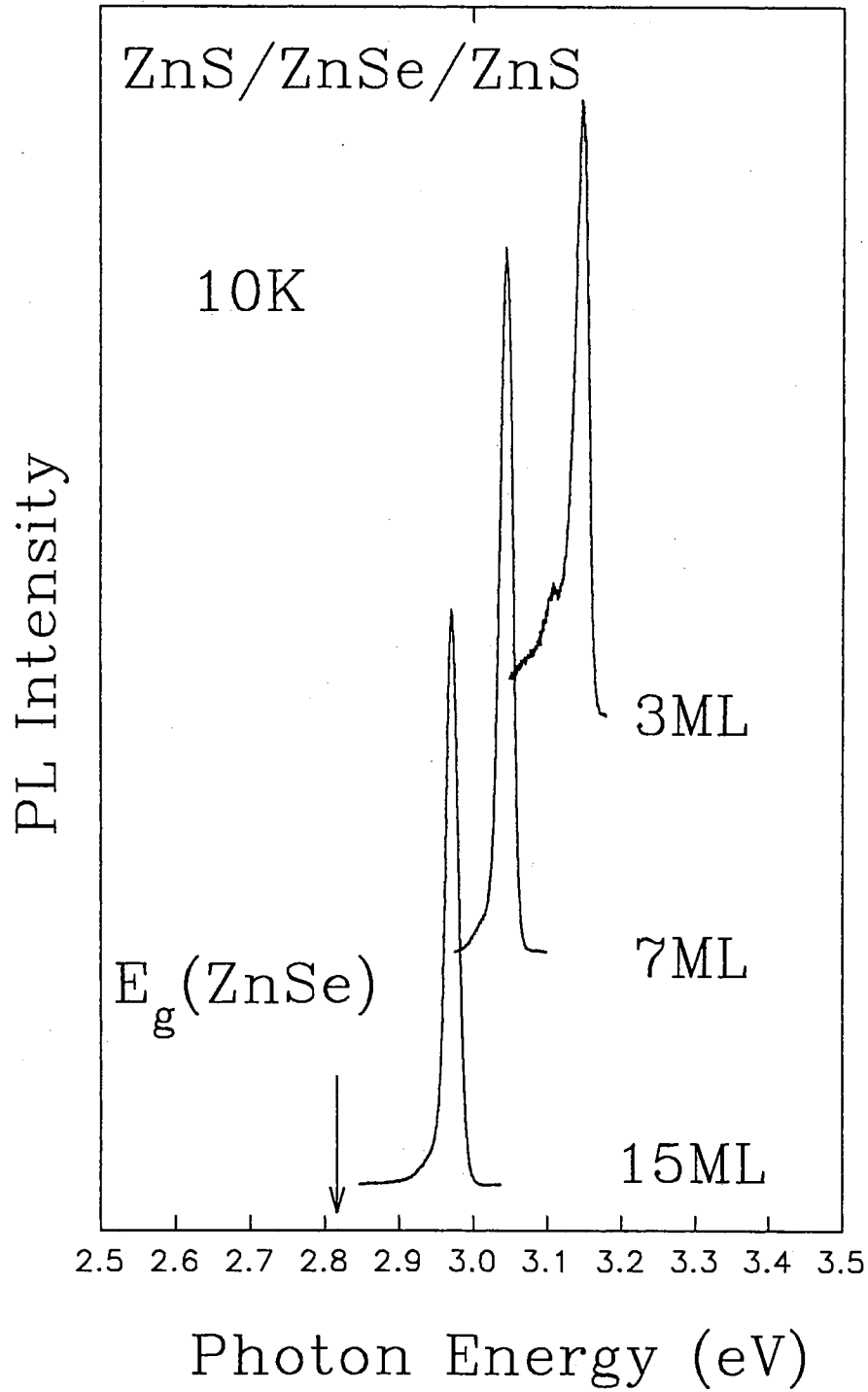
Figure 28. Photoluminescence spectra from the single quantum wells.

of the emission peak from quantum wells thicker than 3 ML varied from 15 to 30

meV. This value is much narrower than the reported half width for ZnSe/ZnS

superlattices.[106-108,111,112] The narrowness of the peak indicates the improved sample

quality of SQW structures over previously grown samples. The thick well (20 ML)

shows relatively broad linewidth (30 meV) with weaker luminescence. This is

probably due to the generation of misfit dislocations which occurs in thick films. The

misfit dislocations will produce nonradiative centers and will broaden the

luminescence. Also seen in Fig. 28 is the low energy tail in the spectra. This

asymmetric line shape has been observed in ZnS/ZnSSe SLS structures and has been

identified as being due to the bound-exciton emission overlapping the free exciton

luminescence.[111]

For samples with well width less than 3 ML, the linewidth broadens abruptly:

86 meV for 2 ML and 115 meV for 1 ML. The broadening mechanisms of the PL line

width are: (1) interface roughness, (2) the interaction of excitons with phonons, and

(3) band filling due to high carrier concentration. The broadening due to the

interaction of excitons with phonons becomes dominant at high temperatures[113], but it

is less important at low temperatures compared to other mechanisms. The broadening

due to the band filling becomes important when the excitation intensity is relatively

high. Therefore, the luminescence broadening due to the interface roughness would be

responsible for the luminescence broadening observed in the present experiments. It is

observed that the linewidth scatters around 20 meV for quantum wells above 3 ML,

while it increases abruptly as the well width decreases below 3ML. Such abrupt

broadening cannot be explained only by considering the fluctuation in the energy level of excitons caused by quantum confinement effect. The lateral confinement of excitons has to be considered.

When a 1 ML thick ZnSe is deposited on a ZnS surface which has a surface roughness of one monolayer, there would be formation of ZnSe islands whose thicknesses are 1ML. If the lateral dimensions of these islands are small compared to the de Broglie wavelength of electrons, additional "lateral" quantum confinement effects should be considered. The ZnSe islands are three-dimensionally covered by ZnS, resulting in a three-dimensional quantum confinement of electrons and holes. This situation is similar to the quantum box with a strong anisotropy. Such confinement would realize "quantum slabs", in which the confinement in the growth direction is of the order of an atomic layer, while the lateral confinement is of the order of excitonic size. Since the lateral dimensions of such quantum slabs are distributed almost randomly, the energy spread of the quantum level would become significant. Consequently, the luminescence broadening occurs. When a 2ML ZnSe well is grown, the lateral confinement is weakened because of the lateral extension of the interface layer. Thus, the energy spread due to the lateral confinement is decreased, which results in a decrease in luminescence broadening compared to the 1ML quantum well. Further deposited ZnSe smears out the lateral quantum confinement abruptly. As a consequence, the luminescence broadening in thick quantum wells will mainly be determined by the fluctuations due to the quantum confinement effect along the growth direction.

Fig. 29 plots the emission peak energy against the ZnSe well width. The dots are the experimental result. It can be seen that as the well width decreases, the emission peak increases. This is due to the quantum confinement effect. The data point of a 20 ML sample has an abnormally high energy value which may be due to the poor quality of this particular sample. The dashed curve shows the dependence of the calculated emission energy on the well thickness based on a simple square well potential model without considering the strain effects. In this model, the band offset ratio used is $\Delta E_c/\Delta E_v = 5\%$. The band offset ratio of $ZnSe/ZnS_xSe_{1-x}$ has been studied thoroughly by both experimental and theoretical work, and it is well established that the conduction band offset is very small (around 5%).[114] The calculated energy position is lower than the experimental data point, especially in the large well situation. When strain effects are included in the calculation by using the model solid theory (see Appendix)[30] , the calculated energy positions are shown as the solid line. Due to the biaxial tensile strain in ZnSe, the energy gap of ZnSe well increases. This results in higher calculated energy positions. This calculation gives an improved agreement with the experimental data. In the emission energy for very thin wells (1-2 ML), there is considerable discrepancy between the calculation and experiment. In such thin quantum wells, the effective mass approximation is not a good approximation, and a more rigorous treatment would be needed. Moreover, in the calculation of the emission energy based on the simple square-well potential model, the variation of binding energy with the well width should be considered. The binding energy of 3D exciton is 20 meV, while that of a two-dimensional limit is 84 meV.
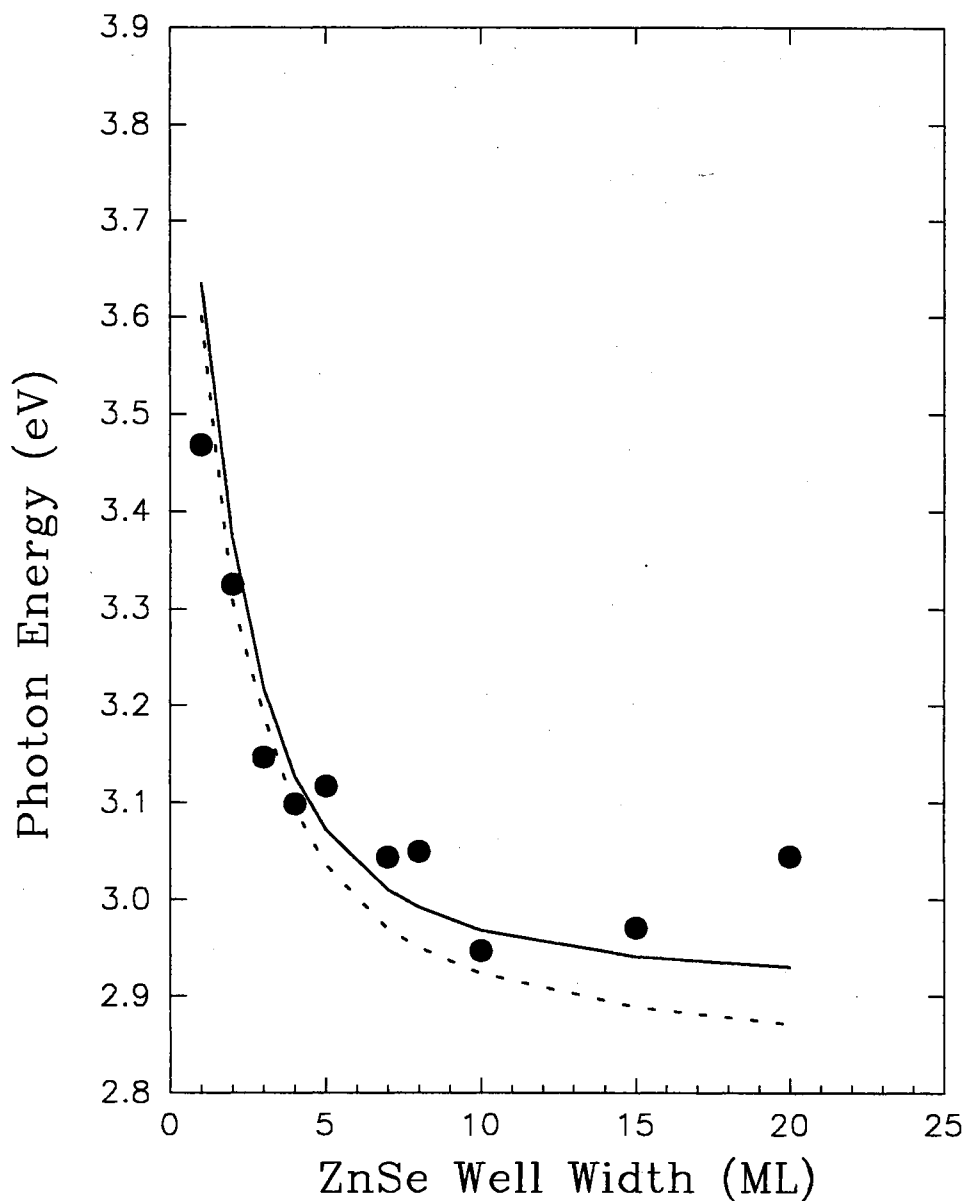
Figure 29. The dependence of emission energy on the well thickness. The dashed
line is the calculation without considering the strain effect,
while the solid line includes the strain effect.

The enhancement of the exciton binding energy becomes important in thin quantum wells. These factors are not considered in the present calculation and should be responsible for the deviation of the calculation from the experimental results.

Conclusion

ZnS/ZnSe/ZnS single quantum well structures (SQW) were fabricated by a combination of MBE and ALE for the first time. The SQW structures show dominant excitonic emission which correlate with quantum confinement effect. The sharp emission peaks indicate the good quality of the samples. The analysis of the dependence of the emission energy on the well width indicates that the conduction band offset is very small. The strain effects in the ZnSe well have to be considered in order for the theory to match the experimental result. The luminescence from wells thicker than 3 ML shows a sharp peak whose line width is typically 15-30 meV, while thinner quantum wells show a much broader luminescence peak. This abrupt broadening cannot be explained only by fluctuations in the electronic energy level associated with quantum confinement effect along the growth direction. It is suggested that the quantum slab structures are formed on the ZnS surface at the beginning of the epitaxy, which causes additional lateral quantum confinement. The lateral fluctuation of the quantum slab size causes additional luminescence broadening.

CHAPTER VIII

SECOND HARMONIC GENERATION

Introduction

Because of their potential applications in optical device technology, the optical properties of II-VI semiconductors, such as ZnSe, have been the subject of widespread and intense investigation. In particular, the nonlinear properties, such as nonlinear absorption and optical bistabilities, have been studied extensively.[115-117] There are also renewed interests in studying the second harmonic generation from ZnSe/GaAs interface in order to characterize the interface properties.[118,119] In this chapter, a preliminary study of the optical nonlinearity of SPVT grown ZnSe was performed experimentally by observing the non-phase-matched second harmonic generation (SHG). A transmission geometry was used in the study. The observed SHG intensity changes as the polarization direction of the pump beam varies. This shows that the SHG is produced in the bulk of the sample rather than in the sample surface. The SHG was observed with a broad range of pump photon energies. We have also investigated the dependence of the observed SHG signals on the sample thickness to quantify any enhancement of SHG due to phase matching.

Theoretical Background

In this section, we will give the basic expressions describing the second order nonlinear optical effect of second harmonic generation. We will also briefly derive the dependence relation of the resultant frequency-doubled signal intensity on the cartesian components of the input fields. The results are then specialized to the case of materials with $\overline{4}3m$ symmetry, such as ZnSe.

In a nonlinear medium, the polarization is made up of a linear and a nonlinear term

$$\vec{P} = \epsilon_0 \chi_L \vec{E} + \vec{P}_{NL}$$

(VIII.1)

where the first term describes the linear process. For a second order nonlinear process $P_{NL} \sim d^{(2)}_{ijk} E_j E_K$, where $d^{(2)}_{ijk}$ are the elements of the second order nonlinear susceptibility and E_i and E_j are the cartesian components of the input beams. For an electromagnetic wave travelling along the z direction in a lossless medium, in the case that the depletion of input beams can be ignored, the Slowly Varying Envelope approximation (SVE) can simplify the Maxwells Equations to one single equation describing the evolution of the frequency-doubled field[120]

$$E'_{3l} = i\omega \sqrt{\frac{\mu_0}{\epsilon_3}} d_{lij} E_{1i} E_{2j} \exp(i\Delta kz)$$

(VIII.2)

where $\Delta k = k_3^l - k_1^i - k_2^j$; μ and ϵ are the permeability and permittivity of the material, respectively. Note that Δk vanishes, or efficient phase matching occurs, only when the refractive index at the fundamental wavelength equals that at the doubled wavelength

for a given component. Integrating Eq. (VIII.2) form z=0 to crystal thickness l gives

$$E_{3l}(l)=2\omega\sqrt{\mu_0/\epsilon_3}d_{lij}E_{1i}E_{2j}\frac{\exp(i\Delta kl-1)}{\Delta kl}$$ (VIII.3)

where the leading factor of 2 results from the sum over i, j.

The quantity in which we are interested is the intensity of lth polarization component in the frequency-doubled beam which is given by

$$[I(l)]_l=\frac{1}{2}\sqrt{\mu_0/\epsilon_3}\omega^2 d_{lij}^2 E_{1i}^2 E_{1j}^2 \frac{\sin^2(\Delta kl/2)}{(\Delta kl/2)^2}$$ (VIII.4)

To describe the dependence of the intensity of the frequency-doubled light as the components of the input fields $E_{1\beta}$ vary, we may fix the field polarization vectors, referring them to a convenient laboratory frame, and allow the crystal to rotate. The effective elements $(d_{ijk})_{eff}$ then change as the crystal rotates and are given by[120]

$$d_{eff}=\sum_{ijk}\hat{b}_i d_{ijk}\hat{a}_j\hat{a}_k$$ (VIII.5)

where â and $\hat{b}$ are the unit polarization vectors of the input field and frequency-doubled field, respectively, referred to the crystallographic axes ijk. $\hat{b}$ can be chosen either parallel or perpendicular to â without loss of generality.

For ZnSe (point group $\overline{4}$3m), all but the following elements d_{ijk} are nonzero[121]

$$d_{123}=d_{132}=d_{213}=d_{231}=d_{312}=d_{321}=d$$ (VIII.6)

Performing the prescribed sum in Eq. leads to

$$d_{eff} = 2d(a_2 a_3 b_1 + a_1 a_3 b_2 + a_1 a_2 b_3) \tag{VIII.7}$$

We now consider a specific case for which the input field propagation vector $\vec{K}$ is parallel to (110) crystallographic direction. Two frames of reference sharing a common origin are required, a laboratory frame and a crystal frame. We denote the laboratory frame the primed frame which can be obtained by rotating the crystal frame about the z-axis through an angle $\Theta = \pi/4$. The vectors $\hat{a}'$ and $\hat{b}'$ referred to the laboratory frame are

$$\hat{a}' = \begin{pmatrix} 0 \\ \sin\phi \\ \cos\phi \end{pmatrix} \tag{VIII.8}$$

$$\hat{b}' = \begin{pmatrix} 0 \\ -\cos\phi \\ \sin\phi \end{pmatrix} \tag{VIII.9}$$

where ϕ is the angle between $\hat{a}'$ and (001). $\hat{a}$ and $\hat{b}$ are then obtained from their primed counterparts by applying the rotation operator R_Θ

$$\hat{a} = R_\Theta \hat{a}'; \qquad \hat{b} = R_\Theta \hat{b}' \tag{VIII.10}$$

where

$$R_\Theta = \begin{pmatrix} \cos\Theta & -\sin\Theta & 0 \\ \sin\Theta & \cos\Theta & 0 \\ 0 & 0 & 1 \end{pmatrix}$$

(VIII.11)

for positive angle Θ. This yields

$$\hat{a} = \begin{pmatrix} -\sin\Theta\sin\phi \\ \cos\Theta\sin\phi \\ \cos\phi \end{pmatrix}$$

(VIII.12)

$$\hat{b} = \begin{pmatrix} \sin\Theta\cos\phi \\ -\cos\Theta\cos\phi \\ \sin\phi \end{pmatrix}$$

(VIII.13)

Using these crystal-frame components in the expression for d_{eff} in Eq. (VIII.7) gives

the angular dependence of the parallel ($\hat{b}//\hat{a}$) and perpendicular ($\hat{b}\perp\hat{a}$) polarization

components of the frequency-doubled light for the case of incidence normal to a (110)

crystallographic face

$$I(2\omega)_{//} \propto (d_{eff})^2_{//}$$
$$\propto \sin^4\phi\cos^2\phi$$

(VIII.14)

$$I(2\omega)_\perp \propto (d_{eff})^2_\perp$$
$$\propto \sin^2\phi(1-3\cos^2\phi)^2$$

(VIII.15)

Again, this treatment assumes that the input field polarization vectors are fixed with

respect to the laboratory frame.

Experimental Procedure

The transmission geometry was used in our experiments. The diagram of the experimental setup is shown in Fig. 30. The excitation source was the Nd: YAG laser pumped nanosecond dye laser. The wavelength of the excitation beam can be broadly tuned. The samples were mounted on a rotational stage so that they can be rotated with respect to the polarization of the input beam. Several samples were investigated in this study. One sample has dimensions of 5 mm x 5mm x 5 mm, and the other samples have 1 mm thickness and variable lengths. The orientation of the samples is as follows: a polished face parallel to the (110) plane, and remaining edges parallel to the ($\bar{1}$10) and (001) planes, respectively. The laser beam was incident on the (110) surface. Neutral density filter (NDF) and blue filters were used to block the fundamental light. The output signal was analyzed with a polarization analyzer before directed to a spectrometer and recorded with a CCD.

Experimental Results

Preliminary results were obtained on the SPVT ZnSe single crystal samples. The angular dependence of the parallel and perpendicular components of SHG signal intensities for incidence on a (110) plane are given by

$$I_{\parallel}(2\omega) \propto P^2_{\parallel}(2\omega) = 9E^2_p(\omega)\chi^2\sin^4\phi\cos^2\phi \qquad \text{(VIII.16)}$$

$$I_{\perp}(2\omega) \propto P^2_{\perp}(2\omega) = E^2_p(\omega)\chi^2\sin^2\phi(1-3\cos^2\phi)^2 \qquad \text{(VIII.17)}$$
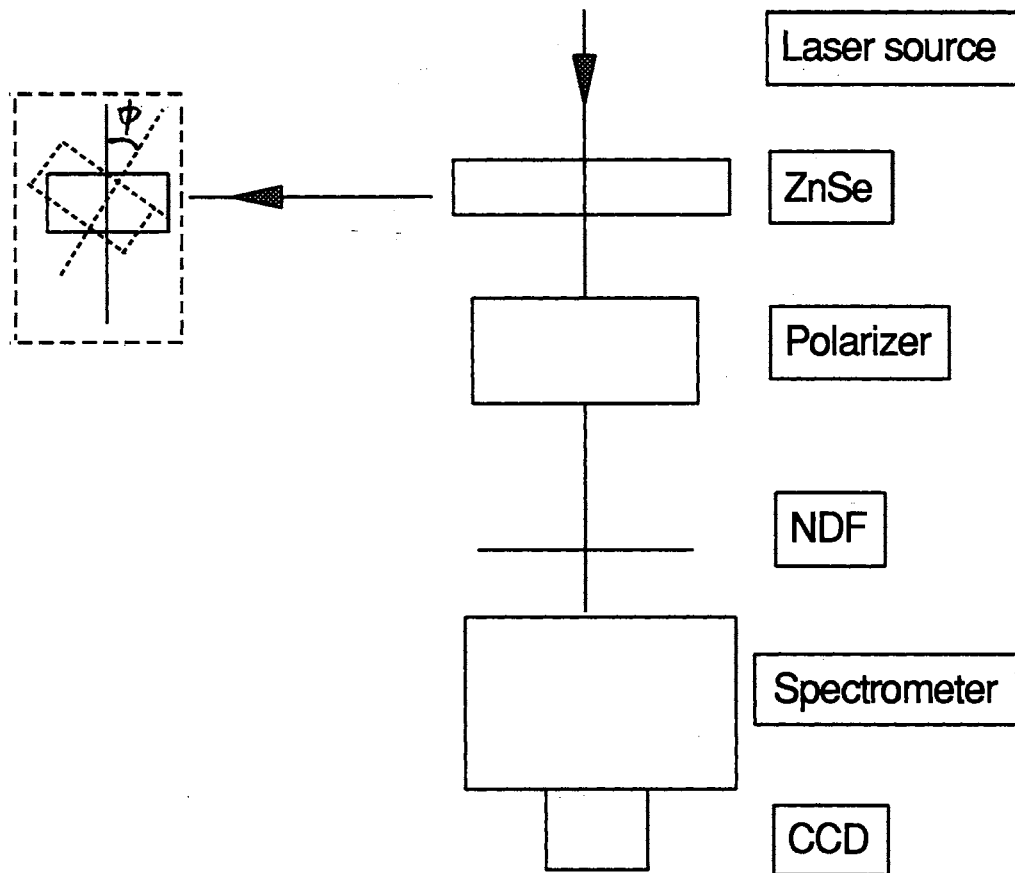
Figure 30. Experimental geometry used in the SHG investigation.

respectively, where $E_p(\omega)$ is the amplitude of the optical electric field oscillating at

angular frequency ω, $P(2\omega)$ is the induced nonlinear polarization oscillating at 2ω,

$\chi=\chi_{123}=\chi_{213}=\chi_{312}$ is the bulk second harmonic generation contribution to $\chi^{(2)}$ in

materials with $\overline{4}3m$ symmetry, and ϕ is the angle between the incident optical electric

field and the (001) crystallographic direction of the sample. The experimentally

observed angular dependence of the polarization components is shown in Fig. 31. The

wavelength of the pumping beam used was 850 nm. The theoretical curves

corresponding to Eqs. (VIII.16) and (VIII.17) are shown as solid lines. Good

agreement with the theory over the full range of angles can be seen.

Fig. 32 shows the SHG signal intensity as a function of the input laser intensity

plotted on a log-log scale. It can be seen that the slope of the curve is around 2 which

agrees with Eq. (VIII.4), as expected. The measurement was performed with the

second harmonic light polarized parallel to the excitation beam, at an angle between

the (001) direction and the polarization vector of the excitation beam that maximized

the frequency-doubled signal. We have measured and compared the signal intensities

in two samples with different interaction lengths: one with 5 mm and the other with 7

mm and found that the signal levels are the same using a pumping wavelength 900

nm. We have tuned the excitation wavelength from 840 nm to 920 nm so that the

frequency-doubled light photon energy was tuned from above to below the band gap

energy of ZnSe while keeping the pump power constant. The SHG signal did not

change appreciably when the frequency-doubled photon energy was tuned across the

band gap. We also varied the sample's temperature from 10K to room temperature and
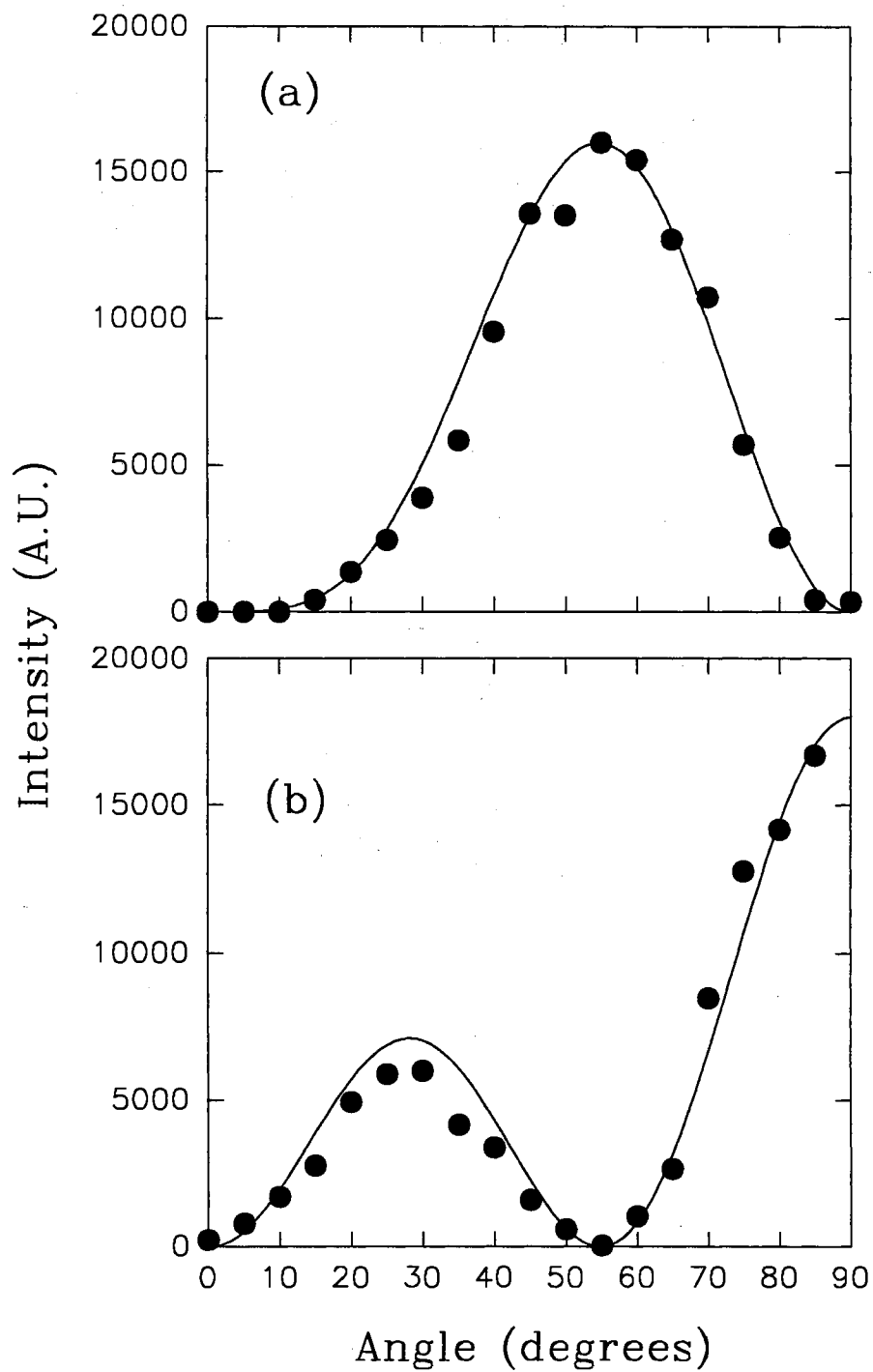
Figure 31. SHG signal intensity as a function of crystal orientation in (110)
orientated ZnSe for (a) $P_{//}$ component, (b) $P_{\perp}$ component. The solid
lines are the corresponding bulk theoretical curves.
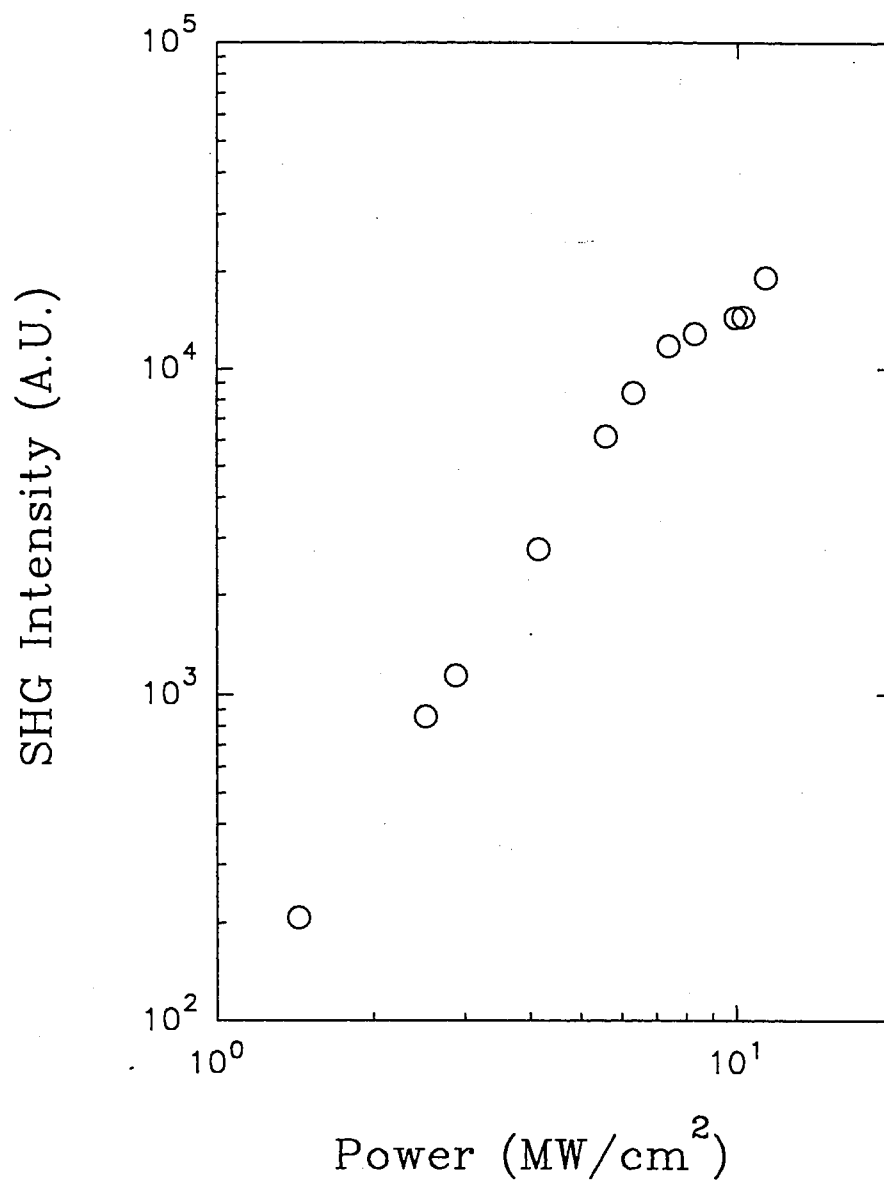
Figure 32. SHG signal intensity as a function of the input laser intensity plotted on a log-log scale.

found that the SHG intensity does not change drastically.

Discussion and Conclusions

The agreement of the data obtained from the polarization rotation experiments with the theoretical curves based on the bulk material is fairly good, suggesting that the observed signal in these samples has its origin in bulk SHG. The non-dependence of the SHG signal intensity on the interaction length can be understood as follows. Generally, the variation of the non-phase-matched and transmitted second harmonic power is an oscillating function of the sample length l. The position of the maximum is determined by the factor of[122,123]

$$\frac{\sin^2(\Delta k l/2)}{(\Delta k l/2)^2} \qquad (VIII.18)$$

where $\Delta k = k^{(2\omega)} - 2k^{(\omega)}$ is the phase mismatch for SHG. This result assumes a low sample electric conductivity. The coherence length l_c is defined as the distance between adjacent peaks of Eq. (VIII.18) and is given by

$$l_c = \frac{\pi}{\Delta k} = \frac{\lambda}{2(n^{(2\omega)} - n^{(\omega)})} \qquad (VIII.19)$$

for free-space fundamental wavelength λ. The coherence length puts an upper limit on the maximum useful thickness of an efficient second harmonic generator. Using the ZnSe refractive indices of 2.47 and 2.69 at 900 nm and 450 nm, respectively[81], we can obtain a coherence length of $l_c = 2.5$ μm. On the other hand, the absorption length l_a, defined as the reciprocal of the absorption coefficient at frequency-doubled

wavelength, is approximately 0.13 μm, using a value of α=8 x 10^4 cm^{-1}.[81] This

suggests that very little enhancements will be obtained by varying sample thickness

even for sample thicknesses approaching the coherence length, since any newly-

generated frequency-doubled light in the bulk is almost immediately absorbed.

Samples less than 0.13 μm thick will be needed to see any thickness dependence. Our

experimental results are consistent, in the limit of negligible pump depletion, with

signals of constant absolute intensity in samples thicker than l_a. This is in contrast to

the sharp increase in efficiency realized in transparent materials where phase matching

techniques can be applied.[120,122]

In summary, we have studied transmission geometry optical second harmonic

generation in ZnSe single crystals and found that the absolute registered second

harmonic intensity is constant for several samples. The angular dependence of the

SHG signal intensity is consistent with signals originating in the material bulk. The

SHG can be observed from a broad range of pumping photon energies. Finally, we

would like to mention that we also observed the SHG signal from a reflection

geometry. With this geometry SHG can be used as a probe to study the buried solid

interfaces at which other optical techniques are not useful.[124]

CHAPTER IX

SUMMARY AND CONCLUSIONS

The experimental results of stimulated emission and lasing studies performed

on the II-VI semiconductor ZnSe-based materials have been reported. Based on the

experimental results, the lasing mechanism at room temperature is determined to be

due to exciton-free carrier scattering, the exciton-hole scattering being the dominant

process. The low lasing threshold of ZnSe and ZnSSe laser bar samples demonstrates

the high quality of MBE and SPVT grown samples. The two-photon pumped blue

lasing was observed which demonstrated the applicability of using near-infrared diode

lasers as the pumping sources to excite the ZnSe-based materials. The mechanism of

the two-photon pumped lasing is due to free exciton-exciton scattering and resultant

band filling. The optical gain was measured using a single beam method by varying

the excitation length. These studies reveal that ZnSe and ZnSSe samples have the

quality suitable for low threshold, high power output blue laser operation.

The quantum size effect was studied in ZnS/ZnSe/ZnS single quantum wells by

the photoluminescence technique. The observed PL energy positions correlate with the

quantum well size through the quantum size effect. The strain effects in the ZnSe well

have to be considered in order for the theory to match the experimental result. The

abrupt broadening of the PL peak from thin well samples was accounted for by the

interface roughness in terms of the lateral quantum confinement effect in quantum slabs formed on islands and valleys at the interface.

We have presented the results of second harmonic generation measurements in a transmission geometry in various thickness ZnSe samples. We find that the second harmonic light originates in the material bulk rather than at the exit surface and that no signal enhancement to the second harmonic light by varying the sample thickness is observed. A broad excitation photon energy can be used to generate the SHG signal.

BIBLIOGRAPHY

1. G.E. Thomas, Phillips Tech. Rev. **44**, 51 (1988).

2. N.G. Basov and O.V. Bogdankevich, "Symp. on Radiative Recombination in Semiconductors", (Paris, 1964).

3. I.V. Kryukova, Soviet Tech. Phys. Lett. **5**, 214 (1979).

4. J.M. Hvam, Phys. Rev. **B4**, 4459 (1971).

5. O.V. Bogdankevich and N.G. Basov, Soviet J. Quantum Electron. **2**, 31 (1972).

6. S.S. Demidov, Soviet J. Quantum Electron. **13**, 54 (1983).

7. S.A. Belyaev, Soviet J. Quantum Electron. **12**, 1117 (1982).

8. E.M. Krasavina and I.V. Kryukova, Soviet J. Quantum Electron. **6**, 1354 (1976).

9. A.S. Nasibov, Soviet J. Quantum Electron. **10**, 503 (1980).

10. R.J. Seymour, B.J. Fitzpatrick, and R.N. Bhargava, IEEE J. Quantum Electron. **QE-14**, 462 (1978).

11. I.M. Catalano, A. Cingolani, M. Ferrara, M. Lugara, Solid State Commun. **43**, 371 (1982).

12. R.A. Baltrameyunas, A.A. Gladyshchuk, V.P. Gribkovskii, E.P. Kuokshtis, and G.P. Yablonskii, Sov. J. Quantum Electron. **11**, 539 (1981).

13. P.R. Newbury, K. Shahzad, and D.A. Cammack, Appl. Phys. Lett. **58**, 1065 (1990).

14. C.A. Zmudzinski, Y. Guan, and P.S. Zory, IEEE Photon. Technol. Lett. **2**, 94 (1990).

15. X.H. Yang, J. Hays, W. Shan, J.J. Song, E. Cantwell, and J. Altridge, Appl. Phys. Lett. **59**, 1681 (1991).

16. X.H. Yang, J. Hays, W. Shan, J.J. Song, and E. Cantwell, unpublished results.

17. G. Sun, K. Shahzad, J.M. Gaines, and J.B. Khurgin, Appl. Phys. Lett. **59**, 310 (1991).

18. I. Suemune, K. Yamada, H. Masato, Y. Kan, and M. Yamanishi, Appl. Phys. Lett. **54**, 981 (1989).

19. K. Nakanishi, I. Suemune, H. Masato, Y. Kuroda, and M. Yamanishi, Jpn. J. Appl. Phys. **29**, L2420 (1990).

20. K. Nakanishi, I. Suemune, Y. Fujji, Y. Kuroda, and M. Yamanishi, Appl. Phys. Lett. **59**, 1401 (1991).

21. D.A. Cammack, R.J. Dalby, H.J. Cornelissen, and J. Khurgin, J. Appl. Phys. **62**, 3071 (1987).

22. K. Nakanishi, I. Suemune, Y. Fuhii, Y. Kuroda, and M. Yamanishi, Jpn. J. Appl. Phys. **30**, L1399 (1991).

23. Y. Fujii, I. Suemune, Y. Kuroda, M. Fujimoto, and M. Yamanishi, Jpn. J. Appl. Phys. **31**, L692 (1992).

24. J. Khurgin, B.J. Fitzpatrick, and W. Seemungal, J. Appl. Phys. **61**, 1606 (1987).

25. Y. Hefetz, J. Nakahara, A.V. Nurmikko, L.A. Kolodziejski, R.L. Gunshor, and S. Datta, Appl. Phys. Lett. **47**, 989 (1985).

26. S.K. Chang, A.V. Nurmikko, J.W. Wu, L.A. Kolodziejski, and R.L. Gunshor, Phys. Rev. **B37**, 1191 (1988).

27. R. Miles, G. Wu, M. Johnson, T. McGill, J.P. Faurie, and S. Sivananthan, Appl. Phys. Lett. **48**, 1383 (1986).

28. Y. Hefetz, D. Lee, A.V. Nurmikko, S. Sivananthan, X. Chu, and J.P. Faurie, Phys. Rev. **B34**, 4423 (1986).

29. D.J. Olego, K. Shahzad, D.A. Cammack, and H. Cornelissen, Phys. Rev. **B38**, 5554 (1988).

30. C.G. Van de Walle, Phys. Rev. **B39**, 1871 (1989).

31. J. Ding, N. Pelekanos, A.V. Nurmikko, H. Luo, N. Samarth, and J.K. Furdyna, Appl. Phys. Lett. **57**, 2885 (1990).

32. W. Waleeki, A.V. Nurmikko, N. Samarth, H. Luo, J. Furdyna, and N. Otsuka,

Appl. Phys. Lett. **57**, 466 (1990).

33. J. Ding, H. Jeon, A.V. Nurmikko, H. Luo, N. Samarth, and J.K. Furdyna, Appl. Phys. Lett. **57**, 2756 (1990).

34. H. Jeon, J. Ding, A.V. Nurmikko, H. Luo, N. Samarth, J.K. Furdyna, W. A. Bonner, and R.E. Nahory, Appl. Phys. Lett. **57**, 2413 (1990).

35. H. Jeon, J. Ding, A.V. Nurmikko, H. Luo, N. Samarth, and J.K. Furdyna, Appl. Phys. Lett. **59**, 1293 (1991).

36. M. Haase, J. Qiu, J.M. DePuydt, and H. Cheng, Appl. Phys. Lett. **59**, 1272 (1991).

37. H. Jeon, J. Ding, W. Patterson, A.V. Nurmikko, W. Xie, D. Grillo, M. Kobayashi, and R.L. Gunshor, Appl. Phys. Lett. **59**, 3619 (1991).

38. H. Jeon, J. Ding, A.V. Nurmikko, W. Xie, D.C. Grillo, M. Kobayashi, R.L. Gunshor, G.C. Hua, and N. Otsuka, Appl. Phys. Lett. **60**, 2045 (1992).

39. Y. Kawakami, S. Yamaguchi, Y. Wu, K. Ichino, S. Fujita, and S. Fujita, Jpn. J. Appl. Phys. **30**, L605 (1991).

40. J. Ding, H. Leon, T. Ishihara, M. Hagarett, A.V. Nurmikko, H. Luo, N. Samarth, and J. Furdyna, Phys. Rev. Lett. **69**, 1701 (1992).

41. J. Ding, H. Leon, T. Ishihara, A.V. Nurmikko, H. Luo, N. Samarth, and J. Furdyna, Surface Sci.**267**, 616 (1992).

42. A.V. Nurmikko, R.L. Gunshor, and M. Kobayashi, J. Cryst. Growth, **117**, 432 (1992).

43. R.L. Gunshor, L.A. Kolodziejski, A.V. Nurmikko, and N. Otsuka, "Semiconductors and Semimetals ", (Academic Press, New York, 1991), Vol. **33**.

44. D. Lee, A. Mysyrowicz, A.V. Murmikko, and B.J. Fitzpatrick, Phys. Rev. Lett. **58**, 1475 (1987).

45. A.M. Glass, K. Tai, R.B. Bylsma, R.D. Feldman, D.H. Olson, and R.F. Austin, Appl. Phys. Lett. **53**, 834 (1988).

46. D. Lee, A.M. Johnson, J.E. Zucker, C.A. Burrus, R.D. Feldman, and R.F. Austin, Appl. Phys. Lett. **60**, 739 (1992).

47. D. Lee, A.M. Johnson, J.E. Zucker, C.A. Burrus, R.D. Feldman, and R.F. Austin, IEEE Photon. Technol. Lett. **4**, 949 (1992).

48. R.B. Bylsma, W.M. Becker, T.C. Bonsett, L.A. Kolodziejski, R.L. Gunshor, M. Yamanishi, and S. Datta, Appl. Phys. Lett. **47**, 1039 (1985).

49. K. Akimoto, H. Okuyama, T. Miyajima, Y. Morinaga, F. Hiei, and M. Ozawa, "Conference of Compact Blue-green Lasers", (New Orleans, 1993).

50. G. Bastard, Phys. Rev. **B24**, 5693 (1981); **B25**, 7594 (1982).

51. B. Ray, "II-VI compounds", (Pergamon Press, Edinburgh, 1969), Chap. 7.

52. Y. Guan, C.A. Zmudzniski, P.S. Zory, and R.M. Park, IEEE Photonics Technol. Lett. **3**, 685 (1991).

53. I.M. Catalano, A. Cingolani, M. Ferrara, and M. Lugara, Solid State Commun. **27**, 1331 (1978).

54. C. Klingshirn and H. Haug, Physics Reports, **70**, 315 (1981).

55. J.J. Hopfield, Phys. Rev. **112**, 1555 (1958).

56. C. Benoit a la Guillaume, J.M. Debever, and F. Salvan, Proc. 9th Intern. Conf. on Phys. Semiconductors, Moscow, 581 (1968) and Phys. Rev. **177**, 567 (1969).

57. H. Haug, and S.W. Koch, Phys. Stat. Sol. **b82**, 531 (1977).

58. S.W. Koch, H. Haug, G. Schmieder, W. Bohnert, and C. Klingshirn, Phys. Stat. Sol. **b89**, 431 (1978).

59. J.M. Hvam, Sol. State Comm. **12**, 95 (1973).

60. K. Era, D.W. Langer, J. Lum.**1,2**, 514 (1970).

61. X.W. Fan, Z.K. Tang, and H. Tian, J. Crystal Growth, **101**, 944 (1990).

62. X.W. Fan, and J. Woods, IEEE Trans. Electron Device ED-28, 428 (1981).

63. T. Yao, Y. Okada, S. Matsui, K. Ishida, and I. Fujimoto, J. Crystal Growth **81**, 518 (1987).

64. K. Ohkawa, T. Mitsuyu, and O. Yamazaki, Phys. Rev. **B.38** 12465 (1988).

65. K. Shahzad, Phys. Rev. B. **38** 8309 (1988).

66. X.H.Yang, J. Hays, W. Shan, J.J. Song, E. Cantwell and J. Aldridge, Appl. Phys. Lett. **60**, 926 (1992).

67. Josef Bille, in Festkorperprobleme XIII, Advances in Solid State Physics, edited by H.J. Queisser (Pergamon, Braunschweig, 1973), p. 111.

68. H. Yoshida, H. Saito, and S. Shionoya, Solid State Commun. **33**, 161 (1980).

69. H. Saito, and S. Shionoya, J. Phys. Soc. Japan, **37**, 423 (1974).

70. T. Fischer, and J. Bille, J. Appl. Phys. **45**, 3937 (1974).

71. W. Maier, and C. Klingshirn, Sol. State Comm. **28**, 13 (1978).

72. Y. Shirakawa, and H. Kukimoto, J. Appl. Phys. **51**, 2014 (1980).

73. U. Heim, and P. Wiesner, Phys. Rev. Lett. **30**, 1205 (1973).

74. R.A. Reynolds, J. Vac. Sci. Technol. **A 7**, 269 (1989), and references therein.

75. R.N. Bhargava, J. Cryst. Growth **86**, 873 (1988).

76. J. Saraie, N. Matsumura, M. Tsubokura, K. Miyagawa, and N. Nakamura, Jpn. J. Appl. Phys. **28**, L108 (1989).

77. H. M. Yates, J.O. Williams, Appl. Phys. Lett. **51**, 809 (1987).

78. I. Suemune, K. Yamada, H. Masato, T. Kanda, Y. Kan, and M. Yamaniahi, Jpn. J. Appl. Phys. **27**, L2195 (1988).

79. P.R. Newbury, K. Shahzad, J. Petruzzello, and D.A. Cammack, J. Appl. Phys. **66**, 4950 (1989).

80. K. Yamada, I. Suemune, T. Kanda, H. Masato, Y. Kan, and M. Yamanishi, Extended Abstract of 1988 International Conference on Solid State Devices and Materials (Business Center for Academic Societies, Tokyo, 1988), P. 403.

81. S. Adachi, and T. Taguchi, Phys. Rev. **B 43**, 9569 (1991).

82. E. Catwell, Technique Report of Eagle Picher Research Lab. 1991 (unpublished).

83. J.I. Pankove , "Optical Processes in Semiconductors", (Dover, New York, 1971),

Chap. 7.

84. H.L. Cotal, A.C. Lewnadowski, B.G. Markey, S.W.S. McKeever, E. Cantwell, and J. Aldridge, J. Appl. Phys. **67**, 448 (1990).

85. A. Taike, M. Migita, and H. Yamamoto, Appl. Phys. Lett. **56**, 1989 (1990).

86. M.A. Haase, and J.E. Potts, J. Appl. Phys. **67**, 448 (1990).

87. K. Ohkawa (provate communication).

88. T. Yao (private communication).

89. M. Migita, A. Taike, and H. Yamamoto, J. Appl. Phys. **68**, 880 (1990).

90. S. Colak, R.N. Bhargava, B.J. Fitzpatrick, and A. Sicignano, J. luminescence, **31 & 32**, 430 (1984).

91. V.P. Gribkovskii, V.A. Zaporozhchenko, V.A. Ivanov, A.V. Kachinskii, V.V. Parashchuk, and G.P. Yablonskii, Sov. J. Quantum Electron. **9**, 1305 (1980).

92. M.H. Weiler, Solid State Commun. **39**, 937 (1981).

93. C.R. Pidgeon, B.S. Wherrett, A.M. Johnston, J. Dempsey, and A. Miller, Phys. Rev. Lett. **42**, 1785 (1979).

94. X.H. Yang, J.J. Song, E. Cantwell, and J. Aldridge, Phys. Stat. Sol. **127**(a), K79(1991).

95. K.L. Shaklee, and R.F. Leheny, Appl. Phys. Lett. **18**, 475 (1971).

96. P. Fabeni, R. Linari, G.P. Pazzi, and A. Ranfagni, Appl. Optics **26**, 5317 (1987).

97. S. Borenstain, D. Fekete, M. Vofsi, R. Sarfaty, E. Cohen, and A. Ron, Appl. Phys. Lett. **50**, 442 (1987).

98. E. Fortin, B.Y. Hua, A.P. Roth, A. Charlebois, S. Fafard, and C. Lacelle, J. Appl. Phys. **66**, 4854 (1989).

99. See, for example, P.W. Milonni, and J.H. Eberly, "Lasers", (Wiley, New York, 1988), pp 283-287.

100. P.J. Dean, P.J. Wright, and B. Cockayne, J. Phys. C **16**, 3493 (1983).

101. M. Aven, D. Marple, and B. Segall, J. Appl. Phys. **32**, 2261 (1961).

102. J.J. Song, and W.C. Wang, J. Appl. Phys. **55**, 660 (1984).

103. K.L. Shaklee, R.E. Nahory, and R.F. Leheny, J. Lumin. **7**, 284 (1973).

104. G.C. Osbourn, IEEE J, Quantum Electron. **QE-22**, 1677 (1986).

105. G.C. Osbourn, J. Appl. Phys. **53**, 1586 (1981).

106. T. Yokogawa, M. Ogura, and T. Kajiwara, Appl. Phys. Lett. **49**, 1702 (1986).

107. H. Fujiyasu, H. Takahashi, H. Shimizu, A. Sasaki, and H. Kuwabara, in Proc. 17th Intern. Conf. on Physics of Semiconductors, San Francisco, CA, 1984.

108. K. Mohamed, D.J. Olego, P. Newbury, D.A. Cammack, R. Dalby, and H. Cornelissen, Appl. Phys. Lett. **50**, 1820 (1987).

109. T. Yao and T. Takeda, Appl. Phys. Lett. **48**, 160 (1986).

110. T. Yao, Z.Q. Zhu, K. Uesugi, S. Kamiyama, and M. Fujimoto, J. Vacuum. Sci. Technol. **A8**, 997 (1990).

111. Y. Kawakami, T. Taguchi, and A. Hiraki, J. Crys. Growth, **93**, 714 (1988).

112. M. Konagai, M. Kobayashi, R. Kimura, and K. Takahashi, J. Cryst. Growth, **86**, 290 (1988).

113. J.L. Lee, E.S. Koteles, and M.O. Vassell, Phys. Rev. **B33**, 5512 (1986).

114. K. Shahzad, D.J. Olego, and C.G. Van de Walle, Phys. Rev. **B38**, 1417 (1988).

115. N. Peyghambarian, S.H. Park, S.W. Koch, A. Jeffery, J.E. Potts, H. Cheng, Appl. Phys. Lett. **52**, 182 (1988).

116. L. Banyai, and S.W. Koch, Z. Phys. **B63**, 283 (1986).

117. M. Taghizadeh, I. Janossy, and S.D. Smith, Appl. Phys. Lett. **46**, 331 (1985).

118. M.S. Yeganeh, J. Qi, J.P. Curver, A.G. Yodh, and M.C. Tamargo, Phys. Rev. **B46**, 1603 (1992).

119. Y. Hase, K. Kumata, S.S. Kano, M. Ohashi, T. Kondo, R. Ito, and Y. Shiraki, Appl. Phys. Lett. **61**, 145 (1992).

120. R. Hopf, and G. Stegeman, "Applied Classical Electrodynamics", (Wiley, New York, 1986).

121. A. Yariv, "quantum Electronics", (Wiley, New York, third edition, 1989).

122. P. Maker, R. Terhune, M. Nisenoff, and C. Savage, Phys. Rev. Lett. **8**, 21 (1962).

123. Y. Shen, "The Principle of Nonlinear Optics", (Wiley, New York, 1984).

124. Y.R. Shen, Nature, **337**, 519 (1989).

125. G.A. Baraff, J.A. Appelbaum, and D.R. Hamann, Phys. Rev. Lett. **38**, 237 (1977).

126. G.B. Bachelet, D.R. Hamann, and M. Schluter, Phys. Rev. **B26**, 4199 (1982).

127. W.R. Frensley, and H. Kroemer, Phys. Rev. **B16**, 2642 (1977).

128. W.A. Harrison, "Electronic Structures and the Properties of Solids" (Freeman, San Francisco, 1980), p. 253.

129. J. Tersoff, Phys. Rev. **B32**, 6968 (1985).

130. C. Tejedor and F. Flores, J. Phys. **C11**, L19 (1979).

131. J.A. Verges, D. Glotzel, M. Cardona, and O.K. Andersen, Phys. Status Solidi **B113**, 519 (1982).

132. M. Cardona and N.E. Christensen, Phys. Rev. **B35**, 6182 (1987).

133. G.C. Van de Walle and R.M. Martin, Phys. Rev. **B34**, 8154 (1987).

134. O.H. Nielsen and R.M. Martin, Phys. Rev. **B32**, 3792 (1985).

APPENDIX A

BAND LINEUPS OF SEMICONDUCTOR HETEROJUNCTIONS

Introduction

When an interface is formed between two semiconductors, the question arises naturally of how the bulk band structures are aligned relative to one another. The band offset is the key quantity in the analysis of the properties of heterostructures. The solution to the problem is complicated by several factors. First, the problem is fundamental to that for a bulk solid. There is no intrinsic energy scale (i.e. no vacuum zero is present) to which all energies can be referred. This ambiguity arises because the long range nature of the coulomb interaction does not allow the zero of the energy of an infinite (bulk) solid to be well defined. Therefore, there exists no unique reference level within each bulk solid with which to compare the potentials for two different solids. Secondly, when an interface is formed, the electronic charges will move across the interface. These charge transfer effects set up dipole moments across the interface which will give rise to a relative shift in the bulk bands. If a complete solution of the interface problem is desired, one must carry out self-consistent calculations in which the electrons are allowed to adjust to the specific environment induced by the interface. The first self-consistent interface calculation (SCIC) was that

112

of Baraff[125] et al. The SCIC uses either empirical pseudopotentials or the ab initio

pseudopotentials. Results for ΔE_v (valence band offset) are presented for a number of

lattice-matched (110) heterointerfaces.[126] Unfortunately, the computational complexity

of such first-principle calculations is very high, which limits their use as a general tool

in the exploration and design of novel heterostructures. Several models have been

proposed that attempt to establish an absolute energy level for each semiconductor.

The existence of such an absolute energy scale implies that one is not dealing with an

infinite solid, but rather with a crystal that has been somehow terminated (i.e. a

surface has now entered the picture). The means by which this surface is defined

underlies and differentiates the various models.

There are several models which deal with the band lineups but do not include

strain effects. Frensley and Kroemer[127] constructed a model solid in which they

superimposed spherical ions and chose the mean interstitial potential in the zinc-blende

structure as the electrostatic reference potential for each semiconductor. The Frensley-

Kroemer scheme in principle offered a very attractive approach for calculating a

reference level. However, the extensive computational requirements render it

impractical for generating accurate values for band offsets. Harrison's theory[128] of

natural band lineups establishes an absolute energy scale by referring all energies to

energy eigenvalues of the free atom. Harrison's model is based on atomic term values,

which are assumed to carry over from atom to solid. In the approach of Tersoff[129] and

Tejedor and Flores[130], screening arguments are used to define a neutral level for each

semiconductor. These levels are aligned when an interface is formed, thus determining

band offsets. In analogy to metal-metal interfaces, these theories assume that dipoles will be set up that will drive the heterointerface system towards alignment of neutrality levels of the materials as would be the case at a heterojunction between two metals in which the Fermi levels line up.

Recently, two other model solid calculations based on an absolute energy reference scale and allowing for the incorporation of misfit strain have been generated. These include; (i) the linear muffin-tin orbitals (LMTO) all-electron calculations of Verges et al.[131] and Cardona and Christensen[132], and (ii) the model solid calculations of Van de Walle and Martin.[133] Contrary to the complex calculations of the LMTO method, the model solid theory is much simpler in calculation and can give some physical insights into the problems. We study the model solid theory in more detail.

Model Solid Theory

In the model-solid theory of Van de Walle and Martin[133], a procedure is developed in obtaining the lineup of an electrostatic potential across the heterointerface by using only information from the bulk constituents. This model retains the spirit of the SCIC and results from an attempt to describe the essential features of the SCIC results, but without having to perform the local-density calculations on a supercell. The infinite (bulk) solid is replaced by a semi-infinite solid having an ideally terminated surface (i.e. one without a surface dipole layer). The semi-infinite model solid is constructed by taking a superposition of neutral atomic spheres. The potential outside each of these neutral spheres goes exponentially to zero, which is taken as the

zero of energy for the model solid. The presence of a surface in this model does not induce any shift in the average potential, since no dipole layer can be set up using neutral spheres. Full information about the atomic potential can be obtained by performing an atomic calculation. Since all calculations for the solid are based on pseudopotentials, we can perform the atomic calculations on the 'pseudoatom'. After carrying out the atomic calculations on the pseudoatom and obtaining the charge density and potentials, the average electrostatic potential in this model solid is well determined on the absolute energy level.[133] The band structures of individual materials can be calculated by performing density-functional calculations on individual bulk semiconductors.[134] The accuracy and margin of error of band structures produced by these calculations is well established. The best-known deficiency is the failure of density-functional theory to produce the correct band gap. In model solid theory, the calculated valence bands are added on the electrostatic potential and the conduction band position is derived by adding the experimental band gap to the valence band position. These calculated energies are all put in an absolute energy scale and this allows us to derive band lineups by simply subtracting values for individual semiconductors.

It is to be noted that taken separately, the results for band position with respect to the average potential and for the average potential itself contain no information, since they depend on the choice of angular momentum used in the pseudopotential. Only the combination of both, which gives band positions on an absolute energy scale, is meaningful and independent of choices in the pseudopotential. A summary of the

results for elemental, III-V and II-VI semiconductors are given in Table I in Ref.[30]

Listed in the table are values for $E_{v,av}$, which is the average over the three uppermost

valence bands at Γ. Since there is an interaction between strain and spin-orbit splitting,

the effect of uniaxial strain, hydrostatic strain and spin-orbit may be added on $E_{v,av}$.

The effect of shear strain is to split the degenerate valence bands. The effect of

hydrostatic strain is to shift the positions of each band , i.e. $\Delta E_{v,av} = a_v \text{Tr}(\varepsilon)$,

$\Delta E_c = a_c \text{Tr}(\varepsilon)$, respectively. The detailed information about model solid theory can be

found in Ref. 30.

APPENDIX B

MATERIAL PROPERTIES OF UNDOPED ZnSe, ZnS

Energy	Band Gap (4K)/(RT)	LO Phonon	Exciton (Binding)	Spin-orbit Splitting
ZnSe	2.83 eV/2.67 eV[a]	31 meV[b]	21 meV[c]	0.43 eV[a]
ZnS	3.84 eV/3.68 eV[a]	42 meV[d]	40 meV[e]	0.07 eV[a]

a. K. Shahzad, D.J. Olego, C.G. Van De Walle, and D.A. Cammack, J. Luminescence **46**, 109 (1990).
b. M. Aven, D.T.F. Marple and B. Segall, J. Appl. Phys. **32**, 2261 (1961).
c. Q. Fu, D. Lee, A. Mysyrowitz, and A.V. Nurmikko, Phys. Rev. **B31**, 8791 (1988).
d. T. Taguchi and T. Yokogawa, J. Phys. **D17**, 1067 (1984).
e. T. Taguchi, T. Yokogawa, and H. Yamashita, Solid State Commun. **49**, 551 (1984).

APPENDIX C

EFFECTIVE MASSES OF ZnSe AND ZnS USED IN LITERATURE

References	ZnS			ZnSe		
	M_e^*/M_e	M_{hh}^*/M_e	M_{lh}^*/M_e	M_e^*/M_e	M_{hh}^*/M_e	M_{lh}^*/M_e
(1)	0.28	1.76	0.23	0.14	1.44	0.149
(2)	0.27	0.49	-	0.17	0.6	-
(3)	0.28	1.4	0.49	-	-	-
(4)	-	-	-	0.16	0.29	-
(5)	0.34	-	-	0.16	-	-
(6)	0.17	(M_h) 0.6	(M_h) 0.6	0.17	(M_h) 0.6	(M_h) 0.6

(1) P. Lawaetz, Phys. Rev. **B4**, 3460 (1971).
(2) K. Shahad, J. Luminescence **46**, 109 (1980).
(3) J.O. Dimmack, *II-VI Semiconducting Compounds*, Thomas, 277 (1967).
(4) N. Kobayashi, Appl. Phys. Lett. **55**, 1235 (1989).
(5) H. Fujiyasu and K. Mochizuki, J. Appl. Phys. **57**, 1235 (1985).
(6) K. Mohammed, D.J. Olego, P. Newbury, D.A. Cammack, R. Dalby, and H. Cornelissen, Appl. Phys. Lett. **50**, 1820 (1987).
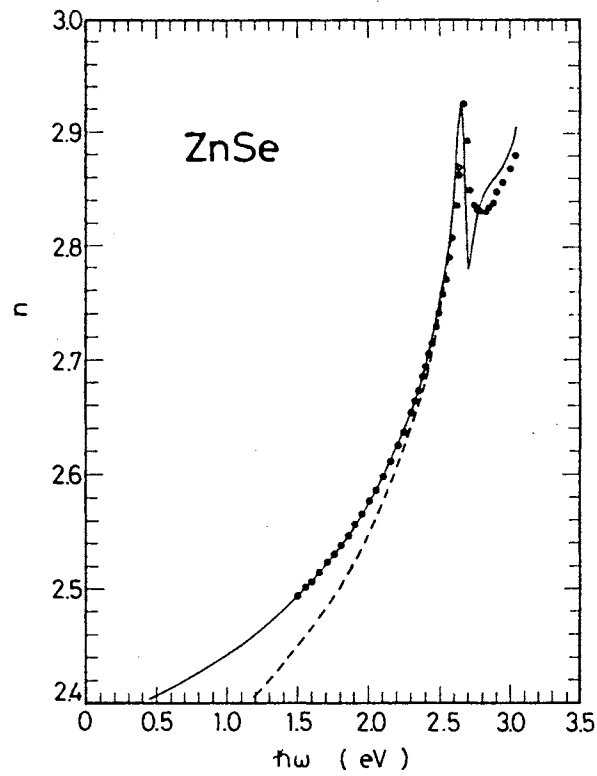
APPENDIX D

COMPARISON OF CALCULATED ABSORPTION COEFFICIENT α (SOLID LINE)

TO THE EXPERIMENTAL DATA FOR ZnSe (REFERENCE 81).
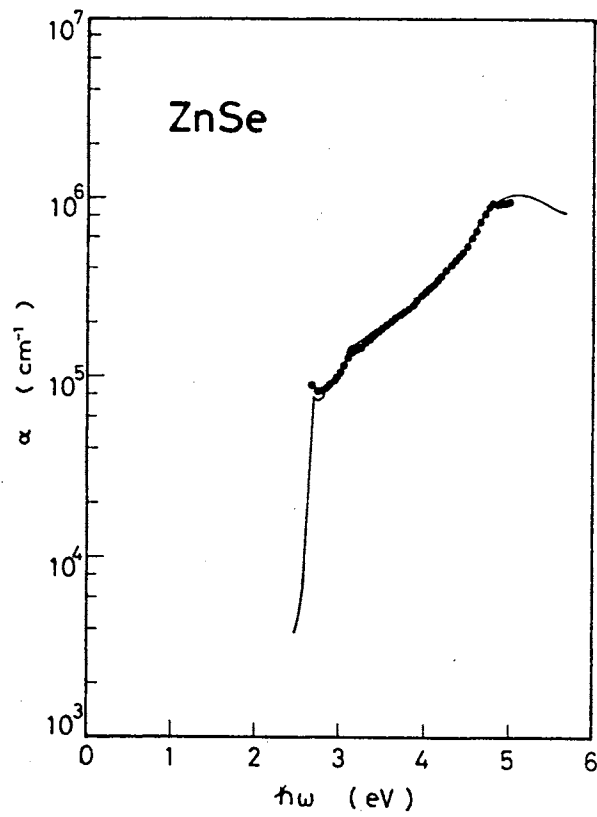
APPENDIX E

COMPARISON OF CALCULATED REFRACTIVE-INDEX DISPERSION (SOLID LINE) TO THE EXPERIMENTAL DATA FOR ZnSe (REFERENCE 81).

VITA

XIAO HUA YANG

Candidate for the Degree of

Doctor of Philosophy

Thesis: LASING AND OPTICAL PROPERTIES OF ZnSe BASED II-
VI COMPOUNDS

Major Field: Physics

Biographical:

   Personal Data: Born in Zhengzhou, China, May 17,
      1962, the son of Han Qing Yang and Yu Qing Gao.

   Education: Graduated from eighth high school
      (Zhengzhou, China) in 1980, received Bachelor of
      Science Degree in physics from Henan Normal
      University in 1984; received Master of Science
      Degree in physics from Oklahoma State University
      in 1988; completed requirements for the Doctor of
      Philosophy Degree at Oklahoma State University in
      July, 1993.